uOttawa

L'Université canadienne
Canada's university

FACULTÉ DES ÉTUDES SUPÉRIEURES ET POSTOCTORALES

uOttawa

L'Université canadienne
Canada's university

FACULTY OF GRADUATE AND POSDOCTORAL STUDIES

David Babineau

AUTEUR DE LA THÈSE / AUTHOR OF THESIS

M.Sc. (Physics)

GRADE / DEGREE

Department of Physics

FACULTÉ, ÉCOLE, DÉPARTEMENT / FACULTY, SCHOOL, DEPARTMENT

Modeling the Electric Field and Natural Environment of Weakly Electric Fish

TITRE DE LA THÈSE / TITLE OF THESIS

Dr. A. Longtin

DIRECTEUR (DIRECTRICE) DE LA THÈSE / THESIS SUPERVISOR

John Lewis

CO-DIRECTEUR (CO-DIRECTRICE) DE LA THÈSE / THESIS CO-SUPERVISOR

EXAMINATEURS (EXAMINATRICES) DE LA THÈSE / THESIS EXAMINERS

Dr. L. Chen

Dr. I. L'Heureux

Dr. B. Jarosz

Gary W. Slater

Le Doyen de la Faculté des études supérieures et postdoctorales / Dean of the Faculty of Graduate and Postdoctoral Studies

MODELING THE ELECTRIC FIELD AND NATURAL ENVIRONMENT OF WEAKLY ELECTRIC FISH

By

DAVID BABINEAU

B.Sc., Université de Moncton, 2003

Thesis submitted to the
Faculty of Graduate and Postdoctoral Studies
In partial fulfillment of the requirements
For the Master's Degree in Physics

Department of Physics
Faculty of Sciences
University of Ottawa

Your file Votre référence
ISBN: 978-0-494-18395-3
Our file Notre référence
ISBN: 978-0-494-18395-3

SUMMARY

Weakly electric fish use a unique sensory modality in order to help them communicate, navigate and find prey. These fish emit electric discharges that are monitored by electroreceptors located in the fish's skin. Surrounding objects perturb these baseline transdermal potentials and create *electric images*. The study of these images has led to a better understanding of general sensory processing principles; however, many aspects of these fish's natural electrosensory environment remain unknown. To this end, a two-dimensional finite element model of *Apteronotus leptorhynchus* was created. Using this model, we suggest new ways by which electric fish are able to locate objects and propose that it is possible for these fish to extract useful information from their environment using their natural scanning behaviour. Our results also reveal important limitations in standard experimental paradigms that aim to mimic the effects of conspecifics. Alternative paradigms that will enable more realistic stimulation are suggested.

SOMMAIRE

Les poissons faiblement électriques utilisent une modalité sensorielle unique qui leur permet de communiquer, naviguer et trouver des proies. Ces poissons émettent des décharges électriques qui sont mesurées par des électrorécepteurs situés dans leur peau. Les objets qui se trouvent autour du poisson perturbent ces différences de potentiels (à travers la peau), et créent ainsi des *images électriques*. L'étude de ces images a amené à une meilleure compréhension des principes généraux de l'information sensorielle. Par contre, l'environnement naturel de ces poissons demeure grandement inconnu. Ainsi, nous avons créé un modèle numérique composé d'éléments finis de *Apteronotus leptorhynchus* en deux dimensions. Ce modèle nous a permis de suggérer de nouvelles méthodes par lesquelles les poissons électriques pourraient localiser des objets et de proposer comment ces poissons pourraient extraire de l'information pertinente de leur milieu en utilisant leur mouvement de « balayage ». Des nouveaux protocoles expérimentaux sont aussi proposés afin de simuler l'effet d'un poisson « voisin » de manière plus efficace.

ACKNOWLEDGEMENTS

I am extremely thankful to André and John for the opportunity they gave me. They were both exceptional supervisors and I am grateful for all their help and also for their friendship. I am also thankful to Christopher Assad for the experimental data he provided. All the people in the fish group made my stay here a lot of fun and also provided me with valuable suggestions during some of my talks (in semi-chronological order): Jay a.k.a. "Mr. Beautiful", Jan, Benji, Brent, Moe, Len, Anne-Marie, Kristina, Erik, Connie, Dan, SuperSally, Shannon, Ginette "Waveform figure" Hupé, Julie, Ben, Jessica, Arielle, Jeff, Alex, Nick, Adrian, Zhaohong and Wudu. Thanks also to non-fish group lab mates J.P., Jim and Iana. Finally, I am deeply thankful to all my friends and family for their support. Mam, Dad, Jeff, pépére et mémére, les Maillet et Serge Emile, merci beaucoup pour votre support et amitié. Dominique, je te dois beaucoup...merci pour ton support, ta patience, ton amitié, et pour ressortir le mieux dans moi...

LIST OF PUBLICATIONS IN THIS THESIS

This is a thesis by articles. It is based in part on work reported in the following two manuscripts:

I. D. Babineau, A. Longtin and J. E. Lewis

Modeling the electric field of weakly electric fish.

Submitted to the Journal of Experimental Biology.

II. D. Babineau, J. E. Lewis and A. Longtin

A Study of Electro-Acuity and Motion Parallax in Weakly Electric Fish.

To be submitted.

TABLE OF CONTENTS

CHAPTER 1

INTRODUCTION

Sight, smell, hearing, taste and touch. These five senses, first classified by Aristotle in antiquity, bring vivid pictures to mind and have been studied exhaustively throughout the ages [3, 14, 15, 22, 29, 34, 37]. As human beings, we are able to relate to these senses because we use each of them at almost every moment of our lives. There are, however, other senses which are foreign to humans and to most other animals. One of these exotic senses is the weakly electric fish's electrosense. Contrary to electric eels, which use strong electrical discharges in order to stun their prey, weakly electric fish use electricity in order to communicate with other fish and to navigate and locate prey (a behaviour called electrolocation), even in the absence of visual cues [12]. Furthermore, these behaviours are effectively performed in natural conditions that involve very low signal-to-noise ratios [28].

One of the reasons why researchers study these fish is in order to gain a better understanding of the human brain, since many of the neural mechanisms and structures responsible for sensory processing in humans are similar to those found in fish [17]. The advantage of studying weakly electric fish, however, lies in the fact that their brains are simpler to study and easier to manipulate experimentally [17]. In fact, weakly electric fish have been singled out as a key model system for elucidating the general principles of sensory processing [8].

The remainder of this chapter will give more details on weakly electric fish and their unique sensory modality and will also explain this thesis' contribution to our understanding of their electrosensory world.

1.1 Weakly Electric Fish: An Introduction

Weakly electric fish are found in dark and murky African and South American waters [11, 27]. Their electric organ discharge (EOD) is emitted from an electric organ (EO) found within the tail-end of their bodies. This EO is formed by specialized "electrocytes" [5] which are organized anatomically in different ways, depending on the species. These electrocytes are activated by spinal electromotor neurons which transmit signals sent out by the fish's brain (the pacemaker nucleus; see [5] for details). Weakly electric fish are generally classified as either pulse-type or wave-type species, depending on the nature of their EOD. Wave-type species emit sine-like discharges while the pulse-type species' EOD has long pauses between discharges (frequencies for wave-type fish vary between approximately 600 and 1800 Hz [27]). These discharges are typically measured as the potential difference found between two electrodes located at the fish's head and tail extremities. Figure 1.1A shows the EOD for the (wave-type) weakly electric fish studied within this thesis, *Apteronotus leptorhynchus* (common name: brown ghost knifefish). A review of weakly electric fish species and their classification can be found in [27].

The electric discharges produced by weakly electric fish creates an electric field all around them which is mainly dipolar in nature ([21]; See Figure 1.1B). This field can be considered as electrostatic, given that the magnetic field is negligible [4] and that the electric signals produced by the fish are rapidly attenuated in water and hence do not

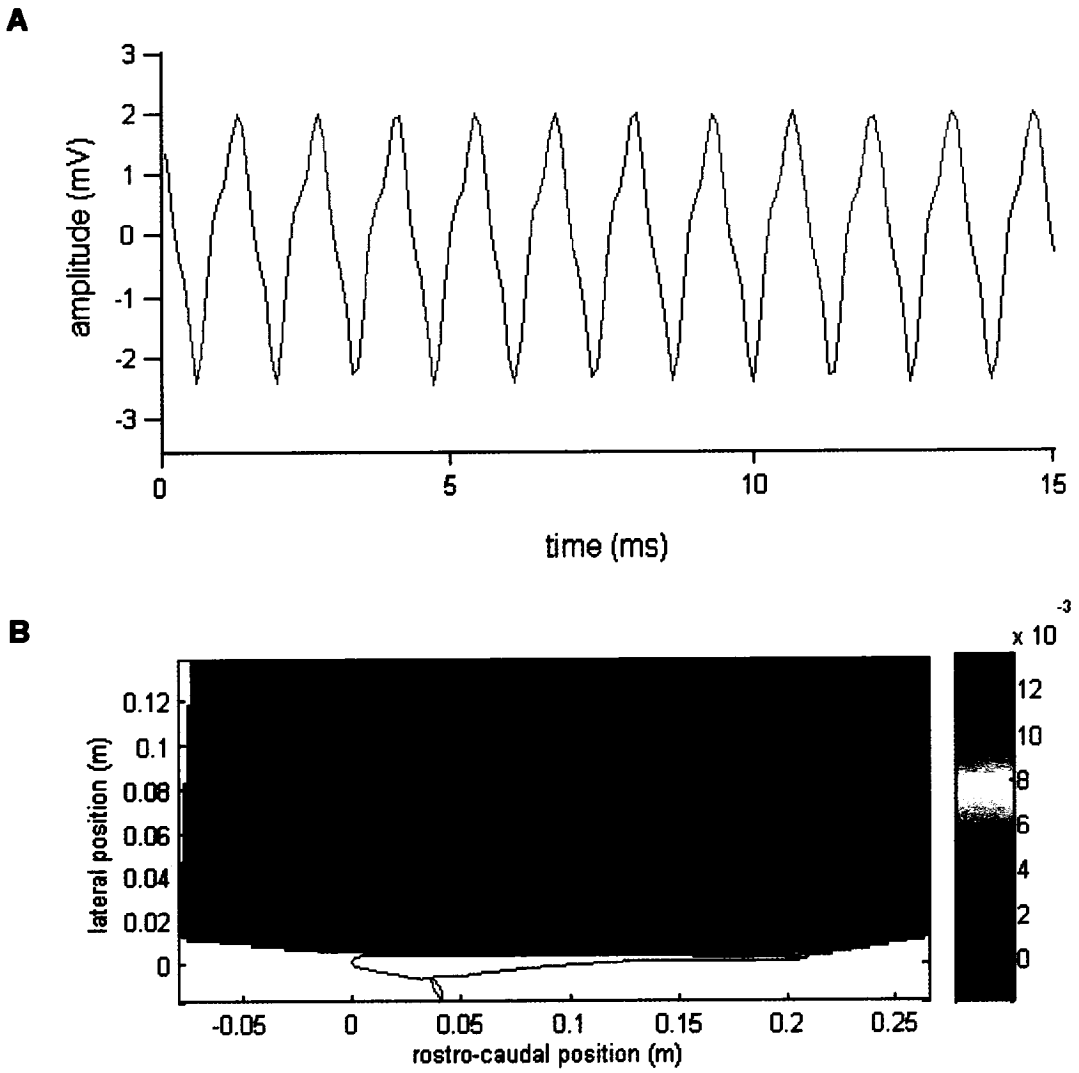

Figure 1.1: Electric discharges produced by the brown ghost knifefish (*Apteronotus leptorhynchus*). (A) Electric organ discharge (EOD) of a male fish (Courtesy Ms. Ginette Hupé). The EOD was measured as the difference in potential between two electrodes placed at the fish's head and tail extremities. The (peak-to-peak) amplitude of this fish's EOD is about 4 mV while its frequency is approximately 900 Hz. (B) Quasi-dipolar field potential surrounding the fish (at one phase of the fish's EOD cycle). The field is characterised by a spatially concentrated, high amplitude pole in the tail region and an elongated, weak amplitude pole in the head regions Potential values, given by the colorscale on the right, are in Volts. The image was produced with MATLAB using the field measurements provided by Christopher Assad (see Chapter 2 for fish specifications).

propagate [19]. The peak-to-peak potentials typically found in the field just outside the fish are on the order of a few millivolts, while the field gradients are in the range of a few millivolts per centimetre. For detailed maps of the fish's electric field and potential at different phases of the EOD cycle, the reader is urged to consult the following papers [2, 31, 32].

How do weakly electric fish locate, or rather, *electrolocate*, nearby objects?[1,2] What happens is that these fish sense perturbations in their self-generated electric field which are caused by nearby objects. For example, an insulating (relative to water conductivity) object would tend to propel current lines away from it (see Figure 1.2A), hence changing the distribution of current at the fish's surface, while a conductive object would produce an opposite effect. This is important since thousands of electroreceptors [9] lie in the fish's epidermis and measure transdermal potentials, i.e. potential differences across the skin (for a review of these electroreceptors see [6]). The distribution of these transdermal potentials all over the fish's surface is commonly referred to as the "electric image" (see Figure 1.2B). These images play an important role in electrosensory perception since this is the first level of electrosensory input for these fish (these images will be investigated throughout this thesis). These initial inputs are then relayed exclusively (via afferent fibres) to a section of the brain called the electrosensory lateral line lobe (ELL) for further processing [17]. From there, information is sent out to higher brain centers, is

[1] Lissman, along with Machin in 1958 [23, 24] were the first to discover that the weak electric discharges produced by weakly electric fish were used for sensing purposes.

[2] Due to the brief nature of this introduction, details of *electrocommunication* will not be covered. However, a review of this behaviour can be found in [18]. Also, exploratory behaviours commonly used by weakly electric are discussed in [35].

processed, and then a decision is made and a relevant motor output is produced (capture prey, flee predator, etc.) The goal of neuroscience is to figure out exactly how all of this works!

A

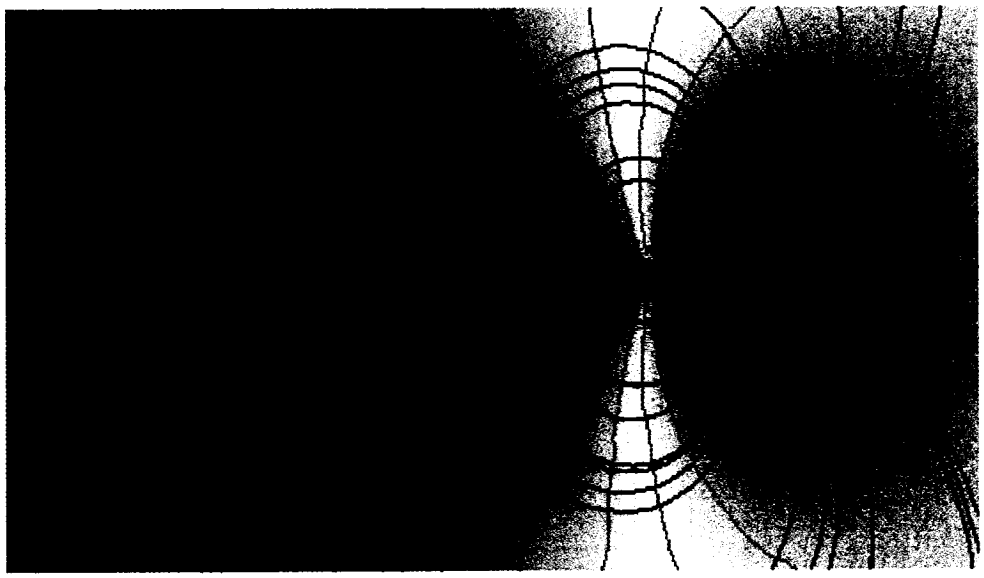

B

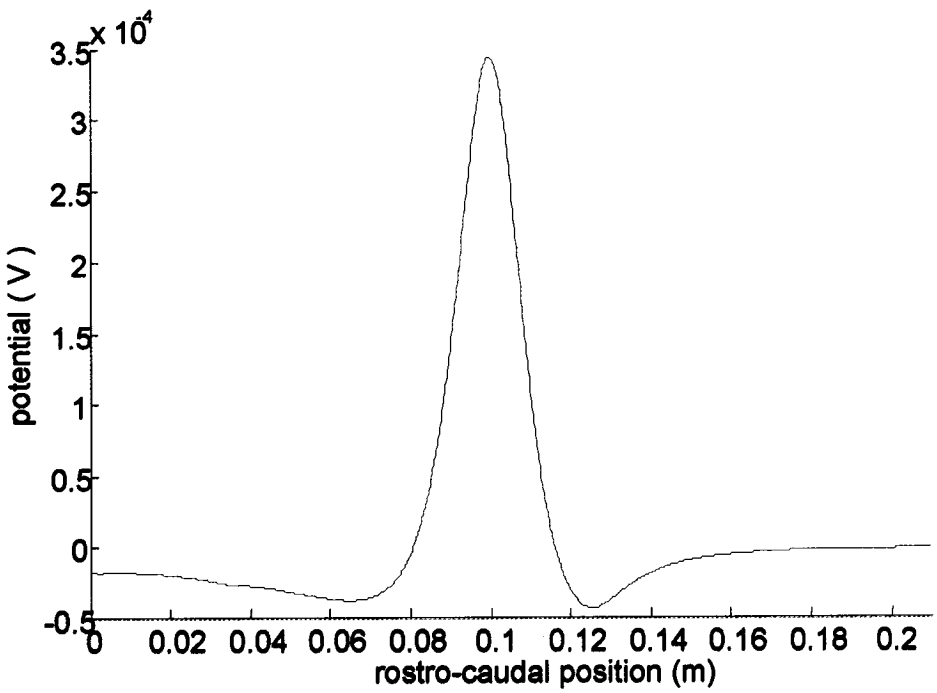

Figure 1.2: Effect of an insulator on the weakly electric fish's electric field. (A) An insulating object (silicon disc with a conductivity of 1 pS/m) diverts current lines (black lines) away from it (compare to unaltered current lines below the fish). A conductive object would draw current lines towards it (not shown). Bluish lines show the equipotentials and once again illustrate the fish's elongated dipolar field. Current lines and equipotentials inside the fish were removed for clarity. This image was produced using the two-dimensional finite element fish model developed within this thesis (see Chapters 2 and 3 for details). (B) Electric image produced by insulating object shown in (A). This image is calculated as the differences in transdermal potential in the presence and absence of an object, all along the fish's body (fish length of 21 cm).

Electric images therefore serve as the weakly electric fish's interface with the outside world. It is believed that these fish can judge a nearby object's conductivity, size and location based on the properties of the electric image ([7, 30, 36]; the word *nearby* is used since it is believed that the range of electrolocation for these fish is less than a body's length away [25]). It would have been nearly impossible, however, to form many of these predictions using only experimental data. Indeed, one can easily imagine how difficult it would be to accurately measure the transdermal potential at every point on the fish's two-dimensional surface, and for all moments in time (with one of the electrodes precisely inserted in the fish's skin). Researchers have therefore resorted to studying the weakly electric fish and its electric field by using different types of analytical, semi-analytical and numerical models. In fact, a new numerical model has been developed in this thesis in order to better understand the weakly electric fish's electroperceptual world. The next section will briefly review some of the previous models of the weakly electric fish to which our new model can be compared.

1.2 Previous Weakly Electric Fish Models

Over the years, there has been a wide array of weakly electric fish models. The first goal of all these models has been to reliably mimic the electric field potential which surrounds these fish. In particular, the majority of these models mimic a single phase of the EOD cycle, one that is fairly dipolar (in actuality, the equipotentials near the fish's head are elongated compared to the ones near the tail: see Figure 1.1B). As such, the first models of weakly electric fish [13, 24] consisted of simple dipoles. While the simulated fields obtained by these models were obviously dipolar, they were not elongated.

Heiligenberg in 1975 [16] improved on these models by using a finite difference method[3] model which solved Laplace's equation[4]. Using this numerical model, Heiligenberg was able to mimic the elongated rostral (headward) pole. He also made the first model-based predictions, such as what the fish's (unmeasured) body resistance should be. This was accomplished by analysing the effects of body conductivity on the simulated electric field. Heiligenberg was also the first to simulate electric images (as transdermal potentials), showing that the amplitude of these images decreases as an object is moved away (laterally). His study also suggested (via simulations) that the natural "tail bending" behaviour exhibited by weakly electric fish is possibly used in order to enhance sensory information contained in the fish's electric images.

The first finite element model was made by Hoshimiya *et al.* [20] in 1980. This model was two-dimensional and solved Laplace's equation. The electric fish's electric organ was modeled using two point charges of opposing polarity and the fish's body was

[3] This numerical method, as well as the finite element method and boundary element method are explained in Chapter 2.

[4] Laplace's equation, as well as Poisson's equation are explained in Chapter 2.

modeled as an ellipse-like structure. This is the first model to explicitly include a skin layer, as Heiligenberg's skin representation consisted of differences in a regular (orthogonal) grid. It should be noted, however, that the thickness of this skin layer was vastly overestimated (about 25-50 times too big). This study reports that the skin resistance must be approximately ten times higher at the head than at the tail in order to reproduce the fish's rostrally-leaning zero-potential line (later measurements have shown large differences in rostrocaudal skin conductivity[5] [1, 26]). Hoshimiya *et al.* also showed that conductive and insulating objects create electric images of differing polarity and that, furthermore, the electric image's peak changes locations as an object is moved rostrocaudally (see Figure 1.2B for an example of an electric image).

In 1983, Bacher [4] presented an analytical model of weakly electric fish that consisted of two line charges of differing lengths (in order to reproduce the elongated dipole field). Chen *et al.* [10] later did a similar model based on Bacher's model using a series of point charges instead of the two line charges. Such analytical models, however, are limited to studying the effects of disc-like objects (or spherical objects in three dimensions). This is because the analytical perturbations that such objects produce can be calculated relatively easily and hence, transdermal potentials (electric images) can be simulated using only the potential at the skin's exterior. Many researchers have indeed used this type of modeling approach. Rasnow [30] outlined a series of comprehensive electrolocation rules based on electric images that were calculated as perturbations of the measured skin potential (semi-analytical model). These models are based on the

[5] An exact rostrocaudal profile of these skin conductivity measurements has not yet been presented.

assumption that the weakly electric fish can be treated as a perfect voltage divider, an assumption that was tested in Chapter 3 of this thesis.

Assad [1], as well as Rother *et al.* [33], use three-dimensional boundary element models in order to mimic the weakly electric fish's electric field[6]. These types of models have the advantage of allowing for three-dimensional representations, but are subject to disadvantages which are discussed in Chapter 3. After considering the pros and cons of the different types of models, a decision was reached to create a two-dimensional, finite element fish model. This model allows for a precise description of the fish's body and solutions can be obtained quickly and easily (see Chapters 2 and 3 for model details).

1.3 Scope of Thesis and Organisation

The main goal of this thesis was to better understand the electrosensory modality, especially in terms of how it relates to the fish's natural, yet relatively unknown [28] environment. Our approach focused on the fish's electric images, the electrosensory system's primary input.

In order to study these images, a computer-based model of the brown ghost knifefish (*Apteronotus leptorhynchus*) was developed. The tools that were used to create this model (numerical method, computer software, physics, etc.) are explained in Chapter 2 while the actual model is described in Chapter 3. The main results of this thesis are presented in Chapters 3, 4, and 5, two of which (Chapters 3 and 4) will be submitted as separate papers for publication. Specifically, Chapter 3 concentrates on the insights that were obtained on the fish's electric field production and electric images. Chapter 4

[6] Assad's model solves Poisson's equation rather than Laplace's equation. This is also the equation which has been solved in the model presented within this thesis.

analyses the accuracy of the electrosense and also studies signal extraction, as related to the fish's natural scanning behaviour. Stimulation paradigms currently used in neurophysiological studies to mimic conspecifics (other fish of the same species) are evaluated in Chapter 5, and several improvements are suggested. Finally, Chapter 6 summarizes the main results found in this thesis and discusses direction for future studies.

1.4 Statement of Contribution

This research project as a whole was suggested to me by Dr. André Longtin and Dr. John Lewis. However, the precise directions which this thesis took on were the result of many synergistic discussions between Dr. André Longtin, Dr. John Lewis and I. All numerical work included in this thesis was done by the author (except for Figure 1.1A which was provided by Ms. Ginette Hupé). All chapters of this thesis (including the two papers) were written by the author, with extensive proof reading on the parts of Dr. André Longtin and Dr. John Lewis.

Bibliography

[1] Assad, C. Electric field maps and boundary element simulations of electrolocation in weakly electric fish. Ph. D. thesis, California Institute of Technology, Pasadena, CA, 1997.

[2] Assad, C., Rasnow, B., and Stoddard, P. K. Electric organ discharges and electric images during electrolocation. *J. Exp. Biol.*, vol. 202, pp. 1185-93, 1999.

[3] Axel, R. The molecular logic of smell. *Sci Am*, vol. 273, pp. 154-159, 1995.

[4] Bacher, M. A new method for the simulation of electric fields, generated by electric fish, and their distorsions by objects. *Biol. Cybern.*, vol. 47, pp. 51-58, 1983.

[5] Bennett, M. V. L. Electric organs. In: *Fish Physiology.* (W. S. Hoar and D. J. Randall, eds.) vol. V, New York: Academic Press, 1971.

[6] Bennett, M. V. L. Electroreception. In: *Fish Physiology.* (W. S. Hoar and D. J. Randall, eds.) vol. V, New York: Academic Press, 1971.

[7] Caputi, A. A., Budelli, R., Grant, K., and Bell, C. C. The electric image in weakly electric fish: physical images of resistive objects in *Gnathonemus petersii*. *J. Exp. Biol.*, vol. 201, pp. 2115-2128, 1998.

[8] Carr, C. E. Neuroethology of electric fish. Principles of coding and processing sensory information. *BioScience*, vol. 40, pp. 259-267, 1990.

[9] Carr, C. E., Maler, L., and Sas, E. Peripheral organization and central projections of the electrosensory nerves in gymnotiform fish. *J. Comp. Neurol.*, vol. 211, pp. 139-153, 1982.

[10] Chen, L., House, J. L., Krahe, R., and Nelson, M. E. Modeling signal and background components of electrosensory scenes. *J. Comp. Physiol. A*, vol. 191, pp. 331-345, 2005.

[11] Crampton, W. G. R. Electric signal design and habitat preferences in a species rich assemblage of gymnotiform fishes from the Upper Amazon basin. *Anais da Academia Brasileira de Cięncias*, vol. 70, pp. 805-847, 1998.

[12] Graff, C., Kaminski, G., Gresty, M., and Ohlmann, T. Fish perform spatial pattern recognition and abstraction by exclusive use of active electrocation. *Curr. Biol.*, vol. 14, pp. 818-823, 2004.

[13] Granath, L. P., Erskine, F. T. I., Maccabee, B. S., and Sachs, H. G. Electric field measurements on a weakly electric fish. *Biophysik* , vol. 4, pp. 370-372, 1968.

[14] Granit, R. Physiology of vision. *Annual Review of Physiology*, vol. 12, pp. 485-502, 1950.

[15] Griffiths, T. D. and Warren, J. D. What is an auditory object? *Nat Rev Neurosci*, vol. 5, pp. 887-892, 2004.

[16] Heiligenberg, W. Theoretical and experimental approaches to spatial aspects of electrolocation. *J. Comp. Physiol.*, vol. 103, pp. 247-272, 1975.

[17] Heiligenberg, W. *Neural Nets in Electric Fish.* Cambridge, Mass.: MIT Press, 1991.

[18] Hopkins, C. D. Electric communication in fish. *Am. Sci.*, vol. 62, pp. 426-437, 1974.

[19] Hopkins, C. D. Temporal structure of non-propagated electric communication signals. *Brain Behav. Evol.*, vol. 28, pp. 43-59, 1986.

[20] Hoshimiya, N., Shogen , K., Matsuo, T., and Chichibu, S. The *Apteronotus* EOD field: waveform and EOD field simulation. *J. Comp. Physiol.*, vol. 135, pp. 283-290, 1980.

[21] Knudsen, E. I. Spatial aspects of the electric fields generated by weakly electric fish. *J. Comp. Physiol.*, vol. 99, pp. 103-118, 1975.

[22] Kung, C. A possible unifying principle for mechanosensation. *Nature*, vol. 436, pp. 647-654, 2005.

[23] Lissman, H. W. On the function and evolution of electric organs in fish. *J. Exp. Biol.*, vol. 35, pp. 156-191, 1958.

[24] Lissman, H. W. and Machin, K. E. The mechanism of object location in *Gymnarchus niloticus* and similar fish. *J. Exp. Biol.*, vol. 35, pp. 451-486,

1958.

[25] MacIver, M. A., Sharabash, N. M., and Nelson, M. E. Prey-capture behavior in gymnotid electric fish: motion analysis and effects of water conductivity. *J. Exp. Biol.*, vol. 204, pp. 543-557, 2001.

[26] Migliaro, A., Caputi, A. A., and Budelli, R. Theoretical analysis of pre-receptor image conditioning in weakly electric fish. *PLoS Comp. Biol.*, vol. 1, pp. e162005.

[27] Moller, P. *Electric Fishes: History and Behavior.* London: Chapman & Hall, 1995.

[28] Nelson, M. E. Target detection, image analysis and modeling. In: *Electroreception (Springer Handbook of Auditory Research)* (T. H. Bullock, C. D. Hopkins, A. N Popper, R. R. Fay, eds.) New York: Springer, 2005.

[29] Price, M. P., Lewin, G. R., McIlwrath, S. L., Cheng, C., Xie, J., Heppenstall, P. A., Stucky, C. L., Mannsfeldt, A. G., Brennan, T. J., Drummond, H. A., Qiao, J., Benson, C. J., Tarr, D. E., Hrstka, R. F., Yang, B., Williamson, R. A., and Welsh, M. J. The mammalian sodium channel BNC1 is required for normal touch sensation. *Nature*, vol. 407, pp. 1007-1011, 2000.

[30] Rasnow, B. The effects of simple objects on the electric field of *Apteronotus*. *J. Comp. Physiol. A*, vol. 178, pp. 397-411, 1996.

[31] Rasnow, B., Assad, C., and Bower, J. M. Phase and amplitude maps of the electric organ discharge of the weakly electric fish, *Apteronotus leptorhynchus*. *J. Comp. Physiol. A*, vol. 172, pp. 481-491, 1993.

[32] Rasnow, B. and Bower, J. M. The electric organ discharges of the gymnotiform fishes: *I. Apteronotus leptorhynchus*. *J. Comp. Physiol. A*, vol. 178, pp. 383-396, 1996.

[33] Rother, D., Migliaro, A., Canetti, R., Gomez, L., Caputi, A., and Budelli, R. Electric images of two low resistance objects in weakly electric fish. *Biosystems*, vol. 71, pp. 171-179, 2003.

[34] Scott, K. Taste recognition: food for thought. *Neuron*, vol. 48, pp. 455-464, 2005.

[35] Toerring, M. J. and Belbenoit, P. Motor programmes and electroreception in Mormyrid fish. *Behav. Ecol. Sociobiol.*, vol. 4, pp. 369-379, 1979.

[36] von der Emde, G., Schwarz, S., Gomez, L., Budelli, R., and Grant, K. Electric fish measure distance in the dark. *Nature*, vol. 395, pp. 890-894, 1998.

[37] Weber, E. H. *The Sense of Touch* (translated by H. E. Ross and D. J. Murray; Original work published 1834). London: Academic Press, 1978.

CHAPTER 2

METHODS

2.1 Introduction

As seen in Chapter 1, researchers have modeled weakly electric fish using a variety of analytical, semi-analytical and numerical methods. These models are necessary given the flexibility they allow in studying these fish. Numerical methods in particular are becoming increasingly popular given the unparalleled processing speed of modern computers. This chapter briefly explains the finite element method (FEM) and the FEM software, COMSOL Multiphysics (COMSOL AB; formerly known as FEMLAB), which was used to create the two-dimensional weakly electric fish model described in this thesis. This chapter also explains the physics underlying the fish model, as well as other technical details.

2.2 Finite Element Method

The problem at hand is to solve a given partial differential equation (PDE), subject to initial conditions and specific boundary conditions. In order to solve this problem numerically, one must first "cut" the given geometry into smaller discrete units (called *elements* in the FEM terminology). The ensemble of these units is called a *mesh* or *grid*. The PDE is then expressed as a discrete equation. Starting from the initial conditions, the final solution can then be found, for example, through an iterative scheme. With a regular grid, this is basically how the finite difference method (FDM) works.

However, with a regular grid, this method is constrained and cannot deal with complex geometries.

The FEM, which can be used to solve problems with complex geometries, solves the initial PDE differently using a specific trick. Let's say the initial PDE f is given by:

$$f = Lu \tag{2.1}$$

where L is a partial differential linear operator that acts on the solution variable u (space and time dependencies will depend on the exact PDE considered). Instead of directly solving this equation, the FEM solves the equation

$$(f \bullet q) = (Lu \bullet q) \tag{2.2}$$

where the $\bullet$ sign signifies the dot product and the test function q is a combination of piecewise polynomials T_1, T_2, T_3, ... These polynomials, which depend solely on the space coordinates, are known as *basis* or *form functions* (can be thought of as weighting functions). The simplest type of basis function is one for which T_i equals one at the i^{th} *node* (or *degree of freedom - DOF*) and equals zero at all other nodes. The solution variable is then approximated by a linear combination of these basis functions:

$$u = u_1 T_1 + u_2 T_2 + u_3 T_3 + ... \tag{2.3}$$

and used for solving the matrix equation (2.2). This is the Galerkin method. There are as many equations as there are DOFs (typical simulations done in this thesis had nearly 100 000 DOFs). Therefore, solving this matrix problem can be quite cumbersome, hence the usefulness of software such as COMSOL Multiphysics (See section 2.3).

A simple intuitive example, as described in Reddy (1984), shall now be shown in order to illustrate the concept of this method (Figure 2.1). Let's say that one wants to measure the circumference of a circle of radius R (Figure 2.1A), without having recourse

to the equation $circumference = 2\pi R$. One way to proceed would be to approximate the circle's circumference with a number of straight lines; the elements (Figure 2.1B). The sum of these lines gives an approximation of the circumference (Figures 2.1 C and 2.1D). As shown in Figure 2.1E, this approximation becomes more and more valid as the number of elements increases. The points which delimit elements are the nodes. In this example, linear elements were used, but, as one might expect, a solution of a given precision would have been attained more quickly using curved elements. Through this simple illustration, one can understand the usefulness of the FEM when it comes to dealing with complex geometries.

For the two-dimensional model created in this thesis, the elements are triangles (called Lagrange-quadratic elements). These element shapes allow for an irregular grid, which consequently allows for a study of irregularly-shaped geometries. The solver used in COMSOL Multiphysics in order to solve the matrix (2.2) is called the "UMFPACK Direct solver". This solver is a set of routines that solves unsymmetric sparse matrices using the Unsymmetric MultiFrontal method and the direct sparse LU factorisation method.

The boundary element method (BEM) is similar to the FEM, except that only the boundaries need to be discretized, not all subdomains. Advantages and disadvantages of both methods are discussed in Chapter 3.

This is a brief outline of the numerical methods used in this thesis. For more details, the reader can consult one of the many books on the subject (see e.g. [5], [6] or [7]).

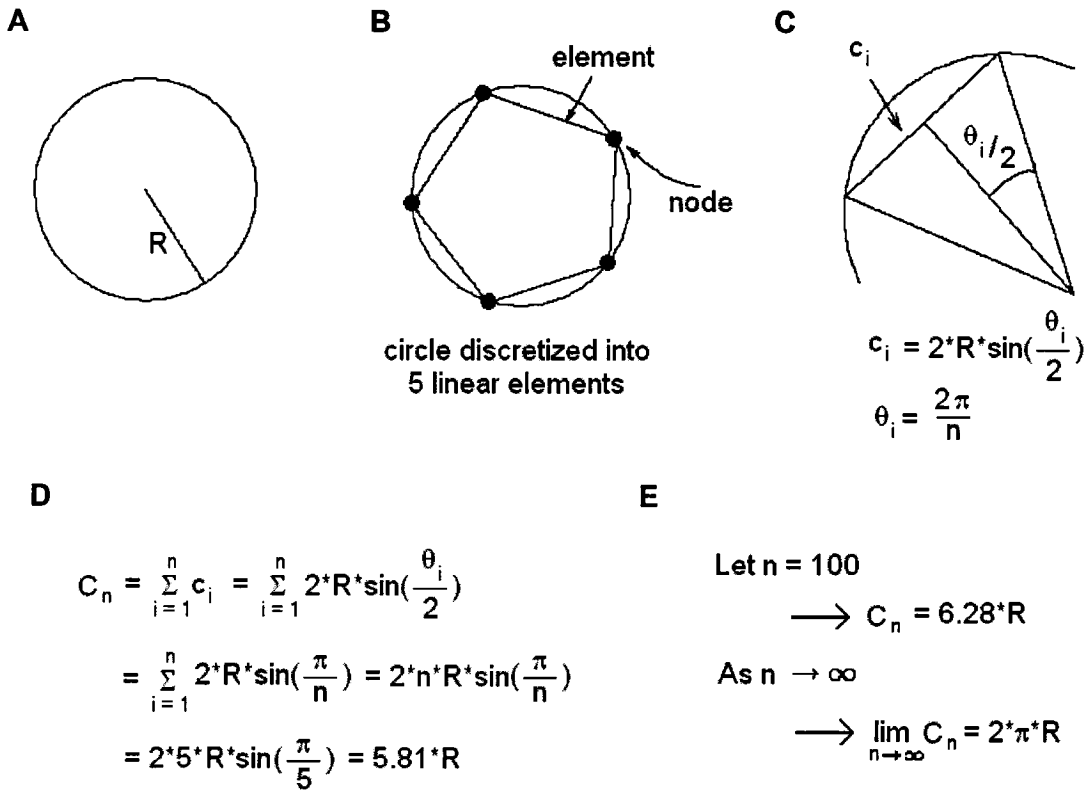

Figure 2.1: Simple intuitive illustration of the finite element method: calculating a circle's circumference. (A) Circle of radius R. (B) Circle discretized into 5 linear elements; as a result, there are 5 nodes. These elements are the simplest types of elements. (C) c_i denotes the length of the i^{th} linear element and θ_i denotes the angle of half the i^{th} element with respect to the circle's center point. (D) The equation for the circumference C as a function of the number of elements n. The equation is solved for 5 elements and one can see that the solution is close to the expected one, $2*\pi*R$. (E) The estimate converges to the solution as n increases.

2.3 COMSOL Multiphysics

2.3.1 Introduction

COMSOL Multiphysics is software that lets the user solve various problems using the finite element method (FEM). The user can either define his or her own PDEs or can choose from one of the several pre-defined PDE application modes (e.g. the "Incompressible Navier-Stokes" application mode or the "Conductive Media DC" application mode). Once a choice has been made, the user must then draw the geometry of the given problem (e.g. create a composite object formed of circles, rectangles, etc. using the computer-aided design tools). Afterwards, the properties must be specified on the various points, boundaries, and subdomains of the geometry (subdomains are regions enclosed within boundaries and exterior to points, if present; see Figure 2.2A). In our case (Conductive Media DC mode; see section 2.3.2 for details), the boundaries can be grounded, set to a specific potential or be electrically isolative (among other conditions). In the final stage, a mesh is created and the problem is solved. The user can choose between several iterative and direct solvers which are in effect different methods to solve the matrix form of the relevant PDE, equation (2.2). Once the problem is solved, the user can do a number of operations in the postprocessing mode of COMSOL Multiphysics in order to view the solution (See Figure 2.2).

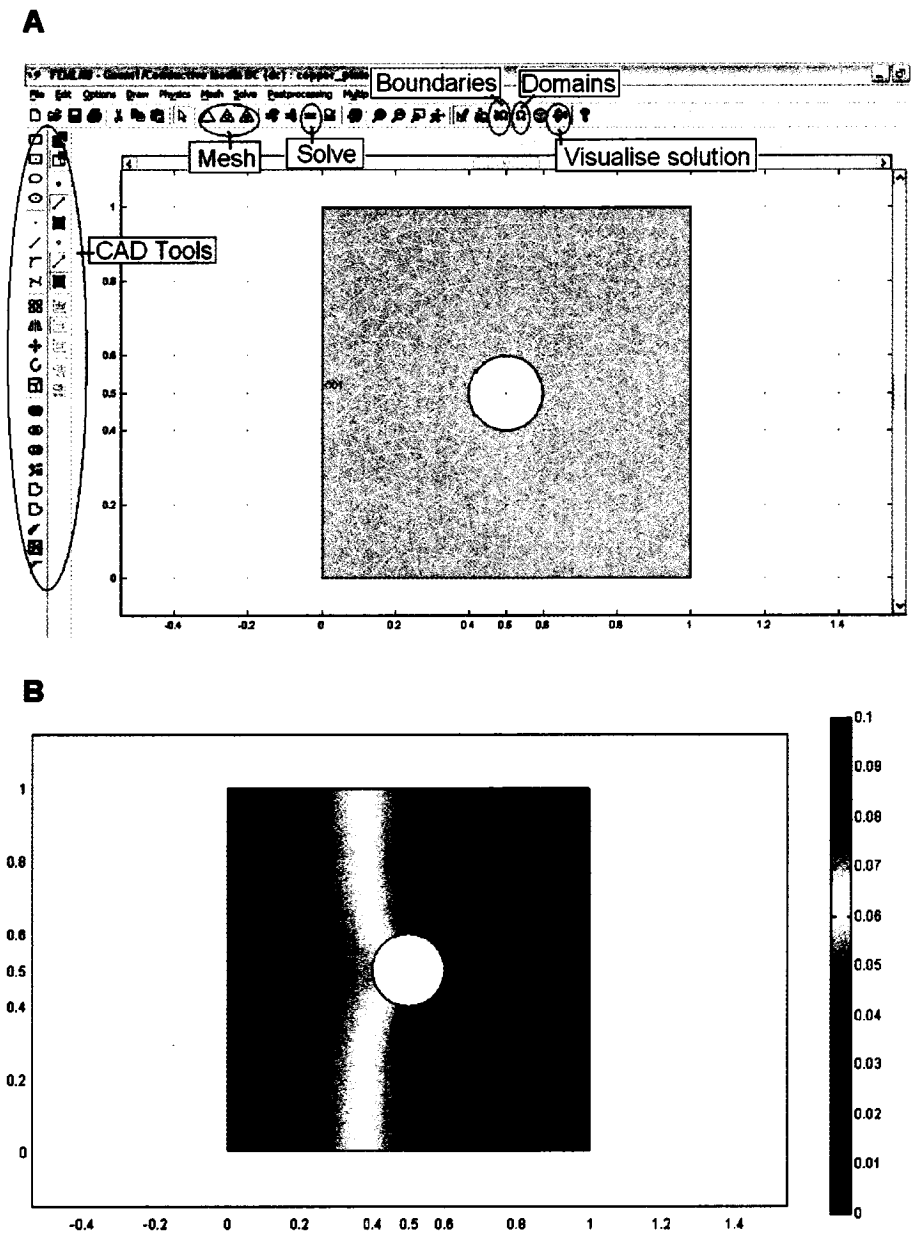

Figure 2.2: Example of the COMSOL Multiphysics software: calculation of a copper plate's potential. (A) Screenshot of the COMSOL Multiphysics graphical interface, including the copper plate geometry. The computer-aided design (CAD) tools can be found at the left while all other buttons, including the ones that create the mesh (shown as grey triangles), calculate the solution, etc. can be found at the top of the interface. (B) Potential distribution on the copper plate (values are given by the color-scale on the right-hand side - in Volts). A potential of 0.1 V was initially set on the left side of the plate while the right side was set to 0V (ground). The resulting potential profile gradually decreases from 0.1 to 0 V, as expected.

2.3.2 Example

In order to illustrate how COMSOL Multiphysics works, a simple example is now provided. Let's say, e.g., that a potential difference is applied between the left and right sides of a copper plate which has a hole in its middle (See Figure 2.2A). A logical question to ask would then be: "What does the potential profile look like on this copper plate?" With COMSOL Multiphysics, this question can be answered quickly by following a few simple steps.

First, the pre-defined (two-dimensional) "Conductive Media DC" application mode is selected. This mode's PDE is Poisson's equation for conductive materials:

$$-\nabla \bullet \left(\sigma \nabla \Phi - \vec{J}^{e}\right) = Q_j \tag{2.4}$$

where σ is the conductivity (in Siemens per meter), Φ is the potential (in Volts), $\vec{J}^{e}$ is the external current density (in Amperes per square meters), and Q_j is the current source (in Amperes per cubic meters[1]; all variables depend on space only: this is considered a static problem). In fact, this is the application mode used for the weakly electric fish models presented in this thesis.

The second step is to represent the problem geometrically. Figure 2.2 shows the geometry which was created and gives an idea of what the COMSOL Multiphysics graphical interface looks like. To create this composite object, a circle was subtracted from a square, using the CAD tools found at the left-hand side of the screen (see Figure 2.2A). This is now a singular object which has one subdomain (in red) and boundaries on the "inside" and on the "outside" of this subdomain.

[1] The units are in A/m^3 even though the simulation is done in two dimensions. This is because COMSOL Multiphysics treats this problem as a three-dimensional case in which the thickness of the model is 1 m in the z-direction. In this manner, the model is "thick" enough to neglect the variation in the z-direction.

The subdomain and boundary properties can then be specified. The conductivity of the subdomain is set to copper's value of 5.998×10^7 S/m (COMSOL Multiphysics uses SI units) while all boundaries, except for the leftmost and rightmost sides of the plate, are set as insulating boundaries. The electric potentials of these sides are set to 0.1 and 0 V (ground), respectively.

Next the mesh is generated and the solution is computed. The resulting potential profile on this copper plate, along with an appropriate color scale, is shown on Figure 2.2B. The potential gradually decreases from 0.1 to 0 V, from left to right, as expected.

2.3.3 Calibration

In order to evaluate the accuracy of COMSOL Multiphysics, the analytical and simulated solutions of a simplistic problem were compared. The problem of a line charge of charge density ρ in the center of a grounded tube of radius r_0 was studied (r_0 was set to 1 for our calibration). While this is in fact a three-dimensional problem, the potential will be the same all along the tube length z (for a given r, θ set of polar coordinates); hence, a two-dimensional cross-section was considered. The solution, easily found using Gauss's theorem, is given by (in SI units):

$$\Phi(r) = -\frac{\rho}{4\pi\varepsilon_0} \ln\left(\frac{r^2}{r_0^2}\right) \tag{2.5}$$

where Φ is the potential, ε_0 is the permittivity of free space and r is the radial variable. The simulated solution was found using COMSOL Multiphysics and the potential for 100 points between $r = 0.1$ and $r = 0.99$ m (along the arbitrary direction $\theta = 0$) was extracted and compared to the analytical potentials (given by equation 2.5) at these

points. A standard root mean square (RMS) error was then calculated using a MATLAB (The MathWorks, Inc.) subroutine. Since the COMSOL Multiphysics user can select the degree of precision for the given mesh, this percent error was calculated for the two modes used exclusively during the fish model simulations (computation time increases with mesh precision and thus constrains the choice of mesh size). All simulations where performed on an IBM computer with a 3.2 GHz Intel Xeon processor. Table 1 shows the RMS % errors (less than 0.5%) as well as the number of degrees of freedom (DOF) and of mesh elements used for each mesh (named "normal" and "coarse"; for this simulation, the "normal" mode had 772 elements while the "coarse" mode had 308). This shows that COMSOL Multiphysics is a very accurate FEM solver, at least for this simple geometry. The geometries used for the fish models are much more complicated and, as a result, no analytical solutions exist. However, given the extreme precision shown here, one can assume that the results will still be very reliable.

Type of mesh	# of DOF	# of mesh elements	RMS error (%)
Normal	1593	772	0.27
Coarse	649	308	0.49

Table 2.1: FEMLAB calibration. RMS error found between the simulated (found using COMSOL Multiphysics) and analytical potentials for a line charge centered in a unit-radius grounded cylindrical tube (see text for details). Calculation is based on 100 points ranging from a value of 0.1 to 0.99 in the radial direction $\theta = 0$. The RMS error (in %) as well as the number of degrees of freedom (DOF) and elements are shown for the two most commonly used mesh settings, i.e. the "normal" and "coarse" meshes (the "normal" setting has more elements and is therefore finer than the "coarse" setting).

2.4 Model Considerations

2.4.1 Field Measurements

The data which was used to calibrate the fish model presented herein was obtained from measurements made by Christopher Assad at the California Institute of Technology on August 24th, 1993 [1]. The electric field he mapped of the 21 cm long female *A. leptorhynchus* had a fundamental EOD frequency of 810 Hz (at the start time of the experiment). The conductivity of the water was 210 μS, its temperature was 29°C and its pH was 6.5.

The potential was measured at 361 irregularly-spaced node locations (accurate to within 500 microns) in the fish's horizontal midplane (view from the top). These nodes, mainly located near the fish, can be seen in Figure 2.3A along with the fish's body contour. The potential at each node was measured for 25 distinct EOD phases, spanning a complete EOD cycle (~ 1.2 milliseconds). The phase for which we calibrated our data is phase #9 and can be seen in Chapter 3, Figure 3.3A (top). In order to calibrate our data, the potentials were calculated for a regular grid by interpolating the potential at the 361 node points (using MATLAB). This regular grid had 248 nodes in the "x" axis, 100 nodes in the "y" axis" (24800 total nodes), and spanned the same space as shown in Figure 2.3A. Figure 2.3B shows how the nodes in Figure 2.3A were re-sampled in order to remove biases produced by over-sampling in the fish's tail region (36 nodes removed; see Chapter 3 for more details). For detailed information regarding the precise measuring techniques used in order to experimentally obtain the weakly electric fish's potential "map", the reader is encouraged to consult Christopher Assad's thesis [1].

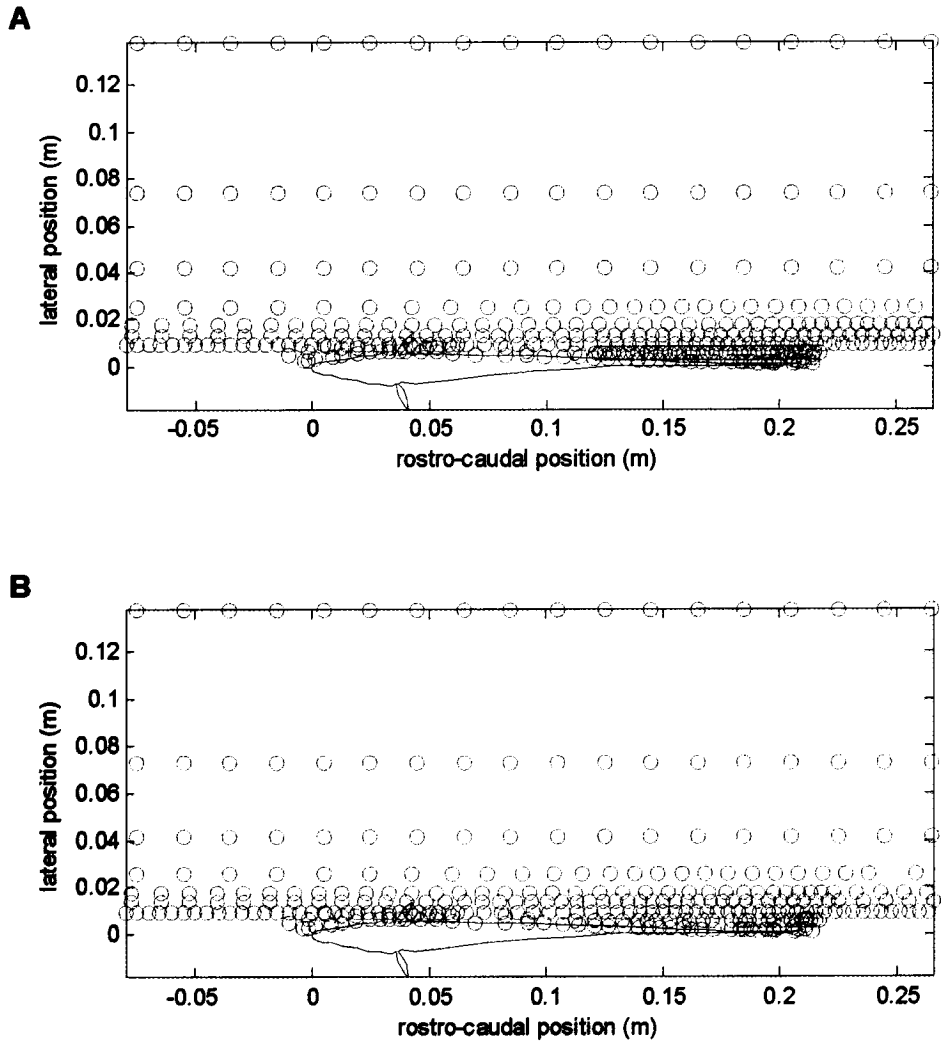

Figure 2.3: Fish body contour and measurement nodes. (A) Un-weighted node locations and body contour mapped by Assad (361 total measurements nodes and 63 total body nodes). (B) Weighted node locations. 36 nodes in total were removed, mostly in the tail region, in order to remove any bias create by the original uneven sampling in (A).

2.4.2 Weakly Electric Fish Physics

Since the fish studied in this thesis is electric in nature, Maxwell's four electromagnetic equations must be used as a starting point in order to describe the physics

of this problem. These are the four fundamental equations which govern electromagnetism. In the case of weakly electric fish, the magnetic field is negligible due to the fish's relatively low frequency [2]. Therefore, the equation of interest is Gauss's law. This law states that the divergence of an electric field $\vec{E}$ in a volume enclosed by a closed surface is proportional to the total charge enclosed within this surface [3]. The differential form of this equation is given by:

$$\vec{\nabla} \bullet \varepsilon \vec{E} = \rho \tag{2.6}$$

where ε is the permittivity of the medium and ρ is the charge density. Since the magnetic field is negligible, the problem at hand is said to be an *electrostatics* one, meaning that the electric field generated is the one that is associated with a static distribution of charge. Under these conditions, the electric field can be approximated as the negative gradient of the scalar potential Φ, $E = -\nabla\Phi$ [3], which leads to Poisson's equation:

$$\nabla \bullet (\varepsilon \nabla \Phi) = -\rho \tag{2.7}.$$

The special case when $\rho = 0$ is called Laplace's equation.

Assad (1997, Chapter 4) has shown that, for the species of weakly electric fish studied in this thesis, the displacement current is negligible compared to the conduction current, meaning that the fish can be treated as a good conductor. Hence, the main equation which we will use for our simulations can be expressed as:

$$\nabla \bullet (\sigma \nabla \Phi) = -Q \tag{2.8}$$

where Q is the current source density (in Amperes per cubic meters: see note on page 21) and σ is the conductivity (in Siemens per meter). All parameters can be defined for

all points in space.

Although the term "electrostatic" is used, a more proper term to use is *quasistatic*, since the changing electric field that surrounds the fish's body for different phases of the EOD cycle can be modeled by a changing electric organ current density (solved for these different phases). This type of modeling can be considered accurate here due to the very small dielectric relaxation time in water due to the fish's relatively low frequency electric discharge and predominately ohmic skin and body [1].

In essence, therefore, one may say that the problem at hand is a quasistatic boundary-value problem. In order to solve this problem, all that needs to be specified is the current source density and conductivity on all domains (initial conditions) and the types of boundary conditions. Since our model consists mainly of three components, a fish, a grounding electrode and an aquarium (Fig. 3.1A), we have three types of boundary conditions (see Chapter 3 for more details). The boundary condition for the grounding electrode is that V = 0 (must be set as ground in order to act as a reference for other potential values). The aquarium is set as an insulating boundary since current cannot pass through. This condition is expressed as $\vec{n} \bullet \vec{J} = 0$, i.e. there can be no normal component of the current density $\vec{J}$ at the boundary. At the interface of two different media, we have the following boundary conditions for the electric field $\vec{E}$ and the electric displacement $\vec{D}$ [4]:

$$\vec{n} \times (\vec{E}_2 - \vec{E}_1) = 0 \tag{2.9}$$

$$\vec{n} \bullet (\vec{D}_2 - \vec{D}_1) = \sigma_s \tag{2.10}$$

where $\vec{n}$ is the normal vector, σ_s is the free surface charge density and the subscripts 2

and 1 denote the two different media. These conditions say that the tangential component of the electric field is continuous while the normal component of the displacement is discontinuous. Taking the derivative of (2.10) with respect to time we have:

$$\vec{n} \bullet (\frac{\partial \vec{D}_2}{\partial t} - \frac{\vec{D}_1}{\partial t}) = \frac{\partial \sigma_s}{\partial t} \qquad (2.11).$$

Furthermore, Ampère's law states that:

$$\frac{\partial \vec{D}}{\partial t} = \nabla \times \vec{H} - \vec{J} = -\vec{J} \qquad (2.12)$$

where $\vec{H}$ is the magnetic field and is considered as negligible in our system. Therefore, combining equations (2.11) and (2.12), we have:

$$\vec{n} \bullet (\vec{J}_2 - \vec{J}_1) = -\frac{\partial \sigma_s}{\partial t} \qquad (2.13).$$

Since we are considering the quasistatic case, we have:

$$\vec{n} \bullet (\vec{J}_2 - \vec{J}_1) = 0 \qquad (2.14).$$

This is the boundary condition which has been applied to all interior boundaries.

The Conductive Media DC application mode used in COMSOL Multiphysics in order to simulate the weakly electric fish's field solves equation 2.8 (see equation 2.4; the external current density is zero in this case). In our study, this was done in the two-dimensional space. The implications of using a two-dimensional model instead of a three-dimensional one are discussed in Chapters 3 and 6.

2.4.3 General Information Concerning the Weakly Electric Fish Model

Although the weakly electric fish model developed in this thesis (see Chapter 3) is designed as a tool to explore the effects of various objects (including conspecifics) on the fish's electric images (see Chapters 3, 4 and 5), much effort went into developing this instrument. Indeed, this model is a result of much research and of much trial and error. For instance, a lot of research initially went into deciding what software was to be used in order to create the fish model. Three options, as determined in conjunction with my supervisors, stood out: a) build on the analytical model developed in Bacher [2], b) use the High Performance Computing Virtual Laboratory (HPCVL) of which the University of Ottawa is a member of or c) use the COMSOL Multiphysics software (then called FEMLAB). The latter was chosen because of its ease of use and flexibility in solving problems with complex geometries.

Once the software was chosen, many different models were tested (e.g. modeling the fish body as an ellipse, modeling the electric organ as two small discs, etc.) These models were later abandoned, however, once Assad's data was obtained and the constraining of a more realistic model was possible (using the fish's measured body contour). Even after this was accomplished, many decisions and much work remained. Should one use the fish's slightly asymmetric body profile as in Assad's experiments or create a symmetric one? How to model the "physics" of the electric fish and which application mode to choose? Which parameters of the fish's body to vary and how? Also, how to calibrate our model with the experimental data? These questions are all answered in Chapter 3 where the model is described in detail. The main point to remember,

however, is that the final model created and used throughout this thesis was not obtained using a turnkey solution, but rather, was the result of much experimentation.

Bibliography

[1] Assad, C. Electric field maps and boundary element simulations of electrolocation in weakly electric fish. Ph. D. thesis, California Institute of Technology, Pasadena, CA, 1997.

[2] Bacher, M. A new method for the simulation of electric fields, generated by electric fish, and their distorsions by objects. *Biol. Cybern.*, vol. 47, pp. 51-58, 1983.

[3] Good, R. H. *Classical Electromagnetism*. Orlando, FL: Saunders College Publishing, 1999.

[4] Jackson, J. D. *Classical Electrodynamics* (3rd edition). New York, NY: John Wiley & Sons, 1999.

[5] Reddy, J. N. *An Introduction to the Finite Element Method*. New York: McGraw-Hill, 1984.

[6] Strang, G. and Fix, G. J. *An Analysis of the Finite Element Method*. Englewood Cliffs, N.J.: Prentice-Hall, Inc., 1973.

[7] Yamashita, E. *Analysis Methods for Electromagnetic Wave Problems*. Boston: Artech House, 1990.

CHAPTER 3

ARTICLE I

Modeling the electric field of weakly electric fish.

D. Babineau, A. Longtin and J. E. Lewis

Submitted to the Journal of Experimental Biology.

Modeling the electric field of weakly electric fish

David Babineau[1], André Longtin[1] and John E. Lewis[2,*]

[1]*Department of Physics, University of Ottawa, Ottawa, Ontario K1N 6N5, Canada and* [2]*Department of Biology, University of Ottawa, Ottawa, Ontario K1N 6N5, Canada*

*Author for correspondence (email: jlewis@uottawa.ca)

Summary

Weakly electric fish characterize the environment in which they live by sensing distortions in their self-generated electric field. These distortions result in electric images that form across their skin. In order to better understand electric field generation and image formation in one particular species of electric fish, *Apteronotus leptorhynchus*, we have developed three different numerical models of a two-dimensional cross-section of the fish's body and its surroundings. One of these models mimics the real contour of the fish; two other geometrically simple models allow for an independent study of the effects of the fish's body geometry and conductivity on electric field and image formation. Using these models, we show that the fish's tapered body shape is mainly responsible for the smooth, uniform field in the rostral region, where most electroreceptors are located. The fish's narrowing body geometry is also responsible for the relatively large electric potential in the caudal region. Numerical tests also confirm the previous hypothesis that the electric fish acts approximately like an ideal voltage divider; this is true especially for the tail region. Next, we calculate electric images produced by simple objects and find

they vary according to the current density profile assigned to the fish's electric organ. This explains some of the qualitative differences previously reported for different modeling approaches. The variation of the electric image's shape as a function of different object locations is explained in terms of the fish's geometrical and electrical parameters. We also discuss novel cues for determining an object's rostro-caudal location and lateral distance using these electric images.

Introduction

In order to extract relevant features from the environment in which they live, animals use both active and passive sensing mechanisms. For species that use an active sensing mechanism, the acquisition of sensory information greatly depends on the efferent signal produced, which can be sensitive to environmental influences. Weakly electric fish detect objects and communicate with conspecifics through a unique modality, the active electric sense. This sense relies on an electric organ discharge (EOD) emitted from the fish's electric organ (EO). The EOD can either be continuous and quasi-sinusoidal ("wave-type" species), or discrete and pulse-like ("pulse-type" species). The species studied in this paper, *A. leptorhynchus*, is a wave-type species with an EOD frequency of approximately 1 kHz. The electric field time course generated by this fish is complex with tri-phasic regions (local waveforms that have three phases, instead of two as in Fig. 1.1A in Chapter 1) close to the skin, but becomes approximately dipolar further away (Knudsen, 1975; Assad *et al.*, 1999). Objects whose electrical properties differ from those of the surrounding water perturb the fish's electric field (Lissman and Machin,

1958) and are sensed by specialized receptors located within the fish's epidermis. Many studies have shown that these electroreceptors respond to transdermal potential differences rather than to transdermal current (e.g. Bennett, 1971; Migliaro *et al.*, 2005). The rostro-caudal, dorso-ventral profile of the transdermal potential differences is commonly referred to as the "electric image". Because these images are the primary source of electrosensory input, a detailed knowledge of the electric field and image formation is required in order to understand the neural mechanisms of electrosensory information processing.

In recent years, different modeling techniques have been used to characterize electric images under various natural scenarios. Two- and three-dimensional numerical and analytical models have been developed, each with its specific advantages and disadvantages. Analytical models (e.g. Bacher, 1983; Chen *et al.*, 2005), while being computationally fast and accurate in some cases, are limited to the study of simplified object geometries and also don't allow for a thorough study of the effects of the fish's body parameters. Numerical models (e.g. Hoshimiya *et al.*, 1980; Assad, 1997; Rother *et al.*, 2003) can mimic the fish's body in a more realistic way, yet are considered more computationally time-demanding. The two main methods used in numerical modeling are the finite element method (FEM) and the boundary element method (BEM). The BEM is advantageous because only the solution at the boundaries is necessary (e.g. at the fish-water interface), therefore reducing the number of calculations and allowing for three-dimensional models (Assad, 1997; Rother *et al.*, 2003). Three-dimensional FEM models are currently not feasible in general due to the large number of elements required to accurately represent, for example, the crucial thin skin layer. On the other hand, the BEM

requires additional calculations to find potentials on non-boundary regions and is harder to implement than the FEM (e.g. boundary integrals are more difficult to evaluate and not all linear problems can be treated; Yamashita, 1990; Assad, 1997).

The goal of this paper was to study the fish in a realistic and accurate manner, using a fast and easily-implementable model. Taking advantage of improved computational power and software, a realistic two-dimensional FEM model, which is both computationally fast and easy to implement, was created. In addition to the realistic model created, two geometrically simple models were created in order to independently study the effects of different fish body geometries and electrical properties for the first time. Using the three distinct models, an analysis of the fish's mid-planar field (view from above) and of the electric images caused by different object sizes and locations is discussed. This study complements other recent studies which have begun to characterize the fish's electric field and electric image formation using different approaches (Caputi and Budelli, 1995; Caputi *et al.*, 1998; Rother *et al.*, 2003; Migliaro *et al.*, 2005; Chen *et al.*, 2005). In addition, our approach allows for future modeling efforts involving realistic electrosensory landscapes.

Materials and methods

Electric field modeling

The two-dimensional, horizontal midplane electric field potential of *A. leptorhynchus* was modeled for a single phase (head-positive). As in previous studies

(Rasnow *et al.*, 1989; Assad, 1997), the problem was treated as an electrostatics boundary-value problem, governed by Poisson's equation,

$$\nabla \bullet \sigma \nabla \Phi = -j \tag{3.1}$$

where Φ is the potential (in Volts), j is the current source density (in Amperes per cubic meter) and σ is the conductivity (in Siemens per meter; each defined for all points in the two-dimensional plane). This equation was solved using finite element method (FEM) software, COMSOL Multiphysics (formerly known as FEMLAB) on an IBM computer with a 3.2 GHz Intel Xeon processor. The current source density units are in A/m^3 because COMSOL Multiphysics treats the problem as a three-dimensional problem in which the model has a 1 m thickness in the z-direction. In this manner, the model is "thick" enough to neglect variations in the z-direction (problem can be solved in two dimensions; however, COMSOL chooses to solve it this way). Second-order Lagrange elements (triangles) were used in the finite element mesh. We chose a pre-defined mesh mode ("normal" mode) which automatically selected element sizes based on the size of the objects located within the geometry. This mode typically produced meshes with ~ 90 000 elements. In order to calibrate the software used, we studied a simple problem whose analytical solution is known: a line charge in the middle of a grounded tube. We found an RMS error of 0.27% (see Chapter 2). This shows that this software is very accurate.

Our studies involve three different fish geometries: one morphologically accurate model (referred to as the "fish" model) and two greatly simplified models (referred to as the "taper" and "box" models; see later for description). Each model is enclosed in a 70 X 70 cm^2 aquarium, which also holds grounding and reference electrodes (Fig. 3.1A). The size, location and conductivity of these components correspond to those found in the

experimental setup of Assad (1997), with whose experimental data we calibrated our fish model.

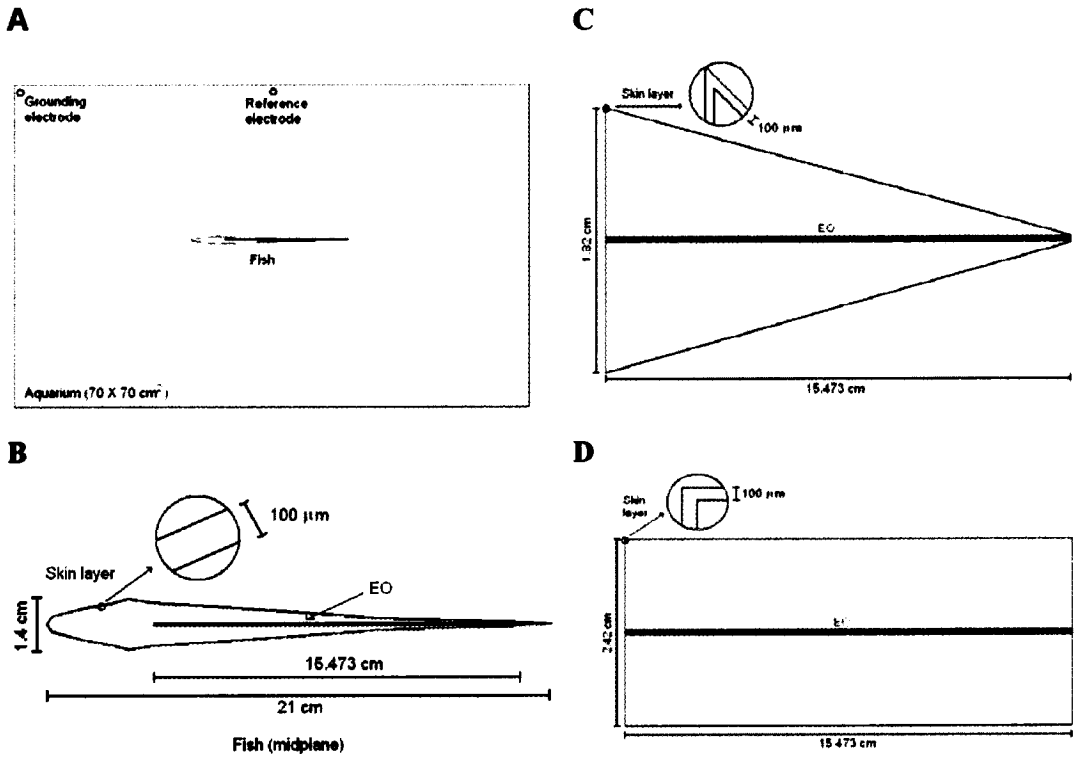

Fig. 3.1: Electric field models. (A) Complete view of the model geometry, composed of an aquarium, grounding and reference electrodes and the model fish. (B) Close-up of morphologically accurate "fish" model consisting of a thin skin layer, an electric organ (EO) and an interior body component (between the EO and skin). The EO is 15.47 cm long and 0.08 cm thick, the skin is 0.01 cm thick and the fish is 21cm long and 1.4 cm wide. (C), (D) Geometrically simple models used for studying (C) different fish tapers (see text for explanation) and (D) various body and skin properties. To achieve different tapers in (C), the left side of the model (here shown for a width of 1.82 cm) is varied. The EO length and skin thickness for (C) and (D) are the same as in (B). Model (C) is referred to as the "taper" model and model (D) is referred to as the "box" model. X and Y axes, as well as grounding and reference electrodes, are not to scale.

Morphologically accurate fish model

For the fish model, the contour of the 21 cm fish was slightly adapted from Assad's original mapping by removing the operculum and by symmetrizing the skin with respect to the rostro-caudal axis, thereby simplifying the interpretation of our results (Fig. 3.1B). These modifications did not negatively affect the data fitting, and, in fact, did improve the overall error by approximately 10 % (see later for error measurement). The size and shape of the EO was adapted from Moller (1995) by approximating the actual shape with an appropriately-sized rectangle. The 100-micron thick skin layer was selected as an acceptable upper bound, based on previous measurements (Bennett, 1971; Zakon, 1986). The fish model therefore has three compartments: an EO, a thin skin layer, and a body component located between the EO and the skin. The reference electrode is placed laterally to the fish, while the grounding electrode is placed in the corner of the tank, as in Assad (1997). Water conductivity was set to 0.023 S/m, also as in Assad (1997), in order to mimic experimental conditions. In Assad (1997), the potential values were obtained by moving an array of electrodes around an immobilized fish. These potentials were differentiated with respect to a fixed electrode located lateral to the fish, near the fish's zero-potential line (see Fig. 3.1A).

Electric field model parameters

Four of the fish model's parameters were varied systematically in order to minimize the error between the simulated and measured potential fields: skin, body and EO conductivity, as well as EO current density profile. EO conductivity was varied from 0.01 to 100 S/m, body conductivity from 0.01 to 10 S/m, and uniform skin conductivity

from 0.00001 to 10 S/m. A non-uniform skin conductivity profile, as predicted by several studies (Heiligenberg, 1975; Hoshimiya *et al.*, 1980; Assad, 1997), was also tested. This profile had three parts: a head conductivity of 0.00025 S/m (first 60% of body length), a tail conductivity of 0.0025 S/m (last 10% of body length) and a mid-body conductivity which varied linearly from 0.00025 to 0.0025 S/m for the middle 30% of the fish's body length (see Fig. 3.8A). These bulk conductivity values, which depend on skin thickness, were re-calculated from Assad (1997) for our chosen skin thickness of 100 μm (versus 200 μm). Assad had chosen 200 μm as a conservative assumption, but we have reduced the skin thickness in order to more accurately mimic values found in the literature, as noted previously.

For the head-positive phase of the EOD cycle studied in this paper, the potential changes polarity along the EO from positive at the fish's head to negative at the tail. In addition, the field is positive for most of the body length and is much stronger in the tail (see Fig. 3.3A). Thus, several zero-mean, bimodal EO current density profiles (linear profile, two component point-line EO, etc.) were tested in order to mimic this field. One profile, however, allowed for a more thorough investigation due to its general nature and amenability to mimic various EOD phases. This current density profile, referred to as "skewed" in this paper, is composed of two Gaussian curves: a rostral positive one and a caudal negative one (see Fig. 3.2A). Such a current density was chosen for its generality; knowledge of the exterior field cannot uniquely determine the distribution of sinks and sources inside of the fish (Rasnow and Bower, 1996), and experimental data is currently unavailable.

In order to find the optimal skewed current density parameters, reasonable estimates for the conductivities of the three separate fish compartments were initially assumed (EO: 1 S/m, body: 1 S/m, skin: previously mentioned non-uniform profile; Scheich and Bullock, 1974; Assad, 1997). The mean and standard deviation of the two Gaussian curves that make up the skewed profile were also initially adjusted in order to mimic the approximately dipolar field. Afterwards, these four current density parameters were altered sequentially in order to minimize the model's error (see next section for error measure). For every set of current density parameters varied, the amplitudes of the two Gaussian curves were adjusted in order to make the mean of the skewed profile as close to zero as possible. This was accomplished by optimizing the rostral curve's amplitude while fixing the caudal curve's amplitude (hence the rostral curve's amplitude was a fifth free current density parameter). Once each skewed current density profile parameter had been optimized, a standard "nonlinear grid search" method (Bevington and Robinson, 2003) was applied in order to obtain a more precise value of the optimal parameter. In short, this method entailed finding the minimum of the error parabola generated by the "optimal" parameter value and the pair of parameter values (less than, and greater than the optimal value) for which the model's error increased. Once the EO current density parameters were established, the EO, body and skin conductivities were varied within the aforementioned ranges and were similarly optimized using the nonlinear grid search method. A second series of optimizations were abandoned since accuracy did not improve greatly.

Model calibration

We calibrated our fish model to experimental data (Assad, 1997) using a weighted RMS percent difference measure (referred to throughout the text as the RMS error). The weighting was done to put more emphasis on the near field, in the range of active electrolocation (MacIver *et al.*, 2001), and because potential falls off to zero in the far field. The overall, n-node weighted RMS error is given by:

$$RMS(\%) = 100 \cdot \sqrt{\frac{1}{\sum_{i}^{n} w_i^2} \sum_{i=1}^{n} w_i^2 \left(\frac{\Phi_i^{sim} - \Phi_i^{\exp}}{\Phi_i^{\exp}} \right)^2} \tag{3.2}$$

where Φ_i^{sim} and $\Phi_i^{\exp}$ are the simulated and experimental potentials at a given node. The weighting function w_i was a factor proportional to the average rostro-caudal field strength: this factor was set to a maximal value of 1 within 2 cm of the fish's skin and had a minimal value of 0.138 near the lateral tank wall (this value was a result of the fact that the field at the lateral tank wall is only 13.8 % of its value close to the fish). The w_i's were set to one when the non-weighted, standard RMS error was calculated. The nodes used to calculate this weighted error were also re-sampled from 361 to 325 (36 nodes withdrawn) in order to remove any bias caused by the original, uneven data sampling (Assad, 1997). Furthermore, the field images shown in Fig. 3 were generated using these re-sampled nodes.

Geometrically simple electric field models

In order to study independently the effect of fish geometry and electrical conductivities of the different body compartments on the electric field and images, two

geometrically simple electric field models were created, differing only in body contour from the fish model. The first geometrically simple model, referred to as the "taper" model (Fig. 1C), has a triangular body contour that touches the EO at both ends. The value of the taper is given by the ratio of the lateral and horizontal extents of the skin contour (on one of the fish's sides). In order to study a given taper (found along the fish model's outer contour), the rostral lateral segment of the taper model was adjusted appropriately. The second geometrically simple model, referred to as the "box" model (Fig. 3.1D), has a rectangular body contour which touches the EO at both ends. The effects of the various body conductivities and of EO-to-skin distance were studied using this model, independent of the effects of taper. For experiments in which the EO-to-skin distance was not varied, a width of 2.42 cm was used by default (see Fig. 3.1D). Results obtained with various widths were qualitatively the same; therefore, the exact choice of the box's width was not important for the comparative studies conducted in this paper. Uniform conductivity parameters were used in these models (optimal values from the fish model; see Results section), unless otherwise stated.

In addition to the optimal skewed EO current density (see Results section), a sinusoidal current density, which held an integer number of wavelengths along the EO, was also tested in these models (profiles with, e.g. 1 or 5 wavelengths, are respectively referred to as "1-cycle" or "5-cycle" sinusoidal waves in this paper). Sinusoidal profiles, which are standard periodic functions, were chosen in order to better compare the results obtained with the more realistic, but skewed current density profile.

Electric field characterization tools

In order to characterize the degree of uniformity or "smoothness" of the electric field around the fish, a quantitative measure was needed. To this end, we used a measure of "energy" (proportional to electric energy density) to quantify the degree of smoothness of the potential Φ along the EO as well as along the interior and exterior skin boundaries. It is defined as:

$$Energy = \int \left(\frac{d\Phi}{dx'} \right)^2 dx' \qquad (3.3).$$

This measure is analogous to the (potential) energy held within a string stretched along a dimension "x" that is perturbed in the "y" dimension. When no energy is applied to the string, there is no variation in the vertical dimension (y; analogous to Φ) as a function of the horizontal dimension (x). However, if the string is suddenly moved up and down repeatedly so that, for example, a sinusoidal pattern results, y will change as a function of x (hence $\frac{dy}{dx} \neq 0$), and therefore equation (3.3) yields a non-zero value for energy. In this sense, the "rougher" the potential variation along a given line is, the higher its associated energy value will be.

To study the electrical filtering effects of the fish body, i.e. how the uniformity of the electric potential profile changes from inside to outside the fish, the energy at the EO level ($Energy_{EO}$) was compared with the energy at the exterior ($Energy_{ext}$) skin level. This filtering effect was quantified as the percentage of energy lost across the body:

$$filtering\ (\%) = 100 \cdot \left(\frac{Energy_{EO} - Energy_{ext}}{Energy_{EO}} \right) \qquad (3.4).$$

With higher filtering values, more energy is being lost (filtered) from the EO to the skin exterior. A 50-cycle sinusoidal current density (see previous section) was used in order to calculate filtering. The EO segment was divided into 50 separate sections and one filtering value was calculated per section (i.e. one filtering value per wavelength). This spatial "frequency", although higher than that of the skewed current density, was selected because it made it possible to visualize the body's filtering effects along the body with good spatial resolution (see e.g. Fig. 3.4B). Further, we found that the filtering curve's main feature, namely a head-to-tail decrease in filtering, remained the same for all frequencies; only the absolute values differed.

In order to test the accuracy of the electric fish as an ideal voltage divider, we compared the simulated (V_{sim}) and theoretical (V_{theo}) transdermal potentials all along the fish's rostro-caudal axis (x) using the taper model (taper ratio = 0.05) with a 5-cycle sinusoidal current density. The following formula, which stems from the standard "perfect voltage divider" equation for an unloaded circuit, was used:

$$V_{theo}(x) = \frac{V_{ext}(x) - V_{EO}(x)}{\left(\frac{\sigma_{skin} \cdot t_{body}(x)}{\sigma_{body} \cdot t_{skin}(x)} + 1 \right)} \tag{3.5}$$

where V_{ext} and V_{EO} are the potentials at the exterior skin level and at the EO level, respectively, σ_{skin} and σ_{body} are the conductivities of the skin and body, respectively, and where t_{skin} and t_{body} are the thicknesses of the skin and body, respectively.

Electric image calculations

Electric images were calculated as the difference between transdermal potentials in the presence (OB) and in the absence (NO) of an object, all along the rostro-caudal axis, as in previous studies (Hoshimiya *et al.*, 1980; Chen *et al.*, 2005; Migliaro *et al.*, 2005):

$$\Delta\Phi(x) = [\Phi_{ext}^{OB}(x) - \Phi_{\text{int}}^{OB}(x)] - [\Phi_{ext}^{NO}(x) - \Phi_{\text{int}}^{NO}(x)] \quad (3.6)$$

where "ext" and "int" denote the exterior and interior boundaries of the skin layer, respectively.

Some of the electric images produced by the skewed current density profile used in this paper are generally bimodal in nature; rostral and caudal peaks of differing polarities are present. Throughout our analysis, the potential difference between the two largest peaks will be referred to as the "peak-to-peak potential", while the horizontal distance between them will be called the "peak-to-peak distance" or "delta". Please note also that the words "images" and "electric images" will be used interchangeably throughout the text.

All electric images in this paper were produced by a 1.1 cm-radius metal (brass; conductivity = 2.13 x 10^7 S/m) disc, unless otherwise stated.

Results

Optimal model parameters

The optimal EO current density is shown in Fig. 3.2A (red trace). It is defined by a difference of Gaussians: a "positive", rostral Gaussian curve (blue trace, centered 15 cm

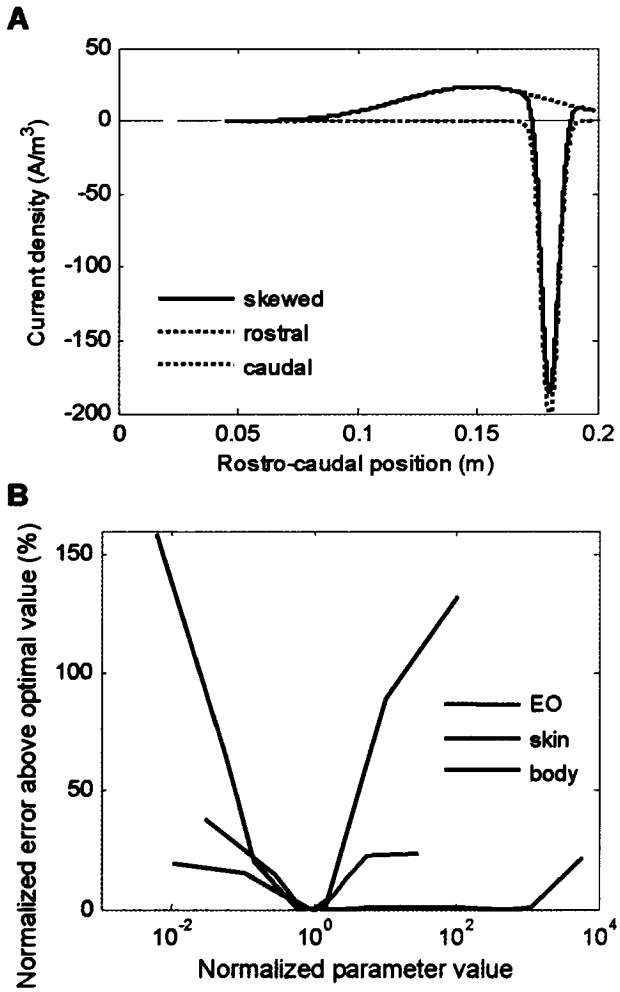

Fig. 3.2: Optimal model parameters. (A) The optimal EO current density profile (red), called "skewed", is the sum of two Gaussian curves: a narrow (dotted green) sink in the tail region and a wide (dotted blue) source in the mid-body. Rostral curve is centered 15 cm from the tip of the head and has a standard deviation of 4.46 cm; caudal curve is centered 18.04 cm from the tip of the head with a standard deviation of 0.5 cm. The ratio of the peak amplitudes of the two curves is 1: 8.38. (B) Optimal conductivity values for the EO (blue), skin (green), and body (red). Optimal parameter values are normalized to one and the errors associated with each optimal parameter value are set to zero. Abscissa values are given as ratios of the optimal parameter value (for each respective curve) and ordinate values are given as field RMS % errors above minimal error (28.6 %; see text for details on error measure). Optimal conductivity values are: EO, 0.927 S/m; body: 0.356 S/m; skin, 0.0017 S/m. Although all parameters here were varied homogeneously, it should be noted that the optimal skin conductivity is not uniform along the length of the fish (see Fig. 8A).

from the tip of the head with a standard deviation of 4.46 cm) and a "negative", caudal Gaussian curve (green trace, centered 18.04 cm from the tip of the head with a standard deviation of 0.5 cm). The ratio of the peak amplitudes, positive to negative, is 1: 8.38, respectively. The electric fields generated from other bimodal current densities (see Materials and methods section) did not match the measured data as well as with this optimal "skewed" profile (data not shown).

Fig. 3.2B shows a sensitivity analysis relative to the optimal (uniform) conductivities values of the different fish compartments. The vertical axis shows error above the minimal weighted RMS error, found with optimal parameters (28.6 %); the horizontal axis shows normalized parameter values (optimal conductivity values each set to one). The optimal parameter values are: EO conductivity, 0.927 S/m, uniform skin conductivity, 0.0017 S/m, body conductivity, 0.356 S/m. Skin conductivity is the least sensitive of the three conductivity parameters. A non-uniform skin conductivity profile was tested as well (see Fig. 3.8A), giving slightly better results (0.5 % less error). Contrary to previous studies, however, we did not find that non-uniform skin conductivity was necessary to reproduce the rostrally-leaning zero-potential line (not shown). Nevertheless, since the error associated with this type of profile was better, it was used by default throughout this paper, except for when the effects of other parameters were studied independently and hence the optimal uniform skin conductivity was used (see later section).

Model calibration

Fig. 3.3A shows the measured (top) and simulated (bottom) field potentials (simulated field shown for optimal set of parameters, including non-uniform skin conductivity). Most qualitative aspects of the measured field, such as the uniform potential in the head region, the elongated dipole field shape, and the rostrally-leaning zero-potential line, are reproduced. Aspects which are not reproduced as effectively are the high potential and rate of field decay in the tail region. This can further be seen in Fig. 3.3C, which shows the absolute potential difference between simulated and experimental data; notice that only the tail region features a discrepancy of several mV (differences over 5 mV are mapped to dark red; maximal difference is ~ 22 mV). Fig. 3.3B shows the un-weighted percent error. The error close to the fish is relatively low (~ 10 % in the rostral near field and similar to that of a recent analytical model; Chen *et al.*, 2005). The error increases further away; this is especially apparent near the zero-potential line, where the measured absolute potentials are very small (micro-volt magnitude; see Fig. 3.3C), hence creating large relative discrepancies with the simulated field. Fig. 3.3D and Fig. 3.3E show the falloff of potential with lateral distance for two different rostro-caudal locations, one at the head (Fig. 3.3D) and one at the tail (Fig. 3.3E). These figures show that even though the error increases further away (see Fig. 3.3B), the falloff is qualitatively similar between our model (red) and the data (blue). The weighted, re-sampled average RMS error is 28 %; the average RMS error (non-weighted, all nodes) is 43%; the average potential difference over the entire field is approximately 1 mV.

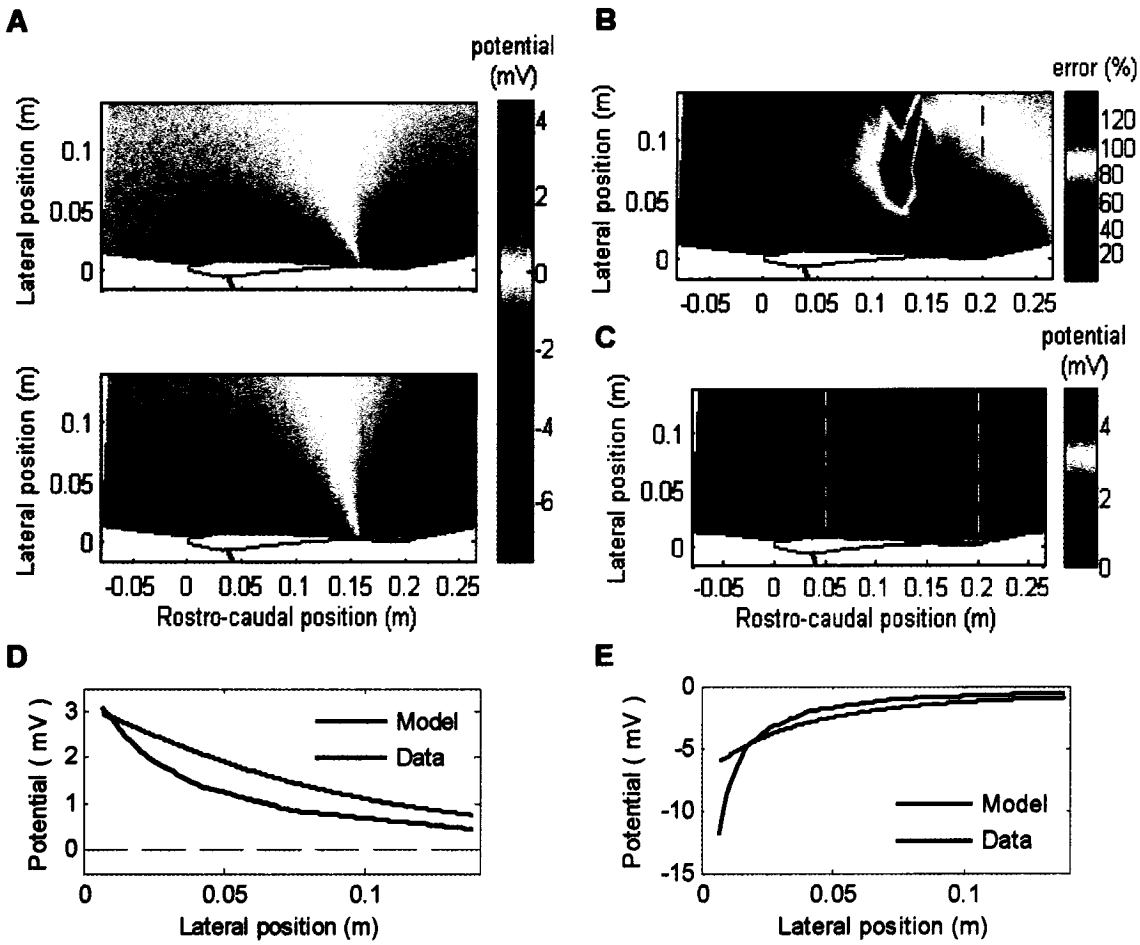

Fig. 3.3: Model calibration. (A) 2D field potential surrounding the fish. Top: experimental data obtained from Assad (1997). Bottom: simulated values obtained with optimal parameters (including non-uniform skin conductivity). Color maps represent potential with respect to an electrode placed laterally to the fish, near its zero-potential line (as in Fig. 1A). All values below ~ -7.6 mV has been mapped to dark blue in order to show a better contrast between the positive and negative regions of the dipolar field (measured potential in tail region reaches ~ -30mV). The zero-potential line is shown in yellow. (B) Un-weighted % error and (C) absolute potential differences between data and simulated values found in (A). Dashed lines show cross-sections at which the potentials are plotted in (D) and (E). Potential differences in (C) greater than 5mV are all mapped to dark red. (D) Potential along dotted line near head (5 cm caudal from the tip of the head) in (B) for model (red) and data (blue). (E) Potential along dotted line near tail (20 cm caudal from the tip of the head) in (B) for model (red) and data (blue).

Electric field characterization

Filtering

Previous studies have noted that the electric field in the head region of *A. leptorhynchus* is relatively uniform along the body (Rasnow *et al.*, 1993; Nelson, 2005), but have not investigated its possible origin. In this section, we quantitatively analyze the degree of electric field uniformity and its possible origin for the first time. In Fig. 3.4A, the potential at the EO level and at the inner and outer skin boundaries of the fish model are shown as a function of normalized EO length (zero corresponding to the rostral end, one to the caudal end) for a 5-cycle sinusoidal current density. The potential at the fish's exterior is much smoother than at the EO level in the head region, and becomes more spatially heterogeneous, or rougher, towards the tail. This was also apparent for sinusoidal current densities of higher and lower frequencies as well as for different current density profiles (data not shown). The EO potential also increases caudally, due to the "narrowing" taper of the fish (this is not due to the EO current density, since in this example its amplitude was the same all along the EO).

Fig. 3.4B further characterizes the smoothness of the exterior potential. The green trace shows that the normalized energy at the exterior skin level approaches a value of zero towards the head, implying that the potential is almost perfectly "flat" in this region; the energy is minimal in the head region situated to the left of the EO (left of red line). The blue trace shows that filtering is maximal rostrally and decreases caudally, with a mean filtering value of 91.5 % (shown for a 50-cycle sinusoidal current density). By contrast, the mean filtering for a 1-cycle sinusoidal current density is 47.3 %. Therefore, the mean filtering value obtained with the skewed current density will be in between

these two values (recall that a higher frequency was used in order to better visualize filtering along the body axis). While the body and skin tend to filter out more of the potential at higher frequencies, the qualitative shape of the filtering curve obtained with lower frequencies remains the same as in Fig. 3.4B (not shown).

Several tests with the two geometrically simple models were carried out in order to understand how different parameters affect the filtering due to the fish's body. By comparing the exterior (red trace) and interior (green trace) potentials in Fig. 3.4A, it is clear that the skin acts as a filter. However, the skin alone cannot account for the head-to-tail drop-off in filtering of nearly 35% in the fish model (see Fig. 3.4C, green trace). Nor can this effect be explained by the different head and tail conductivities found in the non-uniform skin conductivity profile. Tests conducted with body conductivity only predicted differences of a few percent in filtering when varied systematically. Fig. 3.4C shows the filtering effect for two versions of the taper model. The shape of the fish model's filtering curve (green trace) resembles the ones found with the taper models, either rostral to (taper of 0.05, blue trace) or caudal to (taper of 0.0178, black trace) the point of taper change (red dashed line) in the fish model (see Fig. 3.1B for fish model geometry). This can also be understood as differences in effective distance, as a bigger taper value implies that the EO is effectively farther from the exterior skin. The slight caudal discrepancy (green vs. black traces) is likely due to edge effects: the fish model has body tissue located between the end of the EO and the end of the tail that is not present in the taper model.

While a smooth external field may be of functional importance for the fish, as noted previously, it remains that the relevant stimuli for the skin electroreceptors is

transdermal potential (Migliaro *et al.*, 2005). It is thus reasonable to assume that a uniform transdermal potential would be of greater significance to the fish. We calculated the energy of the transdermal potential and found that it was equally "smoothest" in the head region (data not shown). Its shape was similar to the external potential energy curve shown in Fig. 3.4B (green trace), although its peak was shifted rostrally. This can be understood by comparing the external and internal potentials in Fig. 3.4A. At the tail end, both the internal and external potentials are "rough", but the difference between them is relatively uniform.

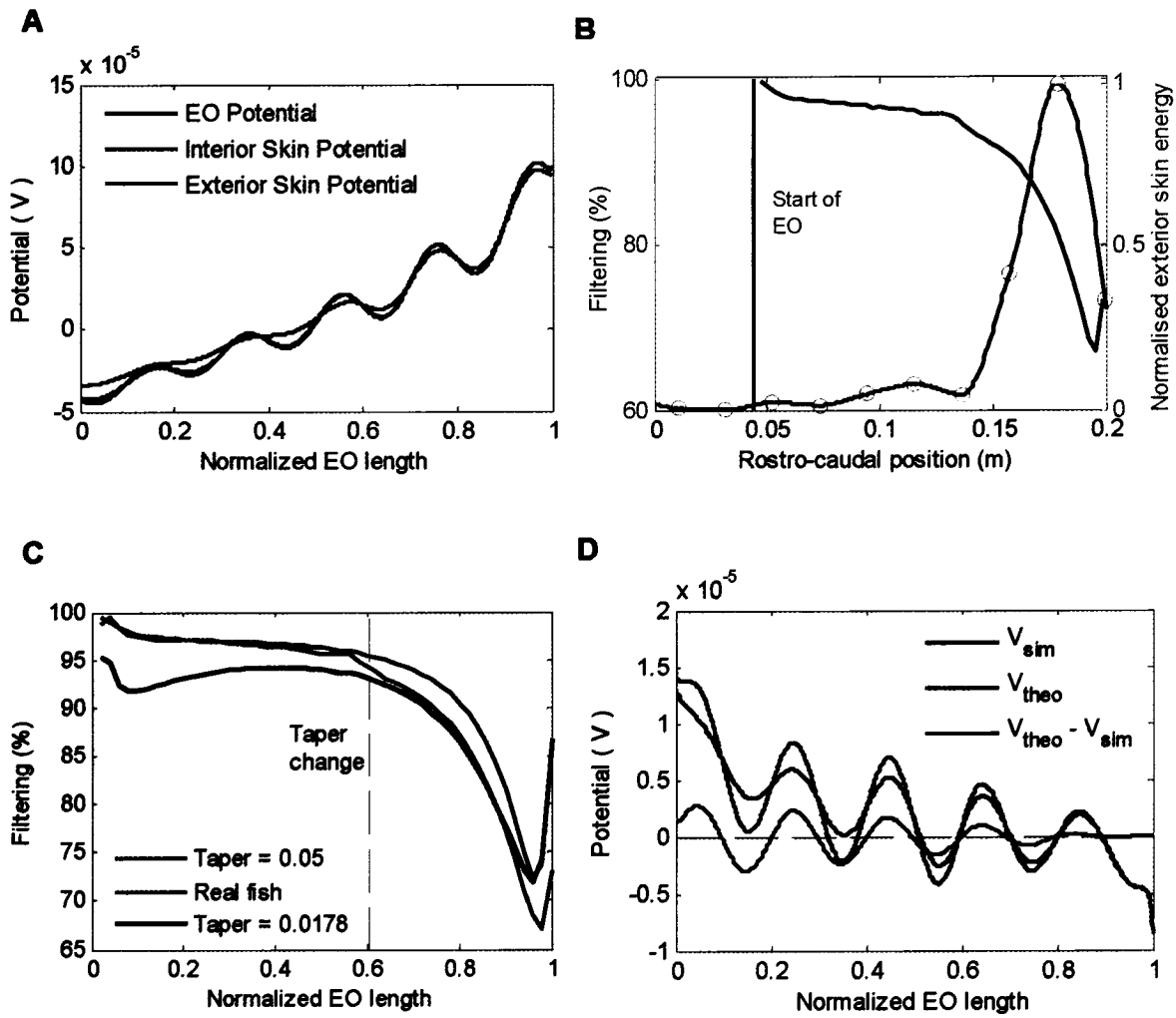

Fig. 3.4: Electric field characterization: study of the fish's filtering properties and comparison with an ideal voltage divider. (A) Potential values at the electric organ (blue) and at the interior (green) and exterior (red) skin boundaries along the EO segment (zero corresponds to the rostral end, one to the caudal end), for a 5-cycle sinusoidal current density (fish model). (B) Right axis, green trace shows the normalized energy of the exterior skin potential curve as a function of rostro-caudal position along the fish body (fish model; solid line was obtained using the "shape-preserving interpolant" fitting function in MATLAB). This energy quantifies the level of "smoothness" of a given trace (see text for details). Left axis, blue trace shows the filtering along the EO segment for a 50-cycle sinusoidal current density (fish model). Filtering quantifies how much the energy has decreased from the EO to the skin (see text for details). The red line represents the start of the EO in the fish model (x = 4.42 cm; see Fig. 1B). (C) Filtering along the EO segment for the fish model (green) and for the taper model with low (black) and high (blue) taper values. Red dashed line represents the location of taper change in the fish model. (D) Comparison between the fish and an ideal voltage divider (taper model, taper = 0.05). Theoretical (green) and simulated (blue) transdermal potentials along the EO segment for a 5-cycle sinusoidal current density. Red trace shows the difference between simulation and theory (see text for details).

Voltage Divider

Previous studies have likened the fish to a voltage divider (Rasnow, 1996; McAnelly *et al.*, 2003), and Fig. 3.4D characterizes the accuracy of such an assumption for the first time. Transdermal potentials calculated for the taper model (simulated, blue trace) and for the ideal voltage divider (theoretical, green trace), as well as the difference between these two quantities (red trace), are shown as a function of normalized EO length for a 5-cycle sinusoidal current density (taper model; see Materials and methods section for details). A taper of 0.05 was chosen, as this is the taper which makes up the longest segment, approximately 25 %, of the fish model's body. Both the simulated and theoretical curves have the same quasi-sinusoidal shape, although their amplitudes differ.

The match between these two curves is especially good towards the tail. On the whole, this analysis validates the assumption that the fish body functions as an ideal voltage divider.

Electric image characterization

Effect of object location on electric images

As in several previous studies (Hoshimiya *et al.*, 1980; Rasnow, 1996; Rother *et al.*, 2003 ; Chen *et al.*, 2005; Migliaro *et al.*, 2005), we have characterized the electric images produced by simple (circular cross-sections) conductive objects. The effects of different lateral and rostro-caudal object locations on electric image shape are displayed in Fig. 3.5. The electric image gets smaller (in amplitude) and wider, as the object is moved away laterally from the fish (Fig. 3.5A). The image amplitude increases (in absolute terms) and then decreases, as the object moves caudally (Fig. 3.5B). Most of the electric images shown in Fig. 3.5B are bimodal in nature: they have a negative rostral peak and a positive caudal one. These images become increasingly more bimodal towards the tail. Also, the distance between successive negative peaks diminishes caudally, even though the different traces are for regularly-spaced object locations (as shown in the inset). This signifies that the offset between the object's location and the location of the electric image's dominant peak on the skin varies with rostro-caudal location.

Bimodal electric image characterization

The electric images shown in Fig. 3.5 are similar to some of those found experimentally (von der Emde *et al.*, 1998; Chen *et al.*, 2005) and numerically using

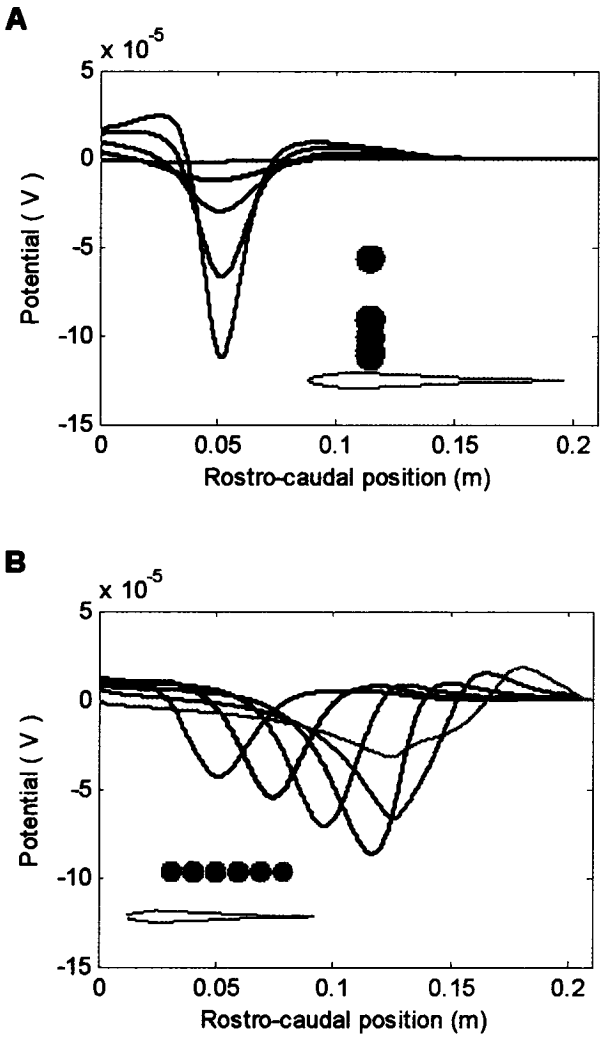

Fig. 3.5: Effect of object location on electric images (fish model). (A) Electric images for an object located 2 (red), 2.5 (blue), 3.5 (green), 5 (black) and 10 (pink) cm lateral of the fish's midline (5 cm caudal from the tip of the head). The electric image is calculated as the change in transdermal potential caused by the object. (B) Electric images for an object located 5 (red), 7.5 (black), 10 (green), 12.5 (blue), 15 (pink), 17.5 (orange) cm caudal from the start of the head at a lateral distance of 3 cm (from the fish's midline). The simulated object for (A) and (B) is a metal disc (brass; conductivity = 2.13 x 10^7 S/m; 1 cm-radius).

different modeling techniques (Hoshimiya *et al.*, 1980; Caputi *et al.*, 1998; Migliaro *et al.*, 2005). However, some qualitative differences exist. In order to investigate these differences, normalized electric images (Fig. 3.6B), which were produced by a rostro-caudally centered metal sphere, were calculated for three separate current densities (Fig. 3.6A): a 1-cycle sinusoidal current density, the optimal skewed current density, as well as a unimodal, pulse-like current density similar to that found in pulse-type electric fish (e.g. Migliaro *et al.*, 2005). The main differences in image shape are a variation in the caudal trough size and discrepancies in the location of the rostral and caudal peaks.

Three points are specified in Fig. 3.6B in order to better characterize the electric image's bimodal shape: the location of the rostral (xR) and caudal (xC) peaks, as well as the location of the null potential (x0) found between these two peaks. It should be noted that other characteristic points could be of importance for other EOD phases or for different rostro-caudal object locations (see Fig. 3.5); however, these were not considered.

The offset between the object and image locations, as observed in Fig. 3.5B, was characterized in Fig. 3.7. Tests were carried out using the box model with 1-cycle sinusoidal (Fig. 3.7A and Fig. 3.7B) and skewed (Fig. 3.7C and Fig. 3.7D) current densities (also, see Fig. 3.6A for reference). These figures show that the locations of the electric image's characteristic points (xR, x0 and xC) change as a function of rostro-caudal object location. The solid black line (identity line) indicates where the location of the image at the skin corresponds exactly to the location of the object. For the sinusoidal current density (Fig. 3.7A), xR (blue trace) is closest to the object's location for the first rostral third of the fish body, x0 (red trace) is closest to it for the middle third, and xC

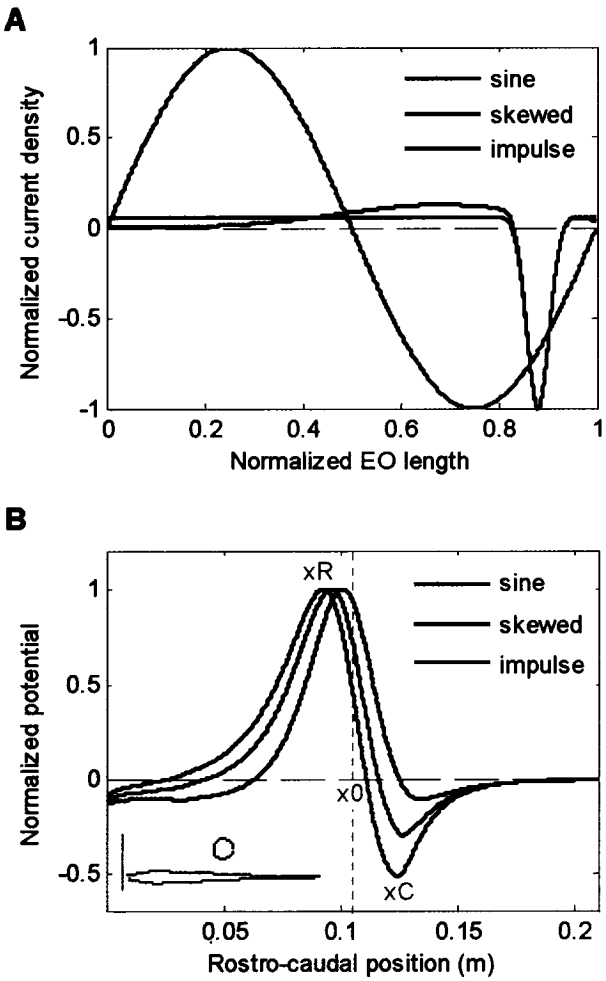

Fig. 3.6: Effect of EO current density profile on electric images (fish model). (A) Normalized current densities versus normalized EO position. The green trace shows the 1-cycle sinusoidal current density; the blue trace shows the optimal skewed current density (sum of two Gaussian curves); the red trace shows the "impulse" current density (single Gaussian function offset in order to have a mean of zero). All current densities are zero-mean. (B) Normalized electric images produced by a metal disc located in the middle of the fish (black vertical line), 3 cm lateral from the midline (see inset), for skewed (blue), impulse (red) and sinusoidal (green) current density profiles. The green markers "xR", "x0", and "xC" illustrate the "x" or rostro-caudal positions of the three points which characterize bimodal electric images: the rostral peak, the zero-crossing (located between rostral and caudal peaks) and the caudal peak, respectively.

(green trace) is closest to it for the last, caudal third of the body (the black dotted lines delimit these zones). This indicates that either the rostral or caudal peak of the bimodal electric image is located closest to the object's position, depending on whether the object is located close to the head or near the tail. A similar phenomenon occurs for the skewed current density (Fig. 3.7C), although in this case the bimodal electric image's rostral peak is closest to the object's actual location over a wider range of the fish's body. It should be noted that for a specific rostro-caudal object location, the electric image's amplitude, at this point, is zero (intersection of solid black and red curves).

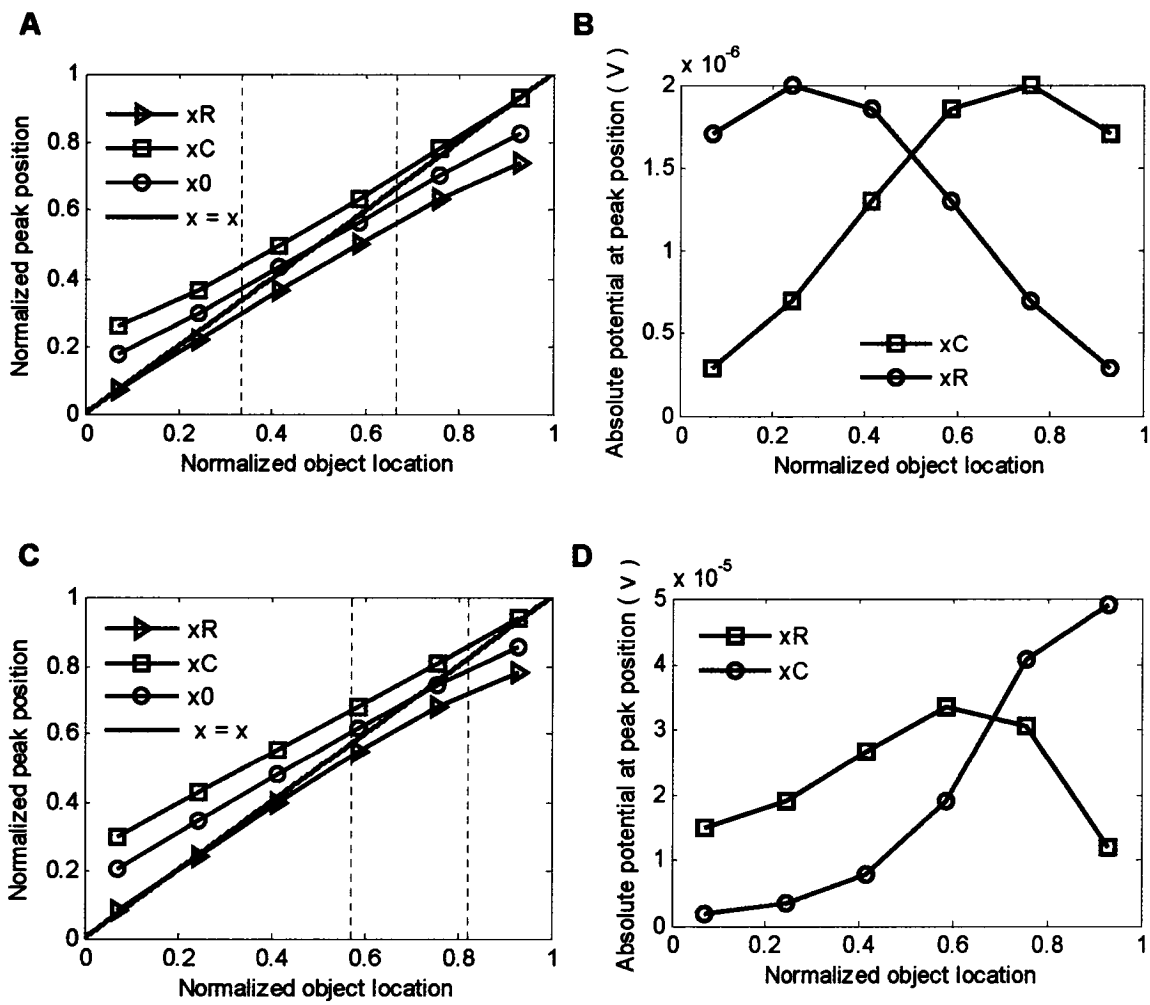

Fig. 3.7: Positions and amplitudes of the bimodal electric image's characteristic points ("xR", "x0" and "xC") for different rostro-caudal object locations (box model; optimal uniform skin conductivity; object centered 3 cm away from the fish's midline). (A), (C) Normalized peak positions for sinusoidal (A) and skewed (C) current densities. Peak positions and object locations are normalized with respect to EO coordinates, with the rostral side corresponding to zero. Blue and green traces are the positions of the rostral and caudal peaks, respectively, while red traces show the positions of the zero-crossings. The solid black curve shows the identity line, where the location of the electric image's dominant peak at the skin corresponds exactly to the rostro-caudal location of the object. Black dotted lines delimit zones in which certain characteristic curves are closest to the solid black trace: e.g., in (C), the blue trace (xR) is closest to the identity line in the rostral zone, i.e. the bimodal image's rostral peak is closest to the object's actual location in this zone. (B), (D) Absolute potentials of the bimodal electric image's rostral and caudal peaks for sinusoidal (B) and skewed (D) current densities. Blue traces show absolute potential values for the rostral peak while caudal peak values are shown in green.

The absolute amplitudes of the rostral and caudal peaks of the bimodal electric image as a function of rostro-caudal object location are shown for sinusoidal (Fig. 3.7B) and skewed (Fig. 3.7D) current densities. Here it can be seen that image amplitude is roughly proportional to the EO potential; hence, the locations of the two amplitude peaks are approximately the same as the locations of the two peaks in a given current density profile (for both profiles). It should be noted that the potentials would have been relatively smaller in the tail region, had the non-uniform skin conductivity profile been used instead of the uniform one.

The effect of skin conductivity profile on electric image shape is studied with the box model in Fig. 3.8. The image (Fig. 3.8B) due to the "real", non-uniform skin conductivity profile (green trace; Fig. 3.8A) either resembles the one obtained with the

uniform head conductivity (0.00025 S/m; red trace) or the one obtained with the uniform tail conductivity (0.0025 S/m; blue trace), depending on rostro-caudal location. The electric image in the middle region shows a transition from the image obtained with one of the uniform conductivities to the other. From this figure, it is also apparent that, as expected, the electric image's amplitude decreases as skin conductivity increases.

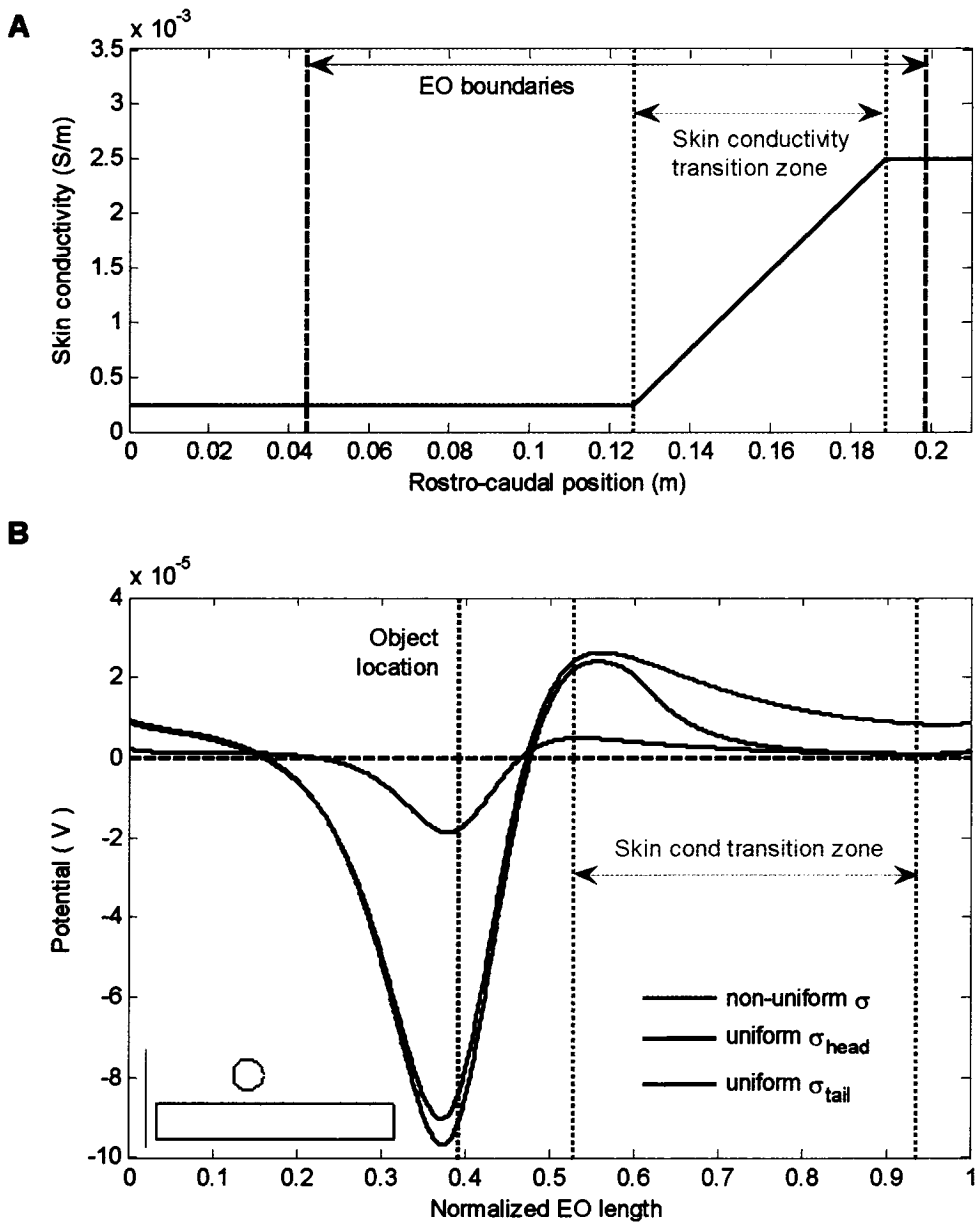

Fig. 3.8: Effect of skin conductivity on electric image shape (box model; skewed current density). (A) Optimal non-uniform skin conductivity profile, which has a low, 0.00025 S/m conductivity at the head, a high, 0.0025 S/m conductivity in the tail region and a linear conductivity increase between the two constant conductivity regions (delimited by pink dotted lines). Black dashed lines delimit the EO. (B) The electric images produced by a 1 cm-radius metal object located at 0.39 along the normalized length of the EO, 3 cm lateral to the fish's midline (black dotted line; see inset) for different values and shapes of skin conductivity are shown. Green trace shows the electric image obtained with the non-uniform skin conductivity. Red and blue traces show the electric images obtained with uniform skin conductivities of 0.00025 S/m (σ_{head}) and 0.0025 S/m (σ_{tail}), respectively.

In Fig. 3.9 we show the bimodal electric images produced by different-sized objects as a function of lateral distance (of the object centers), using the box model (with skewed current density and uniform skin conductivity). Fig. 3.9A and Fig. 3.9C show un-normalized (actual amplitudes) and normalized (with respect to the caudal peak's amplitude) bimodal electric images, respectively, produced by three disc-like objects of different diameters. The amplitude (or peak-to-peak potential) of the electric image produced by the 2 cm object (Fig. 3.9A, red trace) is the largest since all the objects were centered at the same lateral distance of 4 cm; therefore, this object's edge was closest to the fish's skin and thus affected the image more. The normalized bimodal electric images, however, are all very similar (Fig. 3.9C). Fig. 3.9B shows how the peak-to-peak amplitudes of the electric images change as a function of lateral object distance for the three objects: the curves are separated one from another by approximately an order of magnitude (e.g. note peak-to-peak differences at black dotted line). This is in agreement with previous studies that have reported a similar correspondence between un-normalized image amplitude and lateral object distance (Heiligenberg, 1975; Bastian, 1981; Rasnow,

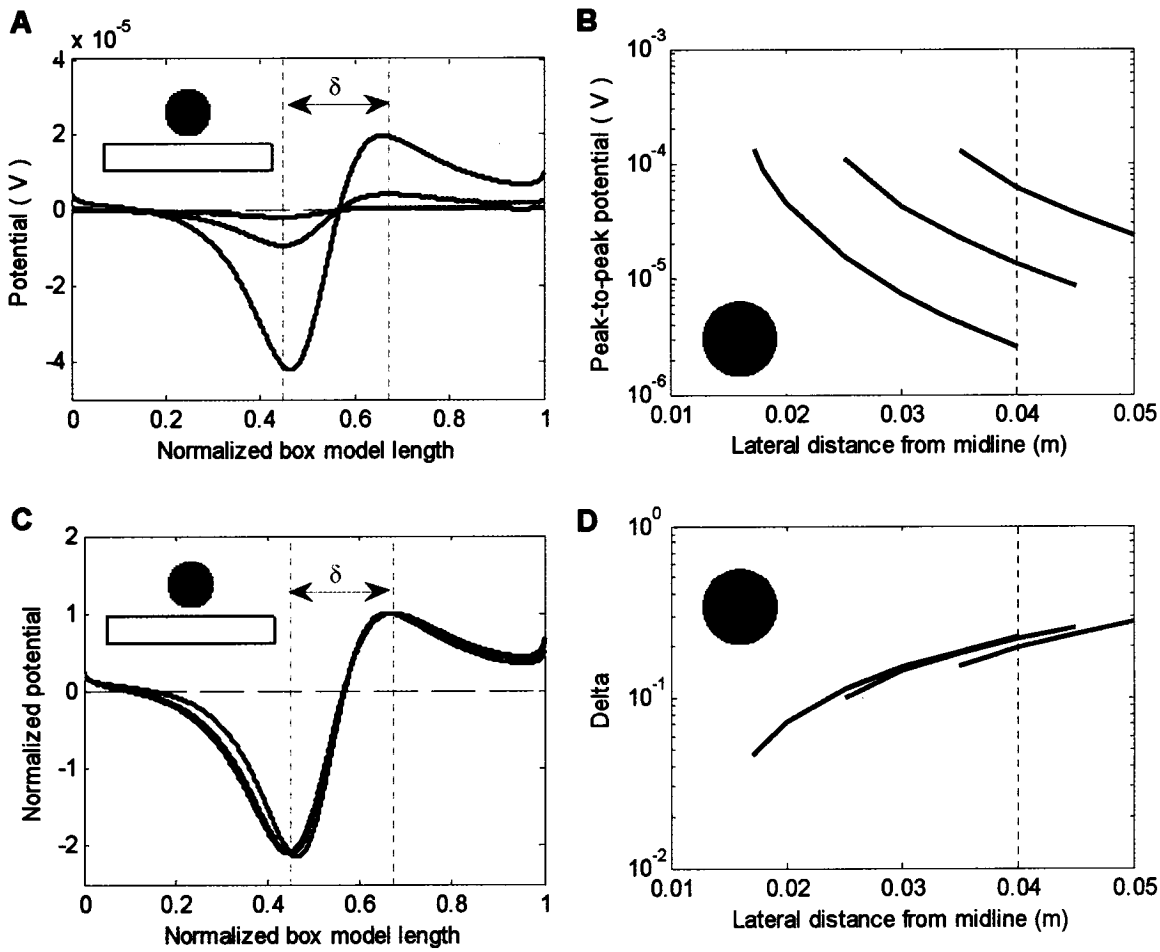

Fig. 3.9: Effect of object size and lateral distance on bimodal electric images (box model; skewed current density; optimal uniform skin conductivity). Lateral distance is measured with respect to object centers. (A) Un-normalized (actual amplitudes) and (C) normalized (with respect to the caudal peak's amplitude) electric images produced by three different-sized metal objects located half way along the fish's body, 4 cm away from the midline: 0.5 (blue), 1.1 (green) and 2 (red) cm-radius (see inset). Both images are plotted versus the normalized box model length, in which the rostral side corresponds to zero. (B) Peak-to-peak potentials of the electric images found in (A) as a function of lateral distance away from the fish's midline for the three different objects (object sizes same as in (A); see inset). (D) Delta, defined as the difference between the rostral and caudal peak locations, found in either (A) or (C), as a function of lateral distance from the fish's midline for the three different objects; delta for the 1.1 cm object is shown in (A) and (C). Black dotted lines in (B) and (D) show the distance (4 cm away from the fish's midline) at which the objects were located for the images shown in (A) and (C).

1996). Thus, the fish cannot unambiguously determine lateral object distance using this measure. This is because small objects placed near the fish's body may create electric images that have the same amplitude as large objects placed farther away from the fish. On the other hand, our analysis shows that the difference between the rostral and caudal peak locations (defined here as "delta") varies consistently with lateral object distance for all three objects (Fig. 3.9D) and could therefore be used by the fish to unambiguously measure lateral object distance. The black dotted line in Fig. 3.9B and in Fig. 3.9D shows the lateral distance (4 cm) for which the electric images in Fig. 3.9A and Fig. 3.9C were calculated. It should be noted that the results shown for the box model also hold for the fish model (not shown). However, the caudal peaks in the fish model are smaller because of the increased conductivity in the tail section (due to the nature of the non-uniform skin conductivity profile; not shown).

Fig. 3.10 shows the same set of panels as in Fig. 3.9, except that lateral distance is now calculated as a function of the object's edge, instead of the object's center. The 0.5 cm-radius (blue) and 1.1 cm-radius (green) objects were moved closer to the fish in Fig. 3.10A and Fig. 3.10C so that their edges were at 2 cm from the midline (same distance as the 2 cm-radius object). The amplitudes have therefore increased in Fig. 3.10C for these two objects since they are closer to the skin surface. There are, however, bigger differences between the normalized electric images of the differently-sized objects, compared to when lateral distance is measured from the object's center. This is reflected in Fig. 3.10D where one can see that the delta values do no longer vary consistently with lateral distance for the three distinct objects. Indeed, this measure seems no more accurate in determining lateral distance than the peak-to-peak potentials shown in Fig. 3.10B.

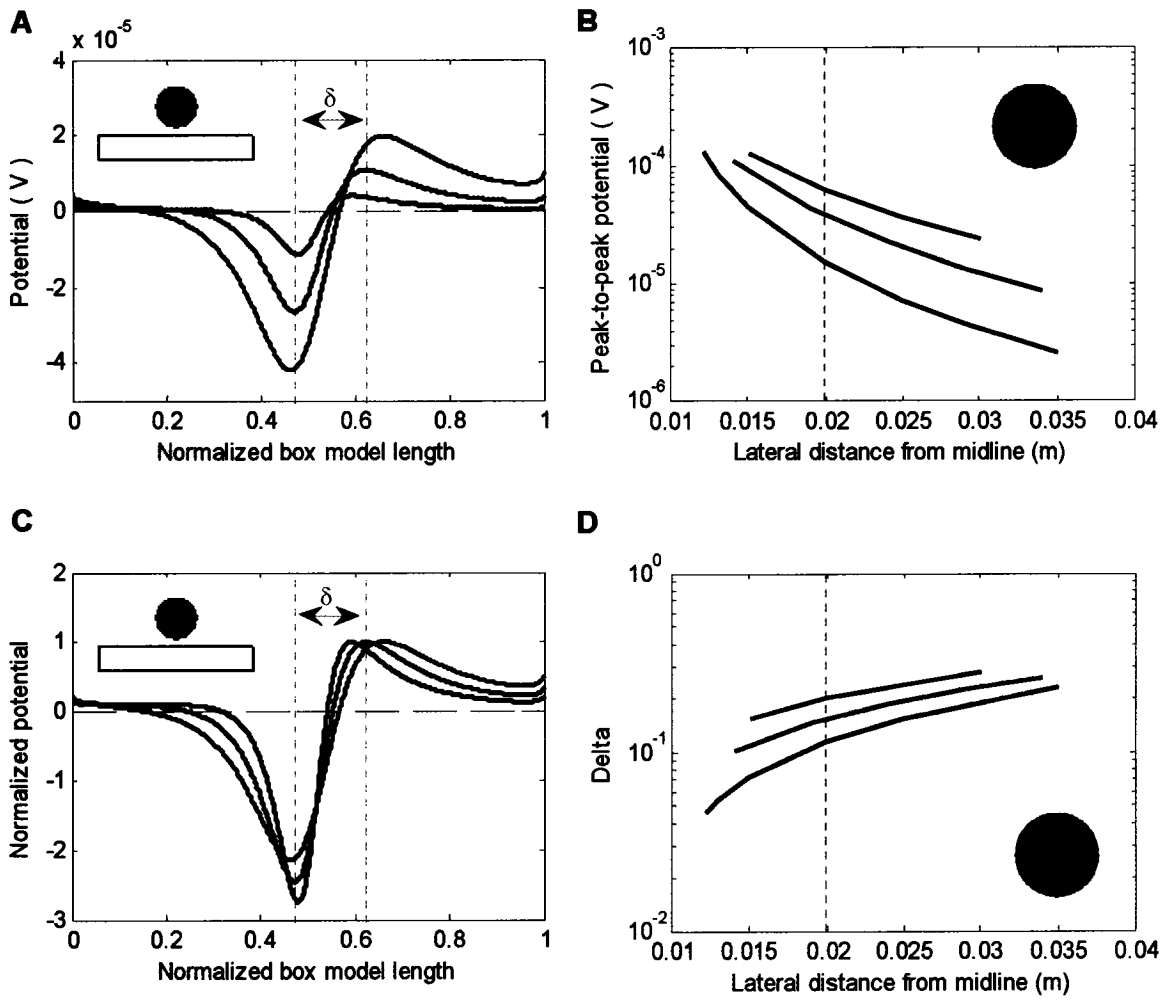

Fig. 3.10: Effect of object size and lateral distance on bimodal electric images. All panels are the same as in Fig. 9 except that lateral distance is measured here with respect to the object's edge. (A) Un-normalized and (C) normalized electric images produced by three different-sized metal objects located half way along the fish's body, with the object edges 2 cm away from the midline: 0.5 (blue), 1.1 (green) and 2 (red) cm-radius (see inset). Red traces are the same as in Fig. 9A and Fig. 9C since a lateral edge distance of 2 cm for the 2 cm-radius object corresponds to a lateral object center distance of 4 cm. (B) Peak-to-peak potentials of the electric images found in (A) as a function of lateral distance away from the fish's midline for the three different objects (object sizes same as in (A); see inset). (D) Delta found in either (A) or (C), as a function of lateral distance from the fish's midline for the three different objects; delta for the 1.1 cm object is shown in (A) and (C). Black dotted lines in (B) and (D) show the distance (2 cm away from the fish's midline) at which the objects were located for the images shown in (A) and (C).

Discussion

In this paper, we have constructed three finite element models in order to study the electric field generated by the weakly electric fish, *A. leptorhynchus*. We have shown, quantitatively, that the relatively homogenous field in the rostral-half of the body is due to the filtering effects of the tapered body shape, and have validated the previous assumption that the fish body acts as an ideal voltage divider. We have also characterized the bimodal electric images produced by simple objects in order to gain further insight into how these fish electrolocate objects. While these images are very similar to those calculated using different models (Hoshimiya *et al.*, 1980; Caputi *et al.*, 1998; Migliaro *et al.*, 2005), there are some potentially important differences.

Electric field modeling

Our two-dimensional, realistic electric field model (referred to as the "fish" model; see Fig. 3.1B) reproduces many spatial aspects of the fish's self-generated EOD potential (Fig. 3.3). For instance, the model duplicated the electric field's dipolar nature and rostrally-leaning zero-potential line. The model was also very accurate near the fish. In particular, the rostral part of the field, where most electroreceptors are located and hence where active electrolocation is mediated (Knudsen, 1975; Carr *et al.*, 1982), has very low error based on comparison's with experimental data (~ 10 %, which is comparable to that found in a recent study; Chen *et al.*, 2005). The high potentials and field decay in the tail region, however, were not reproduced with such low error. This is possibly due to the two-dimensional nature of the model in which the third spatial

dimension does not contribute to the mid-planar field (Assad, 1997). Also, the error between our model and the experimental data does increase further away lateral to the fish. This is because potential values become very small in the far field and hence percent differences can become very large, even though the absolute errors are not large (see e.g. Fig. 3.3C). Fig. 3.3D and Fig. 3.3E show, however, that the field's falloff is qualitatively similar between the model and the data. Therefore, we consider that results which were shown for lateral distances at which the error is larger are still valid, at least qualitatively, in light of the previous argument.

The effects of EO, body and skin conductivity on external potential were studied directly and independently using the two geometrically simple models ("taper" and "box" models; See Fig. 3.1C and Fig. 3.1D). The taper model also allows for an independent study of the fish's geometry. Each model was simple to implement, using the finite element software COMSOL Multiphysics. The models are also computationally fast, solving a mesh containing 89817 nodes in 7.6 seconds (on an IBM computer with a 3.2 GHz Intel Xeon processor). With its realistic electric fish geometry and parameters, the fish model presented in this paper is also an improvement over previous finite element models (Heiligenberg, 1975; Hoshimiya *et al.*, 1980). In particular, compared with the FEM model done by Hoshimiya *et al.* (1980), our model is more morphologically correct (rather than ellipse-like) and has a skin thickness approximately 30 times smaller than in the previous model (and in the range of the measured thickness). Our EO current density was also distributed rostro-caudally along an EO, rather than a two-point dipole used in the previous model. These improvements were enabled in part by our access to increased computational power. The model's main shortcomings are that it is two-dimensional and

that it does not reproduce the potential in the far-field and in the tail region. Also, the model currently only simulates the EOD potential for a single phase of the EOD cycle. However, the model could easily be extended to other phases by modifying the shape of the EO current density appropriately.

The parameters that provide the best fit to Assad's experimental data are in the range of those measured or predicted in the literature. Scheich and Bullock (1974) reported an average body conductivity of 1 S/m, whereas our optimal value is 0.356 S/m. The optimal EO conductivity, 0.927 S/m, is also very similar. Skin conductivity measurements have shown rostro-caudal variations along the fish's body (Scheich and Bullock, 1974; Assad, 1997), and other numerical modeling studies have used a three-component skin conductivity profile in order to model this inhomogeneity (Heiligenberg, 1975; Hoshimiya *et al.*, 1980; Assad, 1997). We have also concluded that this profile (Fig. 3.8A) results in more accuracy, in comparison with uniform skin conductivity profiles. However, we found that in contrast to these previous studies, such a profile was not necessary to reproduce the rostrally-leaning zero-potential line (Fig. 3.3). Thus, for some modeling studies, a uniform conductivity could be used to simplify the models without loss of generality. Here, a uniform skin conductivity of 0.0017 S/m was used for studying the effects of other parameters independently (such as body geometry, for instance). The skewed current density profile (Fig. 3.2A) can be easily adapted to model the time-varying EOD: one only needs to change the mean and standard deviation of the two Gaussian functions in order to mimic different phases. It would be interesting to compare our "simplistic" skewed current density profile with the experimentally

measured one. However, these experiments have only been carried out, as of yet, in pulse-type electric fish (Caputi, 1999).

Electric field characterization

It has been suggested that the uniform field near the head of weakly electric fish could improve their ability to resolve objects, because electroreceptors respond to current flowing perpendicular to the skin surface (Knudsen, 1975; Rasnow and Bower, 1996). We carried out several tests in order to better understand which attributes of the fish body are responsible for this uniform field (Fig. 3.4). We have shown that this spatial filtering is dictated mainly by the tapered shape of the body, and not only, for instance, because of a rostral current density of low amplitude (experiments in pulse-type fish have shown that the electromotive force varied along the fish's body length; see for example Caputi *et al.*, 1989). The field is less smooth caudally because the skin is effectively closer to the EO, therefore reducing the amount of body and skin that can filter out the electric organ's potential. The smooth field in the head region is also aided by the fact that the head region of the fish lacks an EO (Caputi *et al.*, 2002). In fact, we have seen that this region had the lowest exterior energy value (see Fig. 3.4A, green curve; energy rostral of vertical red line is minimal). The importance of skin and body tissues for filtering purposes had been suggested in the past; for example, Rasnow et al. (1993) hypothesized that this was the reason why the fish's EOD propagates less in the trunk. Our geometrically simple models have allowed us to study conductivity and body shape independently and to explain, for the first time, such hypotheses.

We also found that the relevant stimulus for skin electroreceptors, i.e. transdermal potential, was most uniform in the head region. It is possible that electric fish geometry has evolved, in part, to its current shape to increase the field uniformity near the fish's head. The fish's tapered body shape also contributes to the large potentials in the tail region, again due to the effective closeness of the EO and skin layer.

We have also shown that the weakly electric fish acts approximately as an ideal voltage divider (Fig. 3.4D). This is important since certain analytical (Chen *et al.*, 2005) and semi-analytical models (Rasnow, 1996; Nelson *et al.*, 2002), which treat electric images as perturbations of the simulated or measured field at the fish's exterior, are based on such an assumption. Our results indicate that this assumption is good, at least to a first order approximation (especially in the tail region).

Electric image characterization

By positioning an object at various lateral and rostro-caudal locations (Fig. 3.5), we were able to simulate electric images which resemble some of those found experimentally (von der Emde *et al.*, 1998; Chen *et al.*, 2005) and with other numerical models (Hoshimiya *et al.*, 1980; Migliaro *et al.*, 2005). In particular, we found that electric images diminished in amplitude and widened with increasing lateral object distance (Fig. 3.5A), as previously reported (see for example Rasnow, 1996; Caputi *et al.*, 1998). We also found that the electric image's peak-to-peak amplitude decreases with increasing skin conductivity (Fig. 3.8B), which is in agreement with Migliaro *et al.* (2005). The changes in image shape that occur as the object is "moved" rostro-caudally (Fig. 3.5B) can be explained by using the insights obtained with the geometrically simple

models, some of which confirm previous findings. The image amplitude increases at first, due to the EO potential which increases caudally, but then decreases, even though the potential is still increasing towards its (absolute) maximal value. This happens because the conductivity of the skin is increasing, hence reducing the potential drop across the skin and consequently, the image's amplitude. The electric image also widens because the object was moved on a straight line, and therefore the object-to-skin distance increases as the object moves towards the tail. The differences in electric image shape, such as trough sizes, produced by wave-type (skewed current density) and pulse-type (impulse current density) fish can also be explained, at least in part, by the distinct shapes of the EO current densities (Fig. 3.6).

Electric image analysis has been previously used to predict a set of electrolocation rules (Rasnow, 1996; Caputi *et al.*, 1998; von der Emde *et al.*, 1998). It was postulated that the fish could, in principle, compute an object's rostro-caudal location by simply using the location of the electric image's peak (Rasnow, 1996; Caputi *et al.*, 1998) and an object's lateral distance, regardless of its size, by computing the ratio of maximal electric image slope and maximal electric image amplitude (von der Embe *et al.*, 1998). These rules, however, were proposed in the context of either Gaussian-like (Rasnow, 1996) or "Mexican-hat"-like (Caputi *et al.*, 1998; von der Emde *et al.*, 1998) images. While some of the images found here have a "Mexican-hat"-like shape, with a dominant peak surrounded by troughs of opposite polarity on either side, we have also found that in some cases only one of these troughs was significant, resulting in two dominant peaks (Fig. 3.5B). We have characterized these bimodal electric images in order to see how electrolocation rules might differ for such image shapes.

In Fig. 3.7 we studied the bimodal electric images for different rostro-caudal object locations and found that there was an offset between object and electric image locations. Rasnow (1996) also found offsets in his study, but concluded that these were minimal with respect to the width of the electric image. We have shown here that different components of the bimodal electric image, not a single one, are closest to the object's location, as it moves rostro-caudally. When the object is near the head of the fish, the rostral peak of the electric image is closest to the object's location, while the caudal peak is closest when the object is near the tail.

One way that the fish could unambiguously determine which peak is closest to the object's location is by simply comparing the absolute amplitudes of the two peaks: the one with the biggest amplitude indicating that it is closest to the object. The offset between the image peak location and object location could be of functional importance, possibly serving as a prediction of future object location (for an object moving rostro-caudally beside the fish). Nelson & MacIver (1999) postulated this was happening at the electrosensory afferent level, as the peak in afferent activity was located ahead of the transdermal potential peak. The offset in the bimodal electric image could provide another cue for future object location prediction, but would require the use of different peaks, depending on the object's direction of travel. Bacher (1983) has also suggested an algorithm capable of extracting object location using multimodal image shapes; however, his method required the fish to know the object's shape beforehand (and only valid for spheres). The cues suggested here are independent of object shape: the rostro-caudal object location is given by the location of the larger peak of the bimodal electric image (obtained by comparing the amplitudes of the two peaks), with the offset between peak

and object location possibly serving as a future object location predictor. In fact, we have redone the analysis shown in Fig. 3.9 using cube-like objects and have obtained similar results, i.e. that the fish could use delta as an unambiguous lateral distance measure (not shown). One example clearly illustrates how bimodal electric images differ from unimodal ones; for certain object locations, the image has zero amplitude at the corresponding lateral skin position.

In Fig. 3.9 we studied the bimodal electric images produced by different-sized objects as a function of lateral distance. We have shown that the fish could, in principle, use the distance between the rostral and caudal peaks of the electric image (delta) in order to unambiguously determine lateral object distance, regardless of object size. The lateral distance measure presented here is different, yet computationally simpler than the one advanced by von der Emde et al. (1998): only the locations of the two peaks need to be determined by the fish (normalization is not required). The electric fish could subsequently determine the object's size using the bimodal electric image's peak-to-peak amplitude (assuming that the object's conductivity does not change during the electrolocation task, which is a reasonable assumption). Furthermore, we have seen that measuring lateral object distance from the center of objects (Fig. 3.9) seemed much more fruitful than measuring it with respect to the object edges (Fig. 3.10). This corroborates a previous study which noted that measuring lateral object distance with respect to object center had simpler functional forms (Rasnow, 1996). It seems likely, however, that determining the distance of an object's edge would be more relevant for the fish. The fish could then, in principle, extract the edge's distance by using the delta-lateral distance

curve associated with the object's center and then subtract its radius (obtained via the peak-to-peak potential value).

Conclusions

In order to fully understand electrosensory processing, one needs to understand the mechanisms that weakly electric fish use in order to generate electric signals, and how information is extracted from the electric images produced by surrounding objects. Many previous studies have focused on the posteffector mechanisms (Caputi and Budelli, 1995; Rother *et al.*, 2003; Migliaro *et al.*, 2005) and electrolocation principles (Rasnow, 1996; Caputi *et al.*, 1998; von der Emde, 1999; Lewis and Maler, 2002; Chen *et al.*, 2005) employed by weakly electric fish. We have gained further insight into the fish's electric sense using a realistic model of the electric fish *A. leptorhynchus*, as well as two geometrically simple models which have allowed us to study the fish's conductivity and geometry in an independent way. We have also characterized bimodal electric images and seen that electrolocation rules obtained with such images differ from the ones found with Gaussian-like and "Mexican-hat"-like images. Electrolocation rules found using bimodal electric images suggest that weakly electric fish could determine an object's rostro-caudal position by using the location of the peak whose amplitude is greatest and determine its lateral distance by using the distance between the rostral and caudal peaks. More detailed behavioral studies are required to determine which rules are actually used for electrolocation. Finally, our modeling approach also sets the stage for future studies on two poorly understood aspects of the electrolocation behavior: the influence of the time-varying EOD and the nature of complex electrosensory environments.

We would like to thank Christopher Assad for generously sharing his data with us. As well, we would like to extend our thanks to the two referees who reviewed this manuscript for their helpful suggestions. This research was supported by NSERC of Canada grants to AL and JL.

References

Assad, C. (1997). Electric field maps and boundary element simulations of electrolocation in weakly electric fish. Ph. D. thesis, California Institute of Technology, Pasadena, CA.

Assad, C., Rasnow, B., and Stoddard, P. K. (1999). Electric organ discharges and electric images during electrolocation. *J. Exp. Biol.*, vol. 202, pp. 1185-1193.

Bacher, M. (1983). A new method for the simulation of electric fields, generated by electric fish, and their distorsions by objects. *Biol. Cybern.*, vol. 47, pp. 51-58.

Bastian, J. (1981). Electrolocation. I. How the electroreceptors of *Apteronotus albifrons* code for moving objects and other electrical stimuli. *J. Comp. Physiol.*, vol. 144, pp. 481-494.

Bennett, M. V. L. (1971). Electroreception. In: *Fish Physiology.* (W. S. Hoar and D. J. Randall, eds.) vol. V, New York: Academic Press.

Bevington, P. R. and Robinson, D. K. (2003). *Data Reduction and Error Analysis for the Physical Sciences*, 3rd Edn. New York: McGraw-Hill.

Caputi, A., Macadar, O. and Trujillo-Cenoz, O. (1989). Waveform generation of the electric organ discharge in *Gymnotus carapo*. III. Analysis of the fish body as an electric source. *J. Comp. Physiol. A*, vol. 165, pp. 361-370.

Caputi, A. and Budelli, R. (1995). The electric image in weakly electric fish: I. A data-based model of waveform generation in *Gymnotus carapo*. *J. Comput. Neurosci.*, vol. 2, pp. 131-147.

Caputi, A. A. (1999). The electric organ discharge of pulse *gymnotiforms*: the transformation of a simple impulse into a complex spatio-temporal electromotor pattern. *J. Exp. Biol.*, vol. 202, pp. 1229-1241.

Caputi, A. A., Budelli, R., Grant, K. and Bell, C. (1998). The electric image in weakly electric fish: physical images of resistive objects in *Gnathonemus petersii*. *J. Exp. Biol.*, vol. 201, pp. 2115-2128.

Caputi, A. A., Castello, M. E., Aguilera, P., and Trujillo-Cenoz, O. (2002).

Electrolocation and electrocommunication in pulse gymnotids: signal carriers, pre-receptor mechanisms and the electrosensory mosaic. *J. Physiol. Paris*, vol. 96, pp. 493-505.

Carr, C. E., Maler, L., and Sas, E. (1982). Peripheral organization and central projections of the electrosensory nerves in gymnotiform fish. *J. Comp. Neurol.*, vol. 211, pp. 139-153.

Chen, L., House, J. L., Krahe, R., and Nelson, M. E. (2005). Modeling signal and background components of electrosensory scenes. *J. Comp. Physiol. A*, vol. 191, pp. 331-345.

Heiligenberg, W. (1975). Theoretical and experimental approaches to spatial aspects of electrolocation. *J. Comp. Physiol.*, vol. 103, pp. 247-272.

Heiligenberg, W. (1991). *Neural Nets in Electric Fish.* Cambridge, Mass.: MIT Press.

Hoshimiya, N., Shogen , K., Matsuo, T., and Chichibu, S. (1980). The *Apteronotus* EOD field: waveform and EOD field simulation. *J. Comp. Physiol.*, vol. 135, pp. 283-290.

Knudsen, E. I. (1975). Spatial aspects of the electric fields generated by weakly electric fish. *J. Comp. Physiol.*, vol. 99, pp. 103-118.

Lewis, J. E. and Maler, L. (2002). Blurring of the senses: common cues for distance perception in diverse sensory systems. *Neuroscience*, vol. 114, pp. 19-22.

Lissman, H. W. and Machin, K. E. (1958). The mechanism of object location in *Gymnarchus niloticus* and similar fish. *J. Exp. Biol.*, vol. 35, pp. 451-486.

MacIver, M. A., Sharabash, N. M., and Nelson, M. E. (2001). Prey-capture behavior in gymnotid electric fish: motion analysis and effects of water conductivity. *J. Exp. Biol.*, vol. 204, pp. 543-557.

McAnelly, L., Silva, A., and Zakon, H. H. (2003). Cyclic AMP modulates electrical signaling in a weakly electric fish. *J. Comp. Physiol. A.*, vol. 189, pp. 273-282.

Migliaro, A., Caputi, A. A., and Budelli, R. (2005). Theoretical analysis of pre-receptor image conditioning in weakly electric fish. *PLoS Comp. Biol.*, vol. 1, pp. e162005.

Moller, P. (1995). *Electric Fishes: History and Behavior.* London: Chapman & Hall.

Nelson, M. E. (2005). Target detection, image analysis and modeling. In: *Electroreception (Springer Handbook of Auditory Research)* (T. H. Bullock, C. D. Hopkins, A. N Popper, R. R. Fay, eds.) New York: Springer.

Nelson, M. E., MacIver, M. A., and Coombs, S. (2002). Modeling electrosensory and mechanosensory images during the predatory behavior of weakly electric fish. *Brain Behav. Evol.*, vol. 59, pp. 199-210.

Rasnow, B. (1996). The effects of simple objects on the electric field of *Apteronotus*. *J. Comp. Physiol. A*, vol. 178, pp. 397-411.

Rasnow, B., Assad, C., and Bower, J. M. (1993). Phase and amplitude maps of the electric organ discharge of the weakly electric fish, *Apteronotus leptorhynchus*. *J. Comp. Physiol. A*, vol. 172, pp. 481-491.

Rasnow, B., Assad, C., Nelson, M. E., and Bower, J. M. (1989). Simulation and measurement of the electric fields generated by weakly electric fish. In: *Advances in Neural Information Processing Systems.* (Touretzky, D. S., ed.) San Mateo, CA: Kaufmann Publishers.

Rasnow, B. and Bower, J. M. (1996). The electric organ discharges of the gymnotiform fishes: *I. Apteronotus leptorhynchus*. *J. Comp. Physiol. A*, vol. 178, pp. 383-396.

Rother, D., Migliaro, A., Canetti, R., Gomez, L., Caputi, A., and Budelli, R. (2003). Electric images of two low resistance objects in weakly electric fish. *Biosystems*, vol. 71, pp. 171-179.

Scheich, H. and Bullock, T. H. (1974). The detection of electric fields from electric organs. In: *Electroreceptors and Other Specialized Receptors in Lower Vertebrates.* (Fessard, A., ed.) Berlin: Springer-Verlag.

von der Emde, G. (1999). Active electrolocation of objects in weakly electric fish. *J. Exp. Biol.*, vol. 202, pp. 1205-1215.

von der Emde, G., Schwarz, S., Gomez, L., Budelli, R., and Grant, K. (1998). Electric fish measure distance in the dark. *Nature*, vol. 395, pp. 890-894.

Yamashita, E. (1990). *Analysis Methods for Electromagnetic Wave Problems*. Boston: Artech House.

Zakon, H. H. (1986). The electroreceptive periphery. In: *Electroreception* (eds. Heiligenberg, W. and Bullock, T. H.)

CHAPTER 4

ARTICLE II

A Study of Electro-Acuity and Motion Parallax in Weakly Electric Fish.

D. Babineau, J. E. Lewis and A. Longtin

To be submitted.

A Study of Electro-Acuity and Motion Parallax in Weakly Electric Fish

David Babineau[1], John E. Lewis[2] and André Longtin[1,*]

1 Department of Physics, University of Ottawa, Ottawa, Ontario K1N 6N5, Canada, 2 Department of Biology, University of Ottawa, Ottawa, Ontario K1N 6N5, Canada

*To whom correspondence should be addressed. E-mail: alongtin@uottawa.ca

It is well-known that weakly electric fish can exhibit extreme temporal acuity at the behavioral level, discriminating time intervals in the sub-microsecond range. However, relatively little is known about the spatial acuity of the electrosense. Here we use an electric field model of *Apteronotus leptorhynchus* to study spatial acuity and signal extraction in the spatial domain. Using the "just noticeable difference" (JND; measure of spatial acuity) between identical adjacent objects, we show that spatial acuity is highest (i.e. resolution is best) in the fish's midbody, and decreases for objects placed farther away from the fish. Spatial acuity was the same regardless of object conductivity, but improved for low water conductivity values. Spatial acuity also improved with increasing object size, especially near the fish. As a whole, however, spatial acuity was found to be fairly poor in comparison with human visual acuity. Despite this roughness in the electrosense, weakly electric fish are able to extract small signals generated by prey extremely well, even in the presence of large background signals. We have simulated a commonly observed behavior in these fish, back-and-forth scanning, and show that a small prey-like object can be discerned from a large plant-like context due to "motion

parallax"-like cues. We find that while the electric image component due to the prey changes location during fish scanning, the component due to the plant-like context does not. This is the first study that suggests how weakly electric fish might use scanning cues to electrolocate objects. Furthermore, we show that this task could, in principle, be accomplished by the fish using either of two distinct neural computations, i.e. subtraction or scaling.

Introduction

Weakly electric fish, which live in dark and murky South American and African waters [1, 2], use a unique sensory modality, called the "electrosense", to help them navigate, communicate and find prey in the absence of strong visual cues [3]. These fish emit an electric discharge from an electric organ situated within their body resulting in a dipolar electric field in the surrounding waters [4]. The transdermal potential, called "electric image", is continuously monitored via electro-receptors found in the skin layer. Changes in the electric image's shape (likely) act as cues that help the fish determine the location, size and electrical properties of nearby objects [5-8].

Recent studies have shed new light on the weakly electric fish's perceptual world. Lewis and Maler [9] have reported that for distance perception, some electrosensory cues (contained in electric images) were analogous to visual contrast and blur. In addition, Rother *et al.* [10] have shown that the electric image produced by an object is distorted by nearby objects; consequently, conductive objects can act as "electrosensory mirrors". In contrast with the visual sense, however, it has been suggested that the electrosense is

limited to the near-field, and is hence considered as a "rough" sensory modality [11-13]. In fact, research has shown that the range of active electrolocation in weakly electric fish is only about one body length away from the fish [7], and considerably less for small prey-like objects [14]. Within this range, much is known about the fish's temporal acuity [15, 16], but relatively little is known about the fish's ability to resolve multiple nearby objects (spatial acuity).

The first goal of this paper was therefore to quantify this spatial acuity. To this end, we have introduced the notion of "electro-acuity", analogous to the notion of visual acuity found in the visuo-sensory lexicon, in order to estimate the "sharpness" of the fish's electrosense in the spatial domain. A common measure of acuity as applied to other sensory systems is the Just Noticeable Difference (JND). The JND is the minimum difference between two stimuli such that a difference can be perceived [17] (e.g the minimal separation between two sharp points touching a human's skin such that the human is still able to differentiate between these points). In the present context, we consider this difference to be the minimum spatial separation of two objects for there to be two distinct peaks in the fish's electric image. Using a two-dimensional finite element method model of *Apteronotus leptorhynchus'* electric field (previously described in [8]), we show that the JND is smallest in the fish's midbody, and decreases for objects placed further away from the fish. This is surprising given the high density of electroreceptors in the skin of the head region [18], often assumed to the electric "fovea" of the fish [14]. We also find that electro-acuity is poor, relative to visual acuity in humans.

Despite the apparent low-acuity in the electrosensory modality, weakly electric fish are known to be remarkably efficient in detecting small prey, even in the presence of

extremely noisy background signals [7, 19]. The second goal of this paper was to explore this phenomenon. It is believed that some of the natural behaviors exhibited by the fish play a central role in this signal extraction task. Particularly, simulations have shown that tail bending could, in principle, improve the information gathered from an electrosensory scene [11, 12]. It has also been suggested that the back-and-forth hovering, or scanning, motion observed in these fish could be used to generate specific electrolocation cues [20, 21], although this has not been shown as of yet. We have simulated this motion and shown that this behavior could indeed assist in extracting small prey-like signals from large background ones. We show that, while the electric image produced by objects in the background does not change during scanning, the one produced by the prey, albeit miniscule in comparison, does. By comparing the dynamic prey images to the relatively constant background image, we illustrate that prey information can easily be extracted from background clutter. This suggests that weakly electric fish hover back and forth in order to generate motion parallax-like cues, and thereby separate small nearby objects from farther away, larger ones.

Results

In the following, we use our previously described finite element model of the electric field produced by *Apteronotus leptorhynchus* (see Materials and Methods section and [8]). Figure 4.1A shows the simulated dipolar potential map of this fish in the presence of two prey-like objects (see Materials and Methods section for object specifications). The objects do not greatly perturb the fish's "natural" field due to their

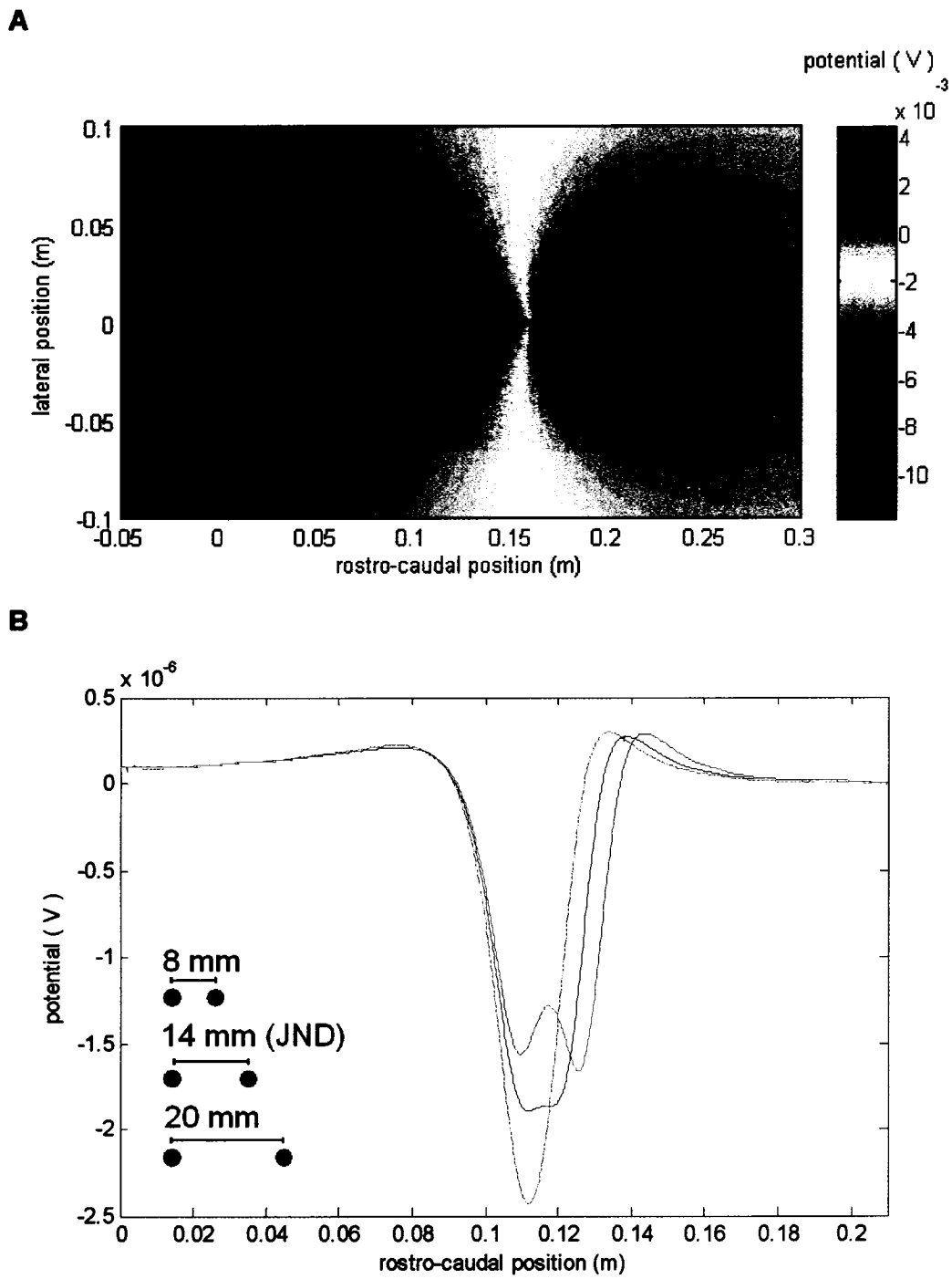

Figure 4.1. Electric Images Produced by Two Prey-like Objects and Just Noticeable Difference (JND)

(A) Electric field potential in the presence of two identical prey-like objects (modeled as 3 mm-diameter discs with a conductivity of 0.0303 S/m; water conductivity: 0.023 S/m).

Objects do not affect the field much due to their size and conductivity. The JND (14 mm) is also shown for a specific prey position (left prey located 11 cm caudally from the tip of the head and 12 mm laterally to the skin).
(B) Electric images for three distinct inter-prey distances (see inset). Blue trace shows JND, when the two peaks in the electric image are just noticeable.

minute size and due to their conductivity which isn't significantly different from that of the water. Figure 4.1B shows the electric images produced by the objects for three different inter-object distances (shown in inset). Prey which are located too close together (green trace) produce a single peak in the electric image, while prey separated by a relatively large distance produce two clearly distinct peaks in the electric image (red trace). The blue trace illustrates the electric image in which two peaks are just barely noticeable; the distance between the two prey that produced this image is the just noticeable difference (JND). A small JND indicates good electro-acuity (i.e. good spatial resolution). For this specific rostro-caudal object location, the JND is 14 mm. This suggests that, at this lateral distance, the objects must be separated by 14 mm, a distance approximately 5 times their diameter, for the fish to distinguish the two prey.

Figure 4.2 characterizes electro-acuity for different lateral and rostro-caudal positions (see insets). Figures 4.2A and 4.2C show the effects of object size and conductivity, respectively, on electro-acuity for different lateral positions (rostro-caudal position fixed near the fish's midpoint, 0.11 m). Electro-acuity decreases (JND increases) for objects that are placed farther away from the fish, regardless of object size or conductivity. For objects located close to the fish, electro-acuity is greatly improved for the biggest object. When objects are far from the fish, the JND is roughly independent of object size. Figures 4.2B and 4.2D show the effects of object size and conductivity,

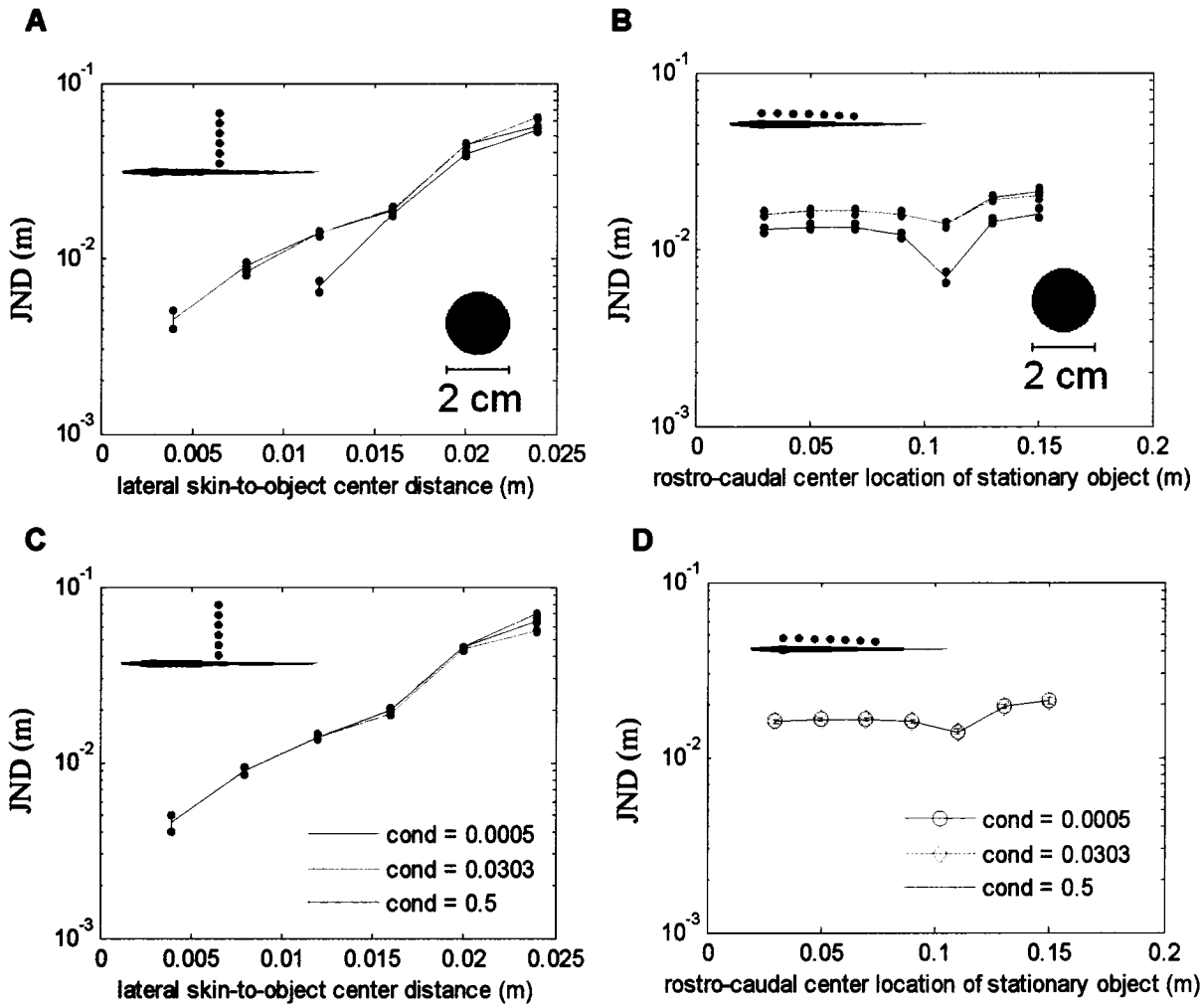

Figure 4.2: Effect of Object Location and Conductivity on Spatial Electro-Acuity
See fish insets for approximate lateral and rostro-caudal locations where the JND was calculated. Error bars represent the sampling which was used in order to calculate the JND (either 0.5 or 1 mm).
(A) Effect of lateral distance on JND for three distinct object diameters. Red: 3 mm (prey size), green: 10 mm, blue: 20 mm. Object conductivity fixed at 0.0303 S/m (prey conductivity).
(B) Effect of rostro-caudal position on JND for same object sizes and conductivity as (A).
(C) Effect of lateral distance on JND for three distinct object conductivities. Red: 0.0005 S/m (plant conductivity), green: 0.0303 S/m (prey conductivity), blue: 0.5 S/m. Object diameters fixed at 3 mm (prey size).
(D) Effect of rostro-caudal position on JND for same object diameter size and conductivities as (C).

respectively, on electro-acuity for different rostro-caudal positions (lateral object center-to-skin distance fixed at 12 mm). Large objects are resolved more efficiently than smaller ones, all along the length of the fish; the 2 cm-diameter objects can actually be distinguished while overlapping (i.e. while the two objects are fused into a new composite object), contrary to smaller objects (e.g. the two 2-cm diameter objects' centers in Figure 4.2B, x = 0.11 m, are separated by only 7 mm). The position x = 0.11 m corresponds to the point of optimal acuity, because this is the rostro-caudal location where electric images are sharpest [8], indicating that two peaks can be distinguished more easily in this region due to the minimal overlap of the individual images. Overall, the JND varies much more in the lateral direction in comparison with the rostro-caudal direction, as can be seen e.g. by comparing Figures 4.2C and 4.2D. This is due to the relatively large changes in image width as lateral object distance increases. Object conductivity has comparatively little effect on the JND in both lateral and rostro-caudal directions.

The effect of water conductivity on electro-acuity was also studied for a specific location (x = 0.11 m, y = 15 mm). For the range of water conductivity values found in the rivers in which *Apteronotus leptorhynchus* live (between 8.5 and 113.5 μS/cm [2]) the JND changes only slightly. As an overall trend, electro-acuity increased as water conductivity diminished: the JND decreased from 15.5 to 12.5 mm as water conductivity decreased from 500 to 5 μS/cm.

In order to understand electro-acuity more thoroughly, the electric images of differently-sized background contexts were studied systematically. In Figure 4.3, the electric images for different numbers of "plant-like" (*Hygrophilia*; see Material and

Methods section) objects are shown (centered rostro-caudally, at a lateral distance of 5 cm). The blue trace shows the electric image produced by a single such object located 11 cm caudally from the tip of the fish's head (blue object in inset located close to the fish's midpoint). The red trace shows the electric image produced by three objects: the central (blue) one plus one (red) disc added 3 cm on each side. Images are shown for up to a total of eleven discs. As the context widens (i.e. larger number of aligned objects), the electric images converge. For a context as wide as the fish (seven discs), the amplitude and overall match is almost the same as with eleven discs. The electric images are each marked by a singular peak because the inter-disc distance is too small (at this lateral distance of 5 cm) to resolve different peaks. The small bumps at approximately 3 and 20 cm are due to abrupt changes in fish geometry near the head and tail, respectively, and are not due to objects. Additionally, tests were conducted for smaller lateral positions, where different peaks were observed in the electric image, and convergence also occurred for broad contexts (not shown). We also tested solid bars of increasing widths and the electric images here too converged (and resembled the ones obtained with the discs; not shown).

Weakly electric fish are able to electrolocate miniscule prey, even in the presence of large background signals. To better understand how this is possibly achieved, we simulated a large, 15-disc plant-like context and a small *Daphnia*-like prey object (Figure 4.4). Even though the prey's center is located only 8 mm away from the fish's skin (compared to the 5 cm lateral position of the context), the electric image with the prey is not much different than the one obtained without the prey (largest deviation between the two curves is 4%). To further illustrate the effects of this type of large context, we

attempted to measure electro-acuity at a specific location (x = 0.11 m, y = 15 mm) for prey-like objects. Whereas a JND of 14 mm was obtained without the context, the two objects were not even distinguishable when separated by 40 mm while in the presence of the plant-like structure (i.e. no separate peaks due to the two prey emerged in the electric images as the objects were separated to this distance).

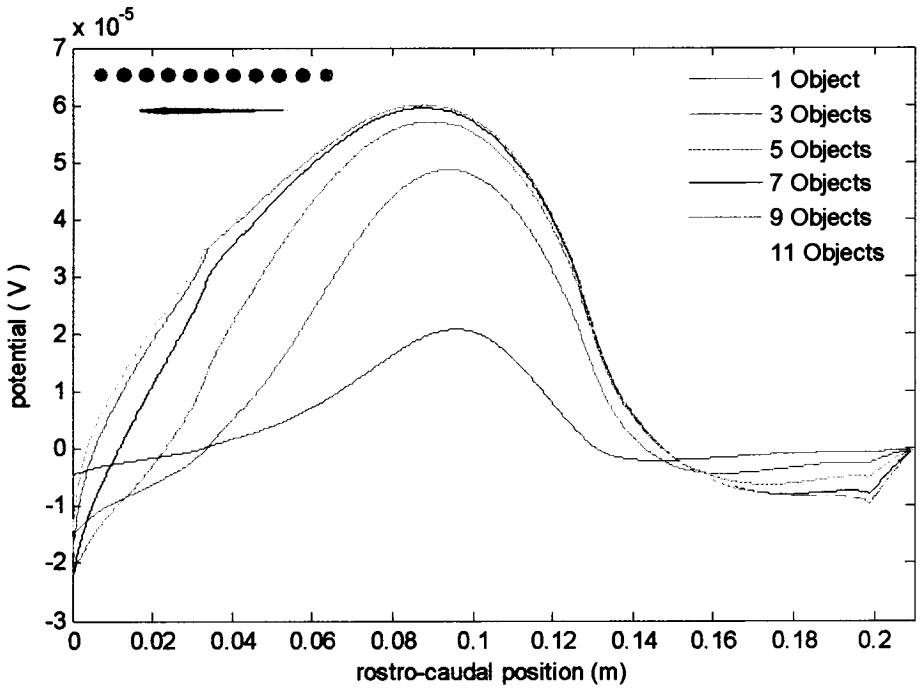

Figure 4.3. Effect of a Plant-like Context on Electric Image Shape
Electric images produced by six distinct context widths, which differ in number of discs (see inset). Blue: 1, red: 3, green: 5, black: 7, cyan: 9, orange: 11. The 2 cm-diameter discs have a conductivity of 0.0005 S/m to mimic the plant *Hygrophilia*. Discs are located 5 cm away laterally from the fish's midline and are separated, one from another, by 3 cm. All series of objects are centered near the fish's midpoint (blue object in inset) and color in inset denotes external objects of a given series.

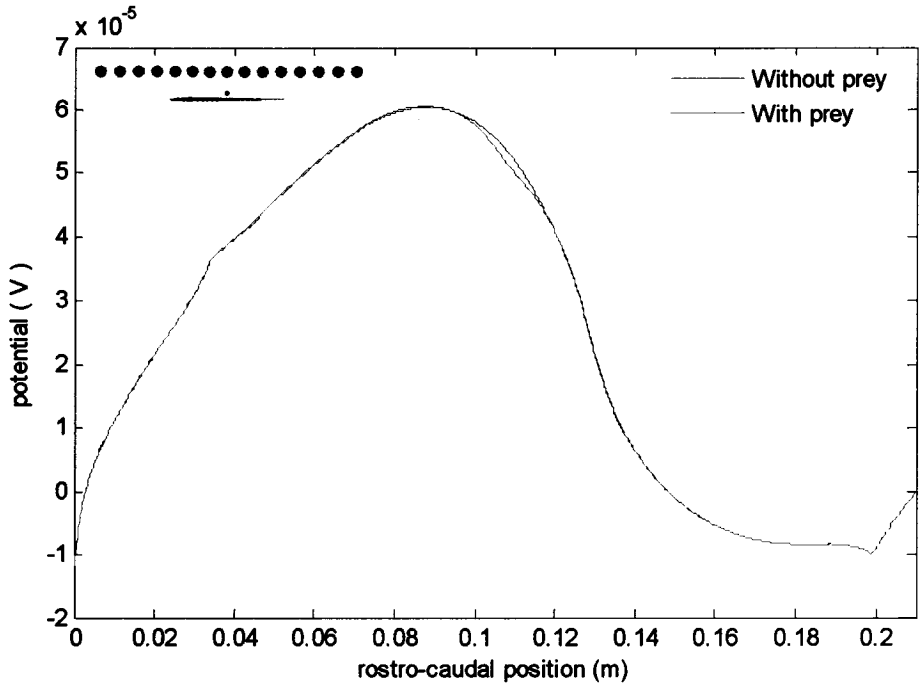

Figure 4.4. Electric Image of a Plant-like Context in the Presence and Absence of a Prey-like Object

Electric image produced by a 15-disc *Hygrophilia* plant-like context (blue trace) is only slightly modified when a small *Daphnia*-like prey object (3 mm-diameter disc; conductivity: 0.0303 S/m) is added (red trace). Prey is located around the fish's midpoint, 8 mm away laterally. Plant context is located 5 cm away laterally.

Electric images produced by an electrosensory scene consisting of a single prey plus a plant-like context were then calculated for different rostro-caudal fish positions (to simulate scanning, Figure 4.5A). Figure 4.5B shows that the prey's presence within the electric image does not stand out, regardless of the fish's position. The small blip created by the prey does, however, change location within the electric image while the electric image component due to the context does not. This demonstrates that the commonly observed scanning behavior [20] of these fish could enable prey detection through a

comparison of the dynamic prey images to the relatively constant "background" image. This comparison could be made in two simple ways (Figures 4.5C and 4.5D); in both, we consider a reference background image as the average of the six images shown in Figure 4.5B. The first method involves dividing the individual images by the reference background image (Figure 4.5C). The second method involves subtracting the reference background image from the individual images (Figure 4.5D; means of resulting images are subtracted to show zero-mean images). Both methods reveal the dynamic component of the image sequence (due to the prey, denoted by the vertical arrows in Figures 4.5C and 4.5D) from the constant background (reference image). The caudal end shows noise in the ratios (for Figure 4.5C) which arise due to the fish's zero-potential line which is situated close by. The rostro-caudal range in Figures 4.5C and 4.5D is shown delimited by dotted lines in Figure 4.5B.

Discussion

In addition to human senses, sensory modalities unique to other species have also garnered much attention in recent years [22]. Indeed, the electrosensory system exhibits many parallels with other senses, including human vision and audition [9, 23]. This indicates that a better understanding of the weakly electric fish's electrosense could hence provide insight into mechanisms and general principles of sensory processing.

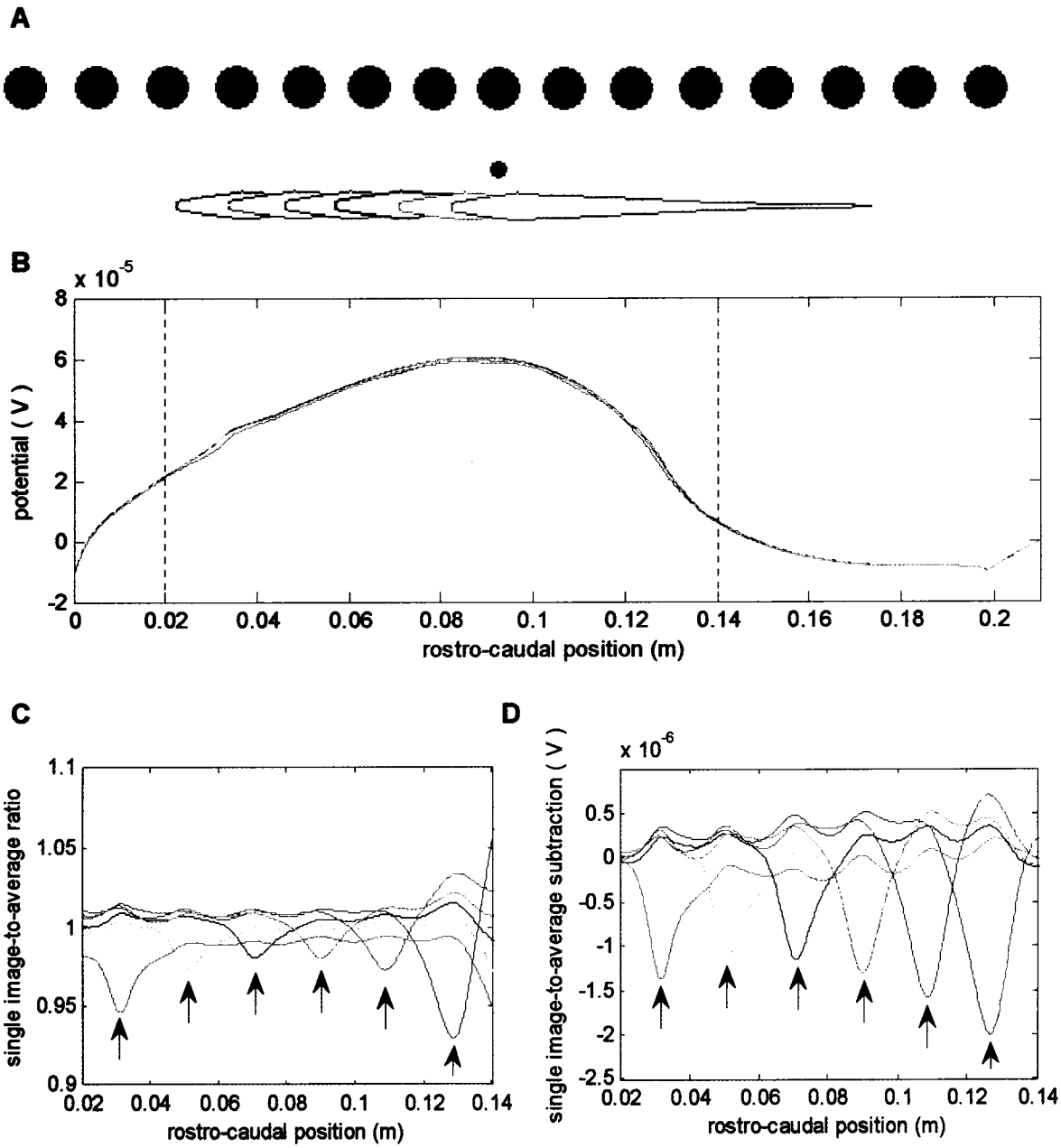

Figure 4.5. Effect of Fish Location on Electric Image Produced by a Plant-like Context and a Prey-like Object

(A) Six rostro-caudal fish positions for which the electric image produced by a 15-disc *Hygrophilia* plant-like context plus a *Daphnia*-like prey were calculated. Positions differ from one another by 2 cm (image not exactly to scale).

(B) Electric images produced by context and prey for six fish locations shown in (A). Vertical dotted lines show rostro-caudal limits used in (C) and (D).
(C) Ratio of single electric images shown in (B) with the average of the six electric images shown in (B). Arrows indicate relevant peaks for each fish position.
(D) Single electric images shown in (B) subtracted from the average of the six electric images shown in (B). The mean was then computed for each resulting curve, and then subtracted from each resulting curve in order to center all curves on zero-mean (for x = [0, 21] cm interval). Arrows indicate relevant peaks for each fish position.

Electro-Acuity Measurement

In order to complement recent studies which have broadened our understanding of the electrosense [8, 19, 21, 24, 25], we have introduced the notion of electro-acuity. This measure, comparable to the notion of visual acuity found in the visuo-sensory lexicon, has helped us quantify the "sharpness" of the electrosense in the spatial domain. Studies have suggested that this was a rather "rough" sensory modality [7, 12], and our findings confirm this. For example, we found a JND of 9 mm for two prey-like objects (3 mm diameter) located within the range of natural prey detection (which is typically less than 2 cm, [14]), i.e. 8 mm lateral from the fish's skin (Figure 4.2). By contrast, this would be equivalent to only being able to visually distinguish two nearby apples if they were separated by 25 cm.

It is interesting to note, however, that for objects located near the fish's surface, bigger objects can be distinguished more efficiently, to the point that they even physically overlap (simulated by merging the two discs into a new composite object). This is a result of the object's proximity to the skin surface, since, when placed far from the fish, all objects are equally discernable. A point of optimal electro-acuity, located in the fish's midbody, has been revealed by our study. This is counter-intuitive since one would think

that this optimal location would be located near the fish's head, where most electroreceptors are localized [18]. However, the combination of body geometry and current density make it so that electric images are sharpest in the midbody [8], thus allowing the objects to be closer in that region without much overlap in the electric images. A trade-off between more receptors rostrally and optimal images more caudally may explain why prey detection occurs at approximately equal rates over all rostro-caudal locations [14].

We have shown that electro-acuity did not vary with object conductivity. This implies that the fish's ability to resolve equally-sized animate and inanimate objects (which differ in conductivity) is the same. However, it is possible that the addition of environmental noise to the electric images would make one of these types of objects more "resolvable", as the signal-to-noise ratio would be greater for high conductivity objects. Water conductivity, on the other hand, does (slightly) affect the JND. Our results are in accord with other findings which state that object detection is best achieved in low-conductivity water [14, 26, 27]. This seems to indicate that water conductivity acts as a type of "electrosensory fog".

The values of JND obtained here can be considered at the same time as upper-bound and as lower-bound limits. On the one hand, they act as upper-bound limits since the fish most likely uses additional cues from the electric image in order to distinguish adjacent objects. Specifically, the electric image produced by two objects which aren't discriminable is still wider than the image of one of the objects alone. On the other hand, our JND values act as lower-bound limits since noise would undoubtedly make the real JND measurements higher. Moreover, the JND measure used in this paper is only valid

for predicting the fish's ability to discern two adjacent objects located in parallel with the fish's contour. Indeed, different JND criteria need to be formulated in order to measure the JND of objects which are situated one "behind" the other (or rather, which are perpendicular to the fish's contour; Rother *et al.* [28] have studied such object locations, but not in the context of spatial acuity). It would be of interest to corrobate our results (predictions) with real JND measurements in weakly electric fish. Measuring the fish's JND could be done using a forced-choice experimental paradigm. In this task, the fish would be trained to choose between a single and a "double" object, with a reward given for the choice of the latter. The accuracy of the choices would be measured as the inter-object distance was decreased to provide an estimate of the JND (see [24, 29, 30] for similar protocols).

Motion Parallax in Weakly Electric Fish

Weakly electric fish are subject to a wide range of stimuli: rocks, plants and prey are just some of the elements which comprise the electrosensory landscape. While some changes in the electric image such as those due to tail bending [7] could in principle be compensated for in the higher brain, other stimuli, such as large conducting boundaries (rocks or the river bottom), constitute huge background clutter which is extraneous to the fish [19]. The fish therefore has the challenging task of extracting small prey signals from enormous background ones.

In order to investigate this scenario, we have modeled a plant-like context. We have shown that, as this context was widened, the electric images converged. In fact, the image is not much different for a context that is 18 cm long than for one that is 30 cm

long. In the visual system, this is similar to a human standing a foot an a half away from a wall and not being able to tell whether this wall is six feet or twenty feet wide. This again illustrates that the electrosense is a rough sensory modality. In the presence of such a large context, the JND was no longer measurable, since the electric image component due to the context drowned out the component due to the two prey.

Figure 4.4 clearly indicates that the effect of a prey is miniscule in the presence of relatively large contextual objects. Even when our simulated fish scanned back-and-forth, at no instant was there a considerable difference in the electric images produced by the context plus prey or the context alone. On the other hand, weakly electric fish are known to detect minuscule signals under natural conditions [31]. We suggest that movement is required, and that for any static "snapshot", the fish would not be able to extract the prey from a large background signal. In fact, the convergent nature of the plant-like objects' image made it so that this fairly constant image did not change with fish scanning, in contrast to the small prey-generated blips (see Figure 4.5B). Therefore, using simple scaling or subtraction algorithms, both of which have been shown to be feasible neuronal computations [32, 33], we show that relevant prey information can be extracted using motion cues.

While it is known that motion parallax plays a central role in object localization in other species (see e.g. [34]), this is the first study that suggests how these cues may be used in weakly electric fish (and hereby possibly explaining the back-and-forth scanning motion described in the literature [20, 35]). This seems to indicate that exploratory behaviors exhibited by weakly electric fish, such as the aforementioned scanning and tail bending, act primarily as tools to help fish extract relevant information from the

surrounding electrosensory scene. Fish might exhibit the behavior that is most suitable to signal extraction, given the context which surrounds them. The scanning technique shown here could be acceptable for "convergent" or relatively constant backgrounds; it might, however, fail for contexts which are more irregular. For such cases, the fish might preferentially use tail bending. It would be very illuminating to study which behaviors are used most frequently by the fish to explore electrosensory landscapes in the presence of varying contexts.

Materials and Methods

The two-dimensional electric field of a 21 cm *Apteronotus leptorhynchus* was simulated using a finite element method model described previously in [8]. Briefly, the model is comprised of three components: an electric organ (EO), a body compartment and a thin skin layer. The EO current density and the conductivities of the three components were optimized using raw data provided by Christopher Assad. Electric images were calculated as the differences in transdermal potential with and without objects (using MATLAB subroutines). All images are shown for the side of the fish body closest to the objects only. Water conductivity was set to 0.023 S/m, as in [28]. The prey chosen, *Daphnia magna*, was modeled as a 3 mm-diameter disc with a conductivity of 0.0303 S/m [13, 14]. The background context simulated throughout this paper is based on the aquatic plant *Hygrophilia*; its conductivity was set to 0.0005 S/m [36] and its geometry was approximated by using a series of 2 cm-diameter discs, spaced 3 cm one from another. The goal here was not to mimic the plant's geometry accurately, but rather

to get a general idea of the effects caused by a context with plant-like conductivity and size.

In order to estimate the fish's ability to resolve two distinct objects (electro-acuity), the Just Noticeable Difference (JND) was calculated. This measure is the inter-object distance which delimits electric images with one peak from those with two peaks (i.e. those caused by the two objects and not the troughs which may appear on either side: see e.g. Figure 4.1B). The rostral object's center coordinates were chosen as the spatial location for which the JND was determined. Therefore, this object was held stationary during a given JND measurement. The caudal object was moved systematically in the rostral direction until two distinct peaks appeared in the electric image (object center-to-skin distance was kept constant). Using this technique, JND measurements were accurate to within 0.5 or 1 mm, representing the chosen sampling (see error bars in Figure 4.2).

Acknowledgements

This research was partially funded by research grants from the Natural Sciences and Engineering Research Council of Canada to AL and JL.

[1] Moller, P. (1995). *Electric Fishes: History and Behavior.* London: Chapman & Hall.

[2] Crampton, W. G. R. (1998). Electric signal design and habitat preferences in a species rich assemblage of gymnotiform fishes from the Upper Amazon basin. *Anais da Academia Brasileira de Cięncias*, vol. 70, pp. 805-847.

[3] Lissman, H. W. and Machin, K. E. (1958). The mechanism of object location in *Gymnarchus niloticus* and similar fish. *J. Exp. Biol.*, vol. 35, pp. 451-486.

[4] Knudsen, E. I. (1975). Spatial aspects of the electric fields generated by weakly electric fish. *J. Comp. Physiol.*, vol. 99, pp. 103-118.

[5] Rasnow, B. (1996). The effects of simple objects on the electric field of *Apteronotus*. *J. Comp. Physiol. A*, vol. 178, pp. 397-411.

[6] Caputi, A. A., Castello, M. E., Aguilera, P., and Trujillo-Cenoz, O. (2002). Electrolocation and electrocommunication in pulse gymnotids: signal carriers, pre-receptor mechanisms and the electrosensory mosaic. *J. Physiol. Paris*, vol. 96, pp. 493-505.

[7] Nelson, M. E. (2005). Target detection, image analysis and modeling. In: *Electroreception (Springer Handbook of Auditory Research)* (T.H. Bullock, C.D. Hopkins, A.N Popper, R.R. Fay, eds.) New York: Springer.

[8] Babineau, D., Longtin, A., and Lewis, J. E. Modeling the electric field of weakly electric fish. *Submitted to the Journal of Experimental Biology.*

[9] Lewis, J. E. and Maler, L. (2002). Blurring of the senses: common cues for distance perception in diverse sensory systems. *Letters to Neuroscience*, vol. 114, pp. 19-22.

[10] Rother, D., Migliaro, A., Canetti, R., Gomez, L., Caputi, A., and Budelli, R. (2003). Electric images of two low resistance objects in weakly electric fish. *Biosystems*, vol. 71, pp. 171-179.

[11] Heiligenberg, W. (1975). Theoretical and experimental approaches to spatial aspects of electrolocation. *J. Comp. Physiol.*, vol. 103, pp. 247-272.

[12] Bacher, M. (1983). A new method for the simulation of electric fields, generated by electric fish, and their distorsions by objects. *Biol. Cybern.*, vol. 47, pp.

51-58.

[13] Nelson, M. E., MacIver, M. A., and Coombs, S. (2002). Modeling electrosensory and mechanosensory images during the predatory behavior of weakly electric fish. *Brain Behav. Evol.*, vol. 59, pp. 199-210.

[14] MacIver, M. A., Sharabash, N. M., and Nelson, M. E. (2001). Prey-capture behavior in gymnotid electric fish: motion analysis and effects of water conductivity. *J. Exp. Biol.*, vol. 204, pp. 543-557.

[15] Rose, G. J. and Heiligenberg, W. (1985). Temporal hyperacuity in the electric sense of fish. *Nature*, vol. 318, pp. 179-180.

[16] Kawasaki, M. (1997). Sensory hyperacuity in the jamming avoidance response of weakly electric fish. *Curr Opin Neurobiol*, vol. 7, pp. 473-479.

[17] Martin, J. H. (1991). Coding and processing of sensory information. In: *Principles of Neural Science*. (E. R. Kandel, J. H. Schwartz, T. M. Jessell, eds.) Norwalk, Conneticut: Appleton & Lange.

[18] Carr, C. E. , Maler, L., and Sas, E. (1982). Peripheral organization and central projections of the electrosensory nerves in gymnotiform fish. *J. Comp. Neurol.*, vol. 211, pp. 139-153.

[19] Chen, L., House, J. L., Krahe, R., and Nelson, M. E. (2005). Modeling signal and background components of electrosensory scenes. *J. Comp. Physiol. A*, vol. 191, pp. 331-345.

[20] Toerring, M. J. and Belbenoit, P. (1979). Motor programmes and electroreception in Mormyrid fish. *Behav. Ecol. Sociobiol.*, vol. 4, pp. 369-379.

[21] Lewis, J. E. and Maler, L. (2001). Neuronal population codes and the perception of object distance in weakly electric fish. *J. Neurosci.*, vol. 21, pp. 2842-2850.

[22] Hughes, H. C. (1999). *Sensory Exotica: A World Beyond Human Experience.* Cambridge: MIT Press.

[23] Montgomery, J., Coombs, S., Conley, R. A., and Bodznick, D. (1995). Hindbrain sensory processing in lateral line, electrosensory and auditory systems: a comparative overview of anatomical and functional similarities. *Auditory*

Neur., vol. 1, pp. 207-231.

[24] von der Emde, G., Schwarz, S., Gomez, L., Budelli, R., and Grant, K. (1998). Electric fish measure distance in the dark. *Nature*, vol. 395, pp. 890-894.

[25] Migliaro, A., Caputi, A. A., and Budelli, R. (2005). Theoretical analysis of pre-receptor image conditioning in weakly electric fish. *PLoS Comp. Biol.*, vol. 1, pp. e162005.

[26] von der Emde, G. (1993). The sensing of electrical capacitances by weakly electric mormyrid fish: effects of water conductivity. *J. Exp. Biol.*, vol. 181, pp. 157-173.

[27] Wojtenek, W., Pei, X., and Wilkens, L. A.. (2001). Paddlefish strike at artificial dipoles simulating the weak electric fields of planktonic prey. *J. Exp. Biol.*, vol. 204, pp. 1391-1399.

[28] Assad, C. (1997). Electric field maps and boundary element simulations of electrolocation in weakly electric fish. Ph. D. thesis, California Institute of Technology, Pasadena, CA.

[29] Schwarz, S. and von der Emde, G. (2001). Distance discrimination during active electrolocation in the weakly electric fish *Gnathonemus petersii. J. Comp. Physiol. A*, vol. 186, pp. 1185-1197.

[30] Graff, C., Kaminski, G., Gresty, M., and Ohlmann, T. (2004). Fish perform spatial pattern recognition and abstraction by exclusive use of active electrocation. *Curr. Biol.*, vol. 14, pp. 818-823.

[31] Nelson, M. E. and MacIver, M. A. (1999). Prey capture in the weakly electric fish *Apteronotus albifrons*: sensory acquisition strategies and electrosensory consequences. *J. Exp. Biol.*, vol. 202, pp. 1195-1203.

[32] Gabbiani, F., Krapp, H. G., Koch, C., and Laurent, G. (2002). Multiplicative computation in a visual neuron sensitive to looming. *Nature*, vol. 420, pp. 320-324.

[33] Pena, J. L. and Konishi, M. (2001). Auditory spatial receptive fields created by multiplication. *Science*, vol. 292, pp. 249-252.

[34] Poteser, M. and Kral, K. (1995). The significance of head movements in distance

discrimination in praying mantis larvae. *J Exp Biol*, vol. 198, pp. 2127-2137.

[35] Toerring, M. J. and Moller, P. (1984). Locomotor and electric displays associated with electrolocation during exploratory behavior in mormyrid fish. *Behav. Brain Res.*, vol. 12, pp. 291-306.

[36] Heiligenberg, W. (1973). Electrolocation of objects in the electric fish *Eigenmannia* (Rhamphichthyidae, Gymnotoidei). *J. Comp. Physiol.*, vol. 87, pp. 137-164.

CHAPTER 5

EFFECT OF CONSPECIFICS ON THE ELECTRIC FIELD OF *APTERONOTUS LEPTORHYNCHUS*

5.1 Introduction

Weakly electric fish conspecifics are able to electrocommunicate with each other using their self-generated electric fields [1, 10, 14]. In order to mimic these communication signals, researchers [3, 6, 7] commonly use a single pair of electrodes, with one electrode on each side of the fish. This type of paradigm, referred to as the "transverse stimulation paradigm", is believed to mimic communication signals due to the spatially diffuse perturbations they produce. There is, however, little knowledge on the types of perturbations that actually occur when a conspecific is near. One study has measured the effect of a parallel and antiparallel conspecific on a pulse species' peak amplitude and waveform [1], but has not studied the rostrocaudal electric images they produce. In most cases, researchers study how simple objects affect the weakly electric fish's electric image [2, 4, 13]. Given the flexibility of the weakly electric fish model presented in Chapter 3, two interacting conspecifics were simulated in this chapter in order to see what types of perturbations occur for common types of relative fish-to-fish orientations. The transverse stimulation paradigm was also compared to such images in order to test how realistic this paradigm actually is and to see if better paradigms exist.

5.2 Methods

The two-dimensional electric field of the 21cm *Apteronotus leptorhynchus* used in this study was obtained using the morphologically accurate finite element fish model described in Chapter 3. All the modeled fish in the present study were identical, having the same head-positive phase described in Chapter 3. Electric images were calculated (using standard MATLAB subroutines) as the differences in transdermal potential in the presence and absence of objects (either a conspecific or a pair of electrodes in this study).

The transverse stimulation paradigm generally used to experimentally mimic the spatially diffuse, "global" stimuli produced by nearby conspecifics is described in [3]. This paradigm consists of two electrodes between which a time-varying electric stimulus is applied. These electrodes, placed at ~ 19 cm on either side of the fish, provide a stimulus of ~ 250 μV/cm (at the fish's midpoint, calibrated without the fish in place). We modeled these electrodes in COMSOL Multiphysics using 0.5 mm-diameter copper discs (conductivity: 5.99 x 10^7 S/m; aquarium size, grounding electrode, etc. as in Chapter 3). Each electrode's current source amplitude was adjusted (in the absence of any fish) until the aforementioned electric field was obtained in the middle of the aquarium, where the model fish is normally situated. Current sources of +/- 350 A/m^3 were found to reproduce the stimulus of ~ 250 μV/cm (note that the electrode amplitudes are of opposing polarity because the net current must be zero). While this may only mimic one phase of the stimulation paradigm, the effect in all other phases would only differ in absolute amplitude.

5.3 Results and Discussion

5.3.1 Effect of Conspecifics on the Electric Field and Electric Images of Weakly Electric Fish

Figure 5.1 shows the electric field potential of two interacting conspecifics for two common relative fish-to-fish orientations, namely when the fish are parallel (Figure 5.1A) and perpendicular (Figure 5.1B) to each other. In this chapter, the "upper" conspecific (oriented either parallel, antiparallel, perpendicular or antiperpendicular) will be considered as the "object" that produces an electric image on the "lower", "receiving" fish (always horizontal). The presence of a conspecific deforms the elongated dipolar electric field of the electric fish (this can be seen by observing the non-symmetric equipotential lines). The maximum (positive) potential value increases for the perpendicular orientation, due to the proximity of the perpendicular fish's head to the horizontal fish head (and thus the head-positive potentials add up).

It should be noted that these two orientations and their respective opposites (antiparallel and antiperpendicular; see Figure 5.5) are by no means considered as a comprehensive analysis of all orientations; the aim of this study is to gain general insights into the perturbations resulting from some common, stereotyped orientations. By the same token, it is unlikely that the oscillating discharges of the two conspecifics would have the same phases. Once again, the innumerable phase-to-phase combinations cannot be studied; the scenario chosen here constitutes a first logical step to study the largely unknown perturbations due to conspecifics. It will also give a good indication as to the efficacy of the currently-used transverse stimulation paradigm.

A

potential (V)

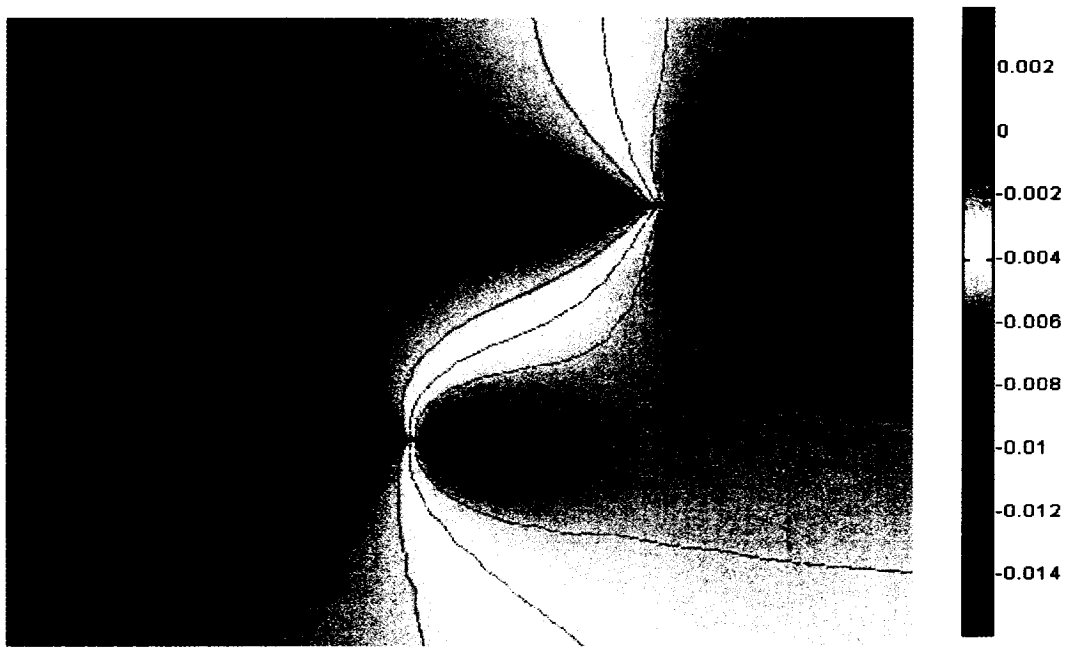

B

potential (V)

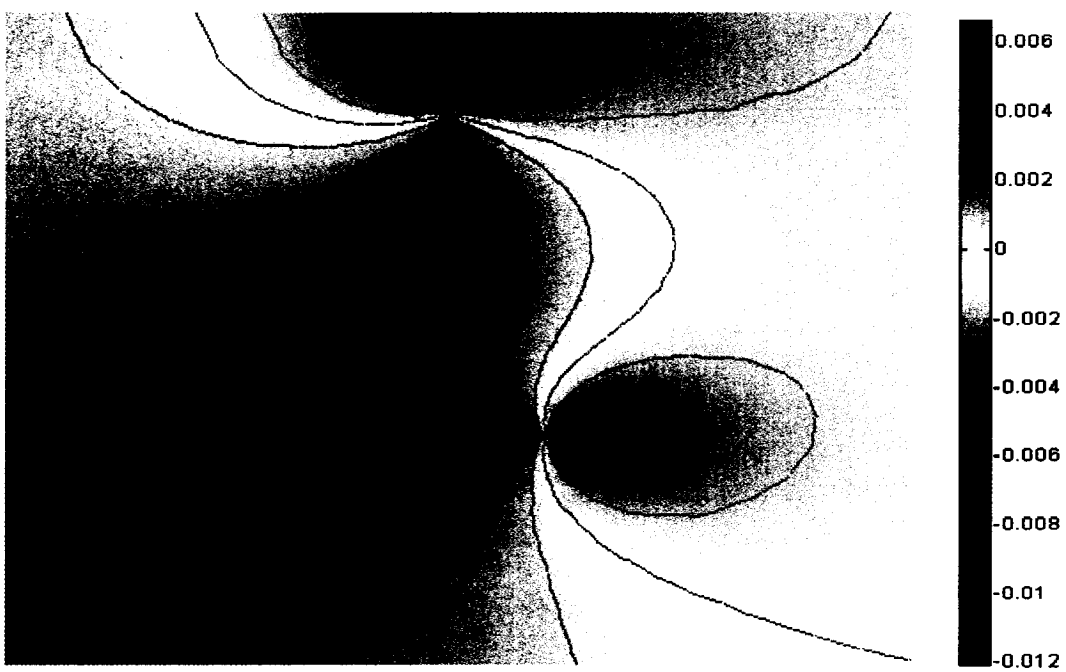

Figure 5.1: Electric field of two weakly electric fish. (A) Potential field of two parallel electric fish. Tips of the fish's head are separated laterally by 19 cm and rostro-caudally by 15 cm. (B) Potential field of two perpendicular electric fish. The vertical "object" fish is centered rostro-caudally at the horizontal, "receiving" fish's midpoint, 10.5 cm. The center of the vertical fish is also laterally situated 19 cm away from the horizontal fish's midline. Both fish used in (A) and (B) are identical, i.e. their length is the same (21 cm) as well as their EOD phase (head positive). X and Y axes not to scale (i.e. "y" dimension was compressed in for viewing purposes).

We have quantified the electric images generated by an adjacent parallel (Figure 5.2A) and perpendicular (Figure 5.2B) conspecific for different relative locations. The effect of simple, disc-like objects has been studied extensively [2, 4, 11, 13], but the effect of a conspecific on a "receiving" electric fish's electric image has remained unstudied. Whereas small, prey-like objects typically produce spatially narrow, Gaussian-like or "Mexican-hat"-like electric images [4, 12, 13], the images produced by another fish are larger in amplitude and more spatially diffuse (and hence their shapes differ greatly from Gaussian or Mexican-hat forms). As the parallel conspecific is moved caudally (Figure 5.2A), it causes the receiving fish's electric image to vary from a very non-uniform one to a spatially uniform one (the small kinks at the head and tail are due to changes in the model fish's geometry in those regions). This non-uniformity is due to the proximity of the parallel conspecifics' tail (which is highly negative) to the receiving fish's rostral field (which is weaker in amplitude).

For simple (disc-like) objects, typically, the electric image amplitude decreases as the object's lateral distance to the fish increases [2, 4, 13]. This also holds for a perpendicular conspecific as its lateral distance increases. However, when this conspecific

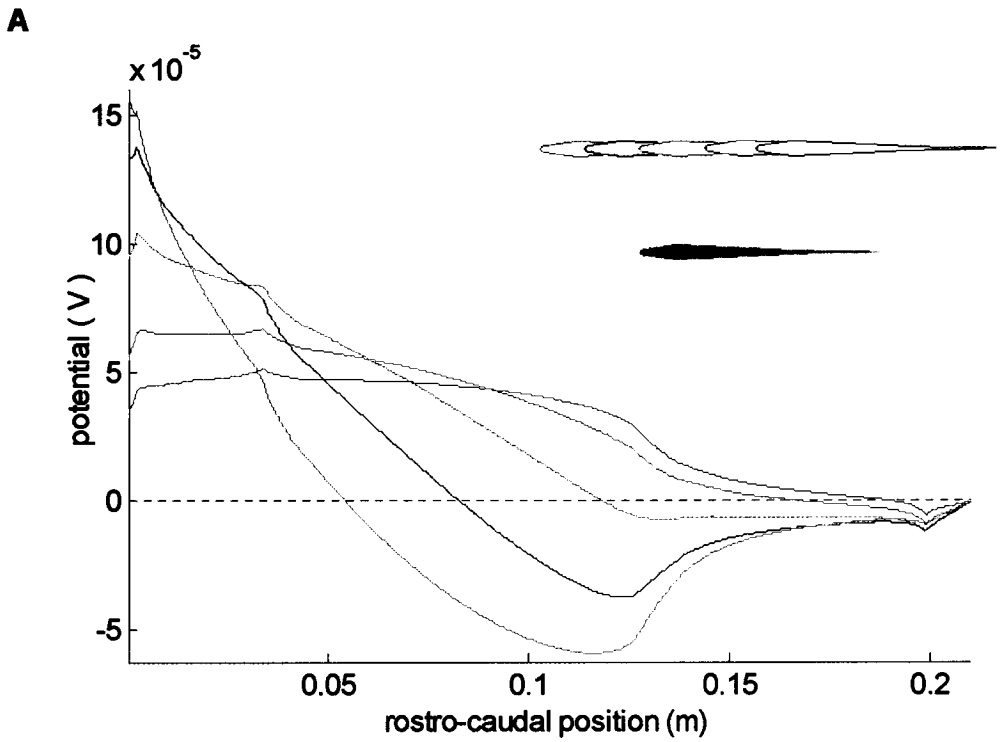
A
x 10^-5
15
10
5
0
-5
potential (V)
0.05
0.1
0.15
0.2
rostro-caudal position (m)

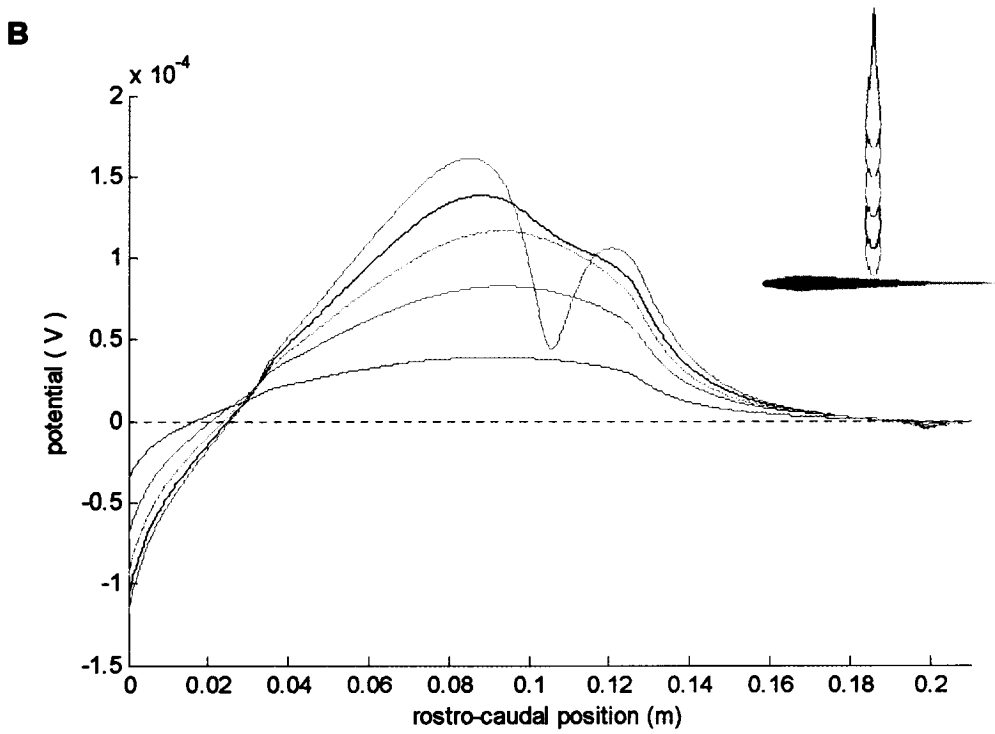
B
x 10^-4
2
1.5
1
0.5
0
-0.5
-1
-1.5
potential (V)
0
0.02
0.04
0.06
0.08
0.1
0.12
0.14
0.16
0.18
0.2
rostro-caudal position (m)

Figure 5.2: Electric images produced by a weakly electric fish conspecific. (A) Electric images produced on the receiving electric fish (grey fish in inset) by a parallel conspecific for different rostro-caudal locations (see inset). Electric images were calculated as the differences in transdermal potentials in the presence, and absence of the "object" conspecific. There is a 5 cm difference from one fish position to the next in the inset; therefore, cyan fish is located 10 cm rostral of the grey fish and blue fish is located 10 cm caudal of grey fish (inset fish positions not to scale). Tips of the fish's head are separated laterally by 19 cm. (B) Images produced on an electric fish (grey fish in inset) by a perpendicular conspecific for different lateral positions (see inset). Distance between the tip of the vertical fish's head and the horizontal fish's midline varies as follows; cyan: 0.5 cm, black: 1.5 cm, green: 3 cm, red: 5.5 cm, blue: 10.5 cm (inset fish positions not to scale). Electric images are shown for one side only: the grey fish's side closest to the conspecific (i.e. the ipsilateral side).

is really close to the receiving fish's body (cyan curve, Figure 5.2B), the electric image's shape changes drastically. This seems to indicate that whereas the insulating property of the fish's head does not affect the receiving fish's electric image for large lateral distances, it does at short distances (hence creating a dip in the image).

The images obtained in Figure 5.2 show that perturbations caused by nearby conspecifics differ greatly in shape and size, and that these perturbations depend on fish orientation and location. Moreover, these images are not as simple as those obtained with simple, prey-like objects. These differences could provide cues to the fish in order to differentiate between prey-like and conspecific-like signals.

The next section takes a look at how researchers currently mimic conspecific signals and offers suggestions on how to deliver more realistic stimuli using a simple pair of electrodes.

5.3.2 Mimicking a Conspecific Using a Pair of Electrodes

In order to simulate conspecific-generated, communication-like signals, researchers commonly use a transverse stimulation paradigm [3, 6, 7]. This experimental paradigm consists of two electrodes equidistantly placed about lateral to the fish, through which a sinusoidal signal (whose amplitude can be varied), in addition to the fish's own electric organ discharge (EOD; recorded from two additional electrodes located at the fish's head and tail, along the midline), is applied (see Figure 5.3A, middle panel). The resulting stimulation signal is characterised by beats (in the temporal domain). This stimulus is believed to mimic the effects of a nearby conspecific since the superposition of two EODs with different frequencies (i.e. the receiving fish's EOD and the nearby conspecific's EOD) will produce beats.

The two recording electrodes used in this paradigm are oriented perpendicularly to the stimulation electrodes in order to avoid any signal contamination. Due to the symmetry that exists between the stimulating and recording electrodes, the signals generated by the stimulation electrodes don't get recorded by the recording electrodes (the contributions of the upper and lower stimulation electrodes cancel out).

We shall now compare the effects of this transverse stimulation paradigm to that of conspecifics. Even though only one phase of the transverse stimulation paradigm is mimicked, other phases would only alter the amplitude of the electric image which it produces, and thus wouldn't qualitatively change the resulting image.

In Figure 5.3 we compare the normalised electric images produced by a parallel (red solid traces) and perpendicular (blue solid traces) conspecific to those obtained with different stimulus electrode configurations (see Figure 5.3A, left and right panels for

conspecific locations). These images were normalised (with respect to the maximal potential of each image) in order to better study the qualitative aspects of the different images and to eliminate discrepancies in amplitude which arose due to the use of the aforementioned electric field stimulus used in [3]. Such differences were to be expected since electric field strength depends on fish size, species, water conductivity, etc. Indeed, the mean electric image produced by the transverse stimulation paradigm (green traces) was roughly five to six times greater than the ones produced by the perpendicular and parallel conspecifics (on the ipsilateral side: side closest to conspecifics in Figure 5.3A).

There are important qualitative differences in the electric images produced by the transverse stimulation paradigm and the parallel and perpendicular conspecifics. This is the case on both sides of the "receiving" fish: ipsilateral (Figure 5.3B) and contralateral (Figure 5.3C). The first thing to point out is that the transverse paradigm (green trace) causes a unimodal perturbation (the image polarity is the same all along the fish), whereas conspecifics sometimes cause strong bimodal perturbations (see e.g. solid red trace, Figure 5.3C). Additionally, there are important qualitative differences between the electric image profiles produced by the conspecifics compared to the one produced by the transverse stimulation paradigm. For example, the image in Figure 5.3B (red trace) drops linearly from head-to-tail until it straightens out at ~ 13 cm, whereas the transverse paradigm is approximately one giant "hump" (image "rises" and "falls" rostrocaudally).

Due to the symmetric nature of the transverse paradigm, the electric image is identical on both sides of the fish. However, this is not the case for "real" conspecifics, as a comparison of Figures 5.3B and 5.3C clearly shows. Moreover, the mean un-normalised electric image produced by the parallel conspecific changes from 28.4 μV on

A

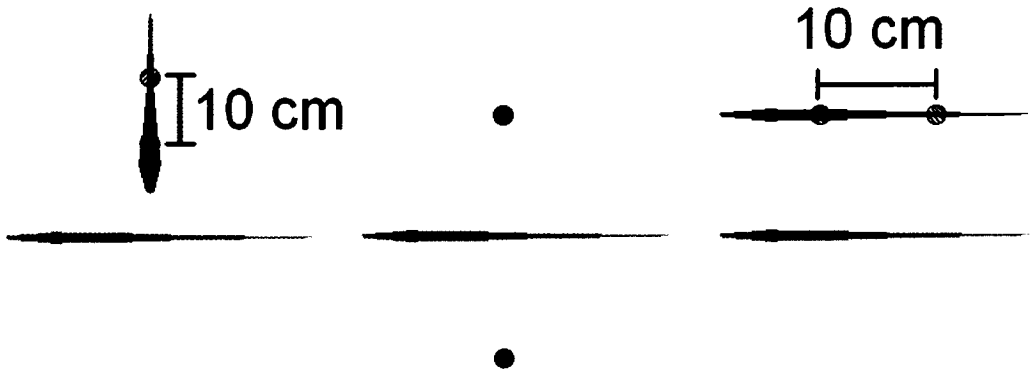
10 cm
10 cm

B

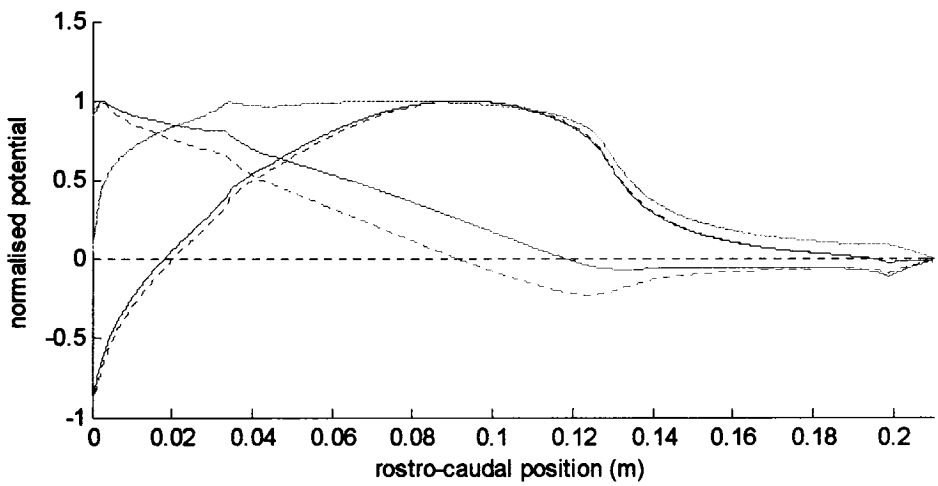
normalised potential
1.5
1
0.5
0
-0.5
-1
0
0.02
0.04
0.06
0.08
0.1
0.12
0.14
0.16
0.18
0.2
rostro-caudal position (m)

C

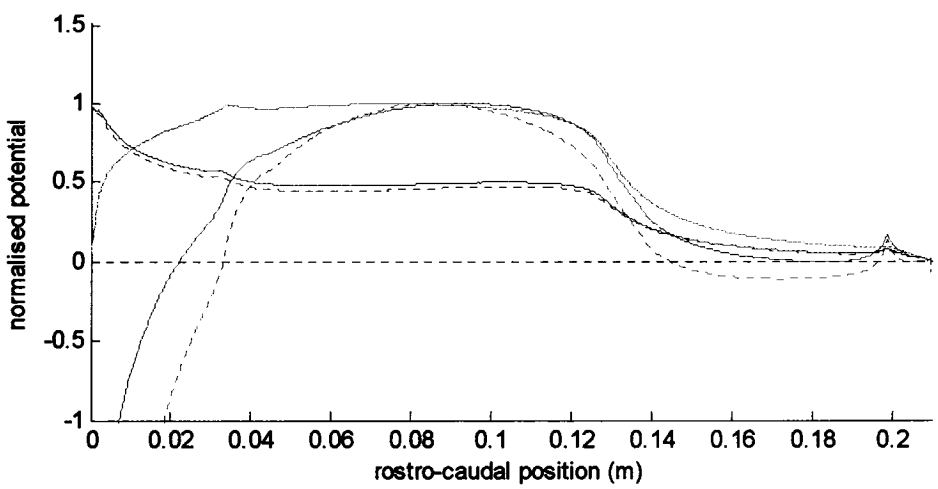
normalised potential
1.5
1
0.5
0
-0.5
-1
0
0.02
0.04
0.06
0.08
0.1
0.12
0.14
0.16
0.18
0.2
rostro-caudal position (m)

Figure 5.3: Mimicking conspecifics with a pair of electrodes. (A) Color-coded conspecific/electrode scenarios for which electric images were calculated in (B) and (C). *Left:* Perpendicular conspecific (blue fish) and pair of electrodes which mimic its effect on a receiving electric fish (grey). *Middle:* Transverse stimulation paradigm (green electrodes) typically used in experiments to mimic effect of conspecifics on an electric fish (grey). Electrodes on either side of the fish are equidistant. *Right:* Parallel conspecific (red fish) and pair of electrodes which mimic its effect on an electric fish (grey). Conspecifics and their respective mimics in left and right panels are centered at the same location as upper electrode in middle panel (at the grey fish's midpoint, 10.5 cm, and 19 cm away laterally). Images produced by "striped" electrodes (for both parallel and perpendicular orientations) are shown as dashed lines in (B) and (C). Diagrams not to scale (e.g. "y" direction in left panel was "compressed" to better view the perpendicular conspecific). (B) Normalised electric images produced by different scenarios shown in (A) on (grey) fish side closest to red "object" fish (ipsilateral side). Color of trace corresponds to color of scenario in (A), i.e. blue traces are for the perpendicular orientation, red traces are for the parallel orientation, and green trace is for the transverse stimulation paradigm. (C) Normalised electric images produced by different scenarios shown in (A) on (grey) fish side farthest to red fish (contralateral side). Trace colors same as in (B).

the ipsilateral side to -9.9 μV on the contralateral side (not shown since images in Figure 5.3 are normalised). This means that a parallel conspecific (for this location) has an effect roughly three times greater on the receiving fish's ipsilateral side. The transverse paradigm's effect, however, is identical on both sides. This is of particular importance, since the fish's electrosensory lateral line lobe is known to receive inputs from both sides of the fish [5, 8, 9].

These results seem to indicate a need for better experimental stimulation paradigms in order to ensure that electrophysiological results are interpreted correctly. To this end, we have mimicked the conspecific fish with an appropriately-aligned pair of electrodes (see left and right panels, Figure 5.3A). These electrodes, whose properties

were identical to the transverse paradigm ones, were separated by 10 cm and centered along the given conspecific's body length (this separation seemed to give the best results, although an exhaustive search was not performed). The electric images obtained with these electrodes (dotted lines, Figures 5.3B and 5.3C), contrary to those obtained with the transverse paradigm, are very similar to the images obtained with the "real" conspecifics, especially for the perpendicular conspecific orientation. While quantitatively not as accurate, the parallel fish's mimic still captured the overall trends in the electric image, for both sides of the fish.

Would these electrode configurations, however, contaminate the recording electrodes? The reason that perpendicular recording electrodes were chosen for the transverse stimulation paradigm was because the contributions of one electrode was offset by the other (due to symmetry). Our proposed stimulation paradigms do not possess this symmetry. However, since the two sets of electrodes are centered (rostro-caudally) along the receiving fish's body, a simple offset (which could be easily calculated using electrostatics) could be applied to these electrodes in order to remove the contamination.

Does the transverse stimulation paradigm mimic the effects of any conspecific location? Figure 5.4 shows that the match between a parallel conspecific displaced 15 cm caudal to the receiving fish (same lateral distance) and the transverse paradigm is reasonable. The transverse paradigm captures the effect of the conspecific extremely well on the ipsilateral side (Figure 5.4A). However, the match on the contralateral side was of lesser quality (Figure 5.4B). Further, this is for the normalised images; in absolute terms,

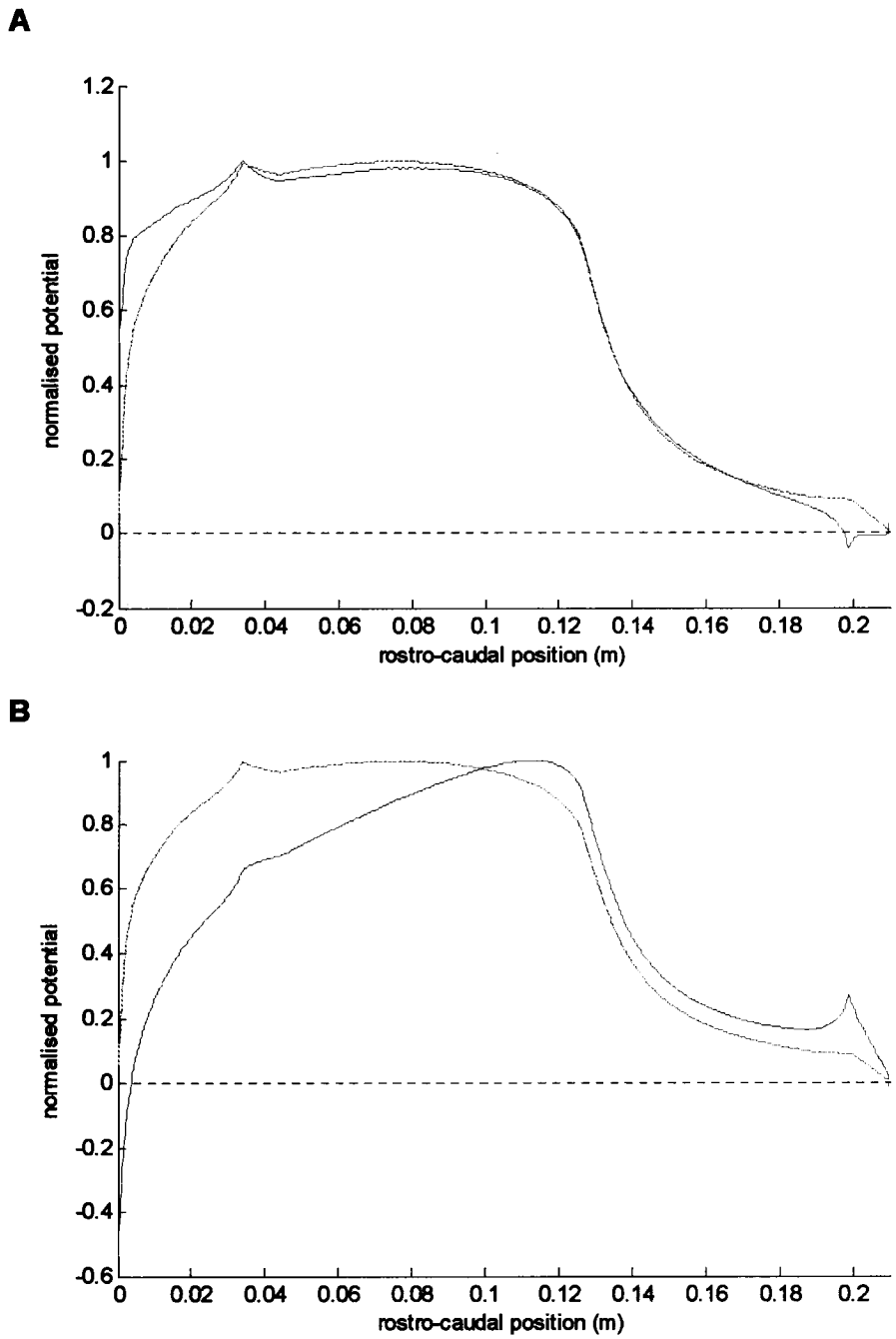

Figure 5.4: Transverse stimulation paradigm versus parallel conspecific. (A) Normalised electric images produced by transverse stimulation paradigm as in Figure 5.3A (green trace) and parallel conspecific (red trace) on electric fish's ipsilateral side (as in Figure 5.3A). Parallel conspecific as in Figure 5.3A, except displaced 15 cm caudally. (B) Normalised images obtained on the fish's contralateral side for same parameters as in (A).

the parallel conspecific's effect on the ipsilateral image was still ~ 40% stronger than on the contralateral side (not shown), while it is identical in the transverse paradigm.

The electric images produced by nearby conspecifics are illustrated in a different way in Figure 5.5 in order to gain further insight into these types of images. The un-normalised electric images for both ipsilateral and contralateral sides (top trace for a given color: ipsilateral) are shown in the same figure for parallel and perpendicular orientations (Figure 5.5A) as well as for antiparallel and antiperpendicular orientations (Figure 5.5B). The differences in the images (due to the conspecifics) between the receiving fish's ipsilateral and contralateral sides are clearly evident (especially red trace, Figure 5.5B). This again points to a need for better stimulation paradigms and such paradigms, as shown in Figure 5.3, could easily be constructed.

5.3.3 Conclusion

Electrocommunication in weakly electric fish has been studied extensively in recent years [3, 6, 7]. These studies use a transverse stimulation paradigm to mimic communication signals and have interpreted their results accordingly. We have studied the effects of a nearby conspecific on the electric images produced in a "receiving" fish, and have compared these images to the ones obtained with the transverse stimulation paradigm. Conspecifics generate bigger and differently shaped signals on the ipsilateral side, compared to the contralateral side, for all conspecific orientations tested. On the other hand, the transverse stimulation paradigm affects both sides of the fish equally. Alternate paradigms have been suggested herein which reproduce the effects of conspecifics with good accuracy. These paradigms should be experimentally tested to see

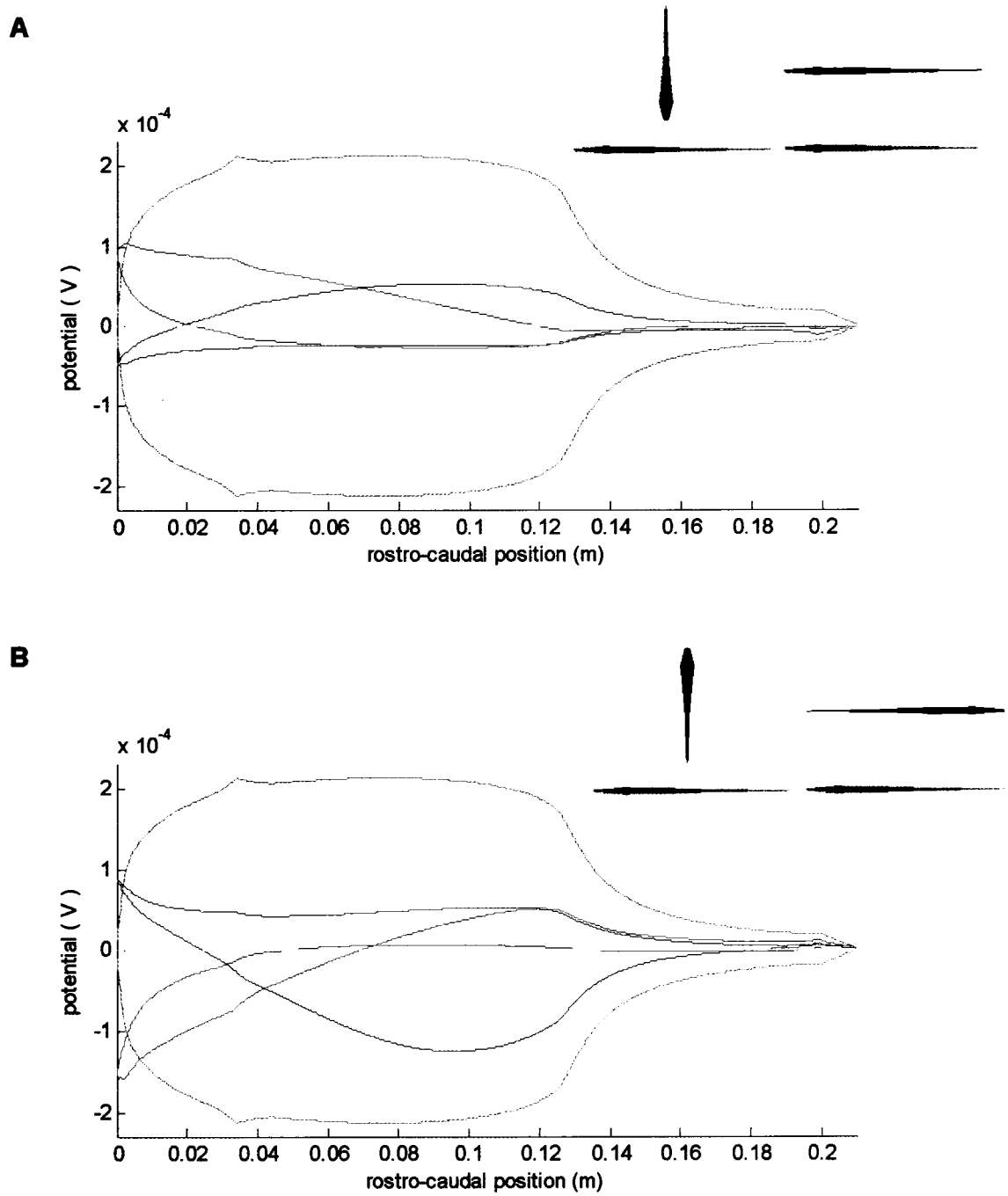

Figure 5.5: Un-normalised electric images produced by conspecifics for different orientations. (A) Images produced by transverse paradigm (same as in Figure 5.3; green trace), parallel conspecific (red trace) and perpendicular conspecific (blue trace) on both sides of the fish body. Images on ipsilateral fish side are top traces of a given color (and mostly positive). (B) Same as in (A) except for opposing fish-to-fish orientations (see insets). Ipsilateral red trace is the one which is most negative in the rostral region.

if results obtained from electrophysiological experiments and theoretical models which try to explain these results still hold. In the very least, however, these results would still be valid for a limited range of conspecific locations (see Figure 5.4). It is possible, however, that fish align in different orientations in order to communicate different messages, and the differences which occur in the electric images due to these different orientations could hold the key to deciphering these messages.

Bibliography

[1] Aguilera, P. A., Castello, M. E., and Caputi, A. A. Electroreception in *Gymnotus carapo*: differences between self-generated and conspecific-generated signal carriers. *J. Exp. Biol.*, vol. 204, pp. 185-198, 2001.

[2] Babineau, D., Longtin, A., and Lewis, J. E. Modeling the electric field of weakly electric fish. *Submitted to the Journal of Experimental Biology.*

[3] Bastian, J., Chacron, M. J., and Maler, L. Receptive field organization determines pyramidal cell stimulus-encoding capability and spatial stimulus selectivity. *J. Neurosci.*, vol. 22, pp. 4577-4590, 2002.

[4] Caputi, A. A., Budelli, R., Grant, K., and Bell, C. C. The electric image in weakly electric fish: physical images of resistive objects in *Gnathonemus petersii*. *J. Exp. Biol.*, vol. 201, pp. 2115-2128, 1998.

[5] Carr, C. E., Maler, L., and Sas, E. Peripheral organization and central projections of the electrosensory nerves in gymnotiform fish. *J. Comp. Neurol.*, vol. 211, pp. 139-153, 1982.

[6] Chacron, M. J., Doiron, B., Maler, L., Longtin, A., and Bastian, J. Non-classical receptive field mediates switch in a sensory neuron's frequency tuning. *Nature*, vol. 423, pp. 77-81, 2003.

[7] Doiron, B., Chacron, M. J., Maler, L., Longtin, A., and Bastian, J. Inhibitory feedback required for network oscillatory responses to communication but not prey stimuli. *Nature*, vol. 421, pp. 539-543, 2003.

[8] Gabbiani, F. and Metzner, W. Encoding and processing of sensory information in neuronal spike trains. *J. Exp. Biol.*, vol. 202, pp. 1267-1279, 1999.

[9] Heiligenberg, W. *Neural Nets in Electric Fish.* Cambridge, Mass.: MIT Press, 1991.

[10] Hopkins, C. D. Electric communication in fish. *Am. Sci.*, vol. 62, pp. 426-437, 1974.

[11] Hoshimiya, N., Shogen , K., Matsuo, T., and Chichibu, S. The *Apteronotus* EOD field: waveform and EOD field simulation. *J. Comp. Physiol.*, vol. 135,

pp. 283-290, 1980.

[12] Nelson, M. E. and MacIver, M. A. Prey capture in the weakly electric fish *Apteronotus albifrons*: sensory acquisition strategies and electrosensory consequences. *J. Exp. Biol.*, vol. 202, pp. 1195-1203, 1999.

[13] Rasnow, B. The effects of simple objects on the electric field of *Apteronotus*. *J. Comp. Physiol. A*, vol. 178, pp. 397-411, 1996.

[14] Tan, E. W., Nizar, J. M., Carrera-G, E., and Fortune, E. S. Electrosensory interference in naturally occurring aggregates of a species of weakly electric fish, *Eigenmannia virescens*. *Behav. Brain. Res.*, vol. 164, pp. 83-92, 2005.

CHAPTER 6

CONCLUSION

6.1 Summary of Results

A two-dimensional model of the weakly electric fish *Apteronotus leptorhynchus'* electric field was created using finite element method software, COMSOL Multiphysics. This model, constructed for a single phase of the fish's oscillating electric organ discharge, reproduces experimental data obtained from Christopher Assad [1], especially near the fish's skin. This model has the advantages of being accurate, fast, easy to modify and flexible. Using this model, many simulations were performed, providing many insights on the weakly electric fish's electric field and natural environment.

In Chapter 3, a study of electric images produced by simple objects suggested some novel rules for electrolocation using bimodal electric images (having two main peaks: a rostral and caudal one). Using these rules, the electric fish might be able to locate lateral objects unambiguously using the distance between the rostral and caudal peaks. This measure is simpler than those previously proposed since the image does not need to be normalised.

The weakly electric fish's field was also analysed using geometrically simple electric field models (see Chapter 3). Using these models, it was discovered that the fish's tapered body shape was mainly responsible for the smooth potential at the head level. The fish was also found to act approximately like a voltage divider, hence providing justification for the use of semi-analytical models under certain conditions.

In Chapter 4, the fish's little-known spatial electro-acuity (fish's ability to distinguish, "hypothetically", two distinct objects) was quantified. Compared to human vision, this sense was found to be very poor (i.e. simulations suggest that objects must be separated by great distances in order for the fish to tell them apart). However, a point of optimal acuity was found in the fish's mid-body, which is somewhat surprising given that the highest density of electroreceptors (the fish's "fovea") is in the head region.

The fish's ability to find small prey-like objects in the presence of large, plant-like contexts was also analysed in Chapter 4. It was found that as the fish scanned about, the electric image component due to the prey, albeit small, changed locations while the component due to the large background context did not (motion parallax). In this fashion, it seems possible that weakly electric fish might extract small, relevant signals by scanning. On a neuronal level, this could in principle be accomplished by either using a subtractive or a scaling algorithm.

The effects of conspecifics were studied in Chapter 5. The electric images produced by conspecifics were found to vary greatly depending on location and orientation (parallel/anti-parallel, perpendicular/anti-perpendicular). These images were, in some cases, found to be drastically different from those produced by the commonly used transverse stimulation paradigm. In particular, this paradigm perturbs both sides of the fish equally, whereas simulations seem to indicate that conspecifics can affect the ipsilateral side up to ~ 3 times more. Conspecifics also produce perturbations which, for a given side, are bimodal (also not mimicked by the current paradigm). It seems possible that different conspecific-to-conspecific orientations are used to communicate different messages, due to the very distinct electric images which they produce.

6.2 Future Work

There are many avenues that can be taken in order to pursue the work done in this thesis and in particular, many theoretical predictions found within it should be verified experimentally.

Firstly, an experiment should be carried out in order to measure the spatial electro-acuity (or, more specifically, the "just noticeable difference") in weakly electric fish. This task, as mentioned in Chapter 4, could be accomplished by using a food-reward paradigm and by forcing the fish to choose between a single object and a "double" object (two objects separated by a given distance). Similar work has been done in weakly electric fish in order to measure the fish's ability to discriminate distances ([4]; the reader is urged to consult this paper for technical experiment details). In this case, however, one would need to calibrate the size of the two different objects (single vs. double) by making the single object larger than the other two objects in the double object. This must be done since the fish would most likely still choose the double object, even for very small inter-object distances, given the larger electric image that two objects would produce as compared to one.

It would also be of interest to see what kinds of exploratory behaviours weakly electric fish use in the presence of different types of backgrounds. If the fish does indeed use the scanning behaviour more frequently while in the presence of "constant" backgrounds, this would seem to corrobate our motion parallax hypothesis (see Chapter 4). A constant background could be mimicked by (e.g.) a long slab of wood while a "messy" background could be produced by scattering chunks of wood here and there.

To follow up the role of scanning in prey detection, we could use a p-afferent (neural) model in order to see whether the small prey blip causes a noticeable change in firing rate (in the presence of a large plant-like context). It would be interesting to see if such an analysis would predict an optimal scanning "speed" and, if so, to compare this speed to behavioural observations.

The study on conspecifics (Chapter 5) was only a "first glimpse" into understanding the effects of their positioning in space on the electric images they produce at the surface of a receiving fish. It might be enlightening to study two conspecifics at different phases or a group of conspecifics (a recent study [5] showed that each fish is typically surrounded by three to five fish), in order to see how such scenarios affect the receiving fish (compared to a single conspecific with the same phase). It would definitely be of interest to determine if electrophysiological results remain the same in the presence of more "realistic" stimuli and if our proposed electrode stimulation paradigm would work (i.e. would not interfere with the recording electrodes). This has serious implications since many important studies [2, 3] have based the interpretation of theirs results on the commonly used transverse stimulation paradigm. Furthermore, electrophysiologists should do recordings in the presence of conspecifics placed in different orientations to see whether or not these might communicate different messages.

The electric fish model created herein easily lends itself to answer a wide range of supplemental questions which were not explored in this thesis. For example, how does a closed container affect the fish's electric image? What does a swarm of prey look like to the fish? What does a worm look like electrically?

Finally, the model itself could be improved by expanding it to the time domain and possibly into the three-dimensional realm. In Chapter 2 it was mentioned that the model could mimic different phases simply by changing the electric organ current density. In order to do this, one would need to change the location, width and amplitudes of the two Gaussian curves which make up the "skewed" profile. One would need to look at the experimental field (as measured by Christopher Assad) for each phase and adjust the aforementioned parameters accordingly. Once these optimal current densities were determined, a script could be written using MATLAB in order to sequentially run COMSOL Multiphysics for the different phases. This model could also be expanded into three dimensions by using a cluster of computers (to improve computing capabilities). This would most likely increase the falloff of the electric field with distance (as mentioned in [1]) and therefore, improve the model's accuracy. Such a model, however, would most likely not negate any of the results found in this thesis since the model was shown to be very accurate near the fish's body, where the (transdermal) electric images were calculated.

Bibliography

[1] Assad, C. Electric field maps and boundary element simulations of electrolocation in weakly electric fish. Ph. D. thesis, California Institute of Technology, Pasadena, CA, 1997.

[2] Chacron, M. J., Doiron, B., Maler, L., Longtin, A., and Bastian, J. Non-classical receptive field mediates switch in a sensory neuron's frequency tuning. *Nature*, vol. 423, pp. 77-81, 2003.

[3] Doiron, B., Chacron, M. J., Maler, L., Longtin, A., and Bastian, J. Inhibitory feedback required for network oscillatory responses to communication but not prey stimuli. *Nature*, vol. 421, pp. 539-543, 2003.

[4] Schwarz, S. and von der Emde, G. Distance discrimination during active electrolocation in the weakly electric fish *Gnathonemus petersii. J. Comp. Physiol. A*, vol. 186, pp. 1185-1197, 2001.

[5] Tan, E. W., Nizar, J. M., Carrera-G, E., and Fortune, E. S. Electrosensory interference in naturally occurring aggregates of a species of weakly electric fish, *Eigenmannia virescens. Behav. Brain. Res.*, vol. 164, pp. 83-92, 2005.